MATHEMATICAL MODELING OF THE TUMOR CELLS POPULATION DYNAMICS IN BREAST CANCER

AMIN OROJI

FACULTY OF SCIENCE
UNIVERSITY OF MALAYA
KUALA LUMPUR

2018

MATHEMATICAL MODELING OF THE TUMOR CELLS POPULATION DYNAMICS IN BREAST CANCER

AMIN OROJI

THESIS SUBMITTED IN FULFILMENT
OF THE REQUIREMENTS
FOR THE DEGREE OF DOCTOR OF PHILOSOPHY

INSTITUTE OF MATHEMATICAL SCIENCES
FACULTY OF SCIENCE
UNIVERSITY OF MALAYA
KUALA LUMPUR

2018

Mathematical modeling of the tumor cells population dynamics in Breast Cancer

ABSTRACT

The role of mathematics in cancer research has steadily increased over time. Multidisciplinary collaboration in cancer research is essential and mathematical applications can significantly contribute to many areas of cancer research. For example, mathematical models can provide deeper insight and establish a framework for understanding properties of cancer cells. Modeling the effects of radiation on cancer cells is one of the most interesting areas in mathematical biology and a variety of models by using the Target theory and DNA fragmentations have been applied to describe how radiation influence tumor cells. In this study, two new mathematical frameworks are proposed to model the population dynamics of heterogeneous tumor cells after the treatment with external beam radiation. The first model is derived based on the Target Theory and Hit Theory. According to these theories, the tumor population is divided into m different sub-populations based on the different effects of ionizing radiations on human cells. This model consists of a system of differential equations with random variable coefficients representing the dynamics transition rates between sub-populations. The model is also describing the heterogeneity of the cell damage and the repair mechanism between two consecutive dose fractions. In the second model, we study the population dynamics of breast cancer cells treated with radiotherapy by using a system of stochastic differential equations. According to the cell cycle, each cell belongs to one of three subpopulations G, S, or M, representing gap, synthesis, and mitosis subpopulations. Cells in the M subpopulation are highly radio-sensitive, whereas cells in the S subpopulation are highly radio-resistant. Therefore, in the process of radiotherapy, cell death rates of different subpopulations are

not equal. In addition, since flow cytometry is unable to detect apoptotic cells accurately, the small changes in cell death rate in each subpopulation during treatment are considered. Therefore, a new definition for the lifespan of the tumor based on population size is introduced. Tumor Lifespan is defined as the minimum number of dose fractions needed to remove the whole tumor. The stability of the first model is studied by considering three cases. For the first and second cases, we assumed that each cell has two and three targets ($m = 2$ and $m = 3$). Applying Routh-Hurwitz criterion, it is proven that the system is stable when the probability that one target becomes deactivated after the application of a dose fraction (q) is greater than or equal to 0.5. Finally, the system stability for the third case is investigated analytically when each cell assumed has m targets. By using Gershgorin theorem, it is shown that the system is stable where $q > 0.5$. In the second model, the existence and uniqueness of the solution are proven and an explicit solution for the SDE model is presented. Moreover, the system stability is investigated via a necessary and sufficient condition on model parameters. The transition rates are estimated in a steady state condition. Subsequently, the model is solved numerically using Euler-Murayama and Milstein methods and the other parameters of the model are estimated using parametric and nonparametric simulated likelihood estimation parameter methods. Finally, we did a number of experiments on MCF-7 breast cancer cell line. The cell cycle analysis assay has been used to analyze experimental data. Then the obtained data is applied and able to calibrate and verify our models.

Keywords: Mathematical Modeling, Tumor Cells Population Dynamics, MCF-7 Breast Cancer Cell Line, Tumor Lifespan, Target Theory, Flowcytometry, Cell Cycle Analysis Assay

Permodelan Matematik untuk Populasi Dinamik Sel Tumor bagi Kanser Payudara

ABSTRAK

Peranan matematik dalam penyelidikan kanser telah meningkat dari semasa ke semasa. Penyelidikan kanser adalah kajian pelbagai disiplin dan matematik gunaan boleh menyumbang dalam banyak perkara. Sebagai contoh, model matematik boleh memberi gambaran yang lebih mendalam untuk memahami ciri-ciri sel kanser. Pemodelan kesan radiasi pada sel kanser adalah salah satu bidang yang menarik matematik biologi dan beberapa model seperti sasaran teori dan DNA fragmentasi dalam menggambarkan bagaimana sel tumor terkesan oleh radiasi. Dalam tesis ini, dua kerangka matematik baru dicadangkan bagi membentuk model heterogen dinamik populasi sel tumor selepas rawatan dengan sinaran pancaran luaran. Model pertama berdasarkan Teori Sasaran dan Teori Hit. Menurut teori ini, populasi tumor dibahagikan kepada m sub-populasi berdasarkan kesan yang berbeza daripada pancaran pengionan pada sel manusia. Model ini dibentuk oleh sistem persamaan pembezaan dengan pekali pembolehubah rawak yang mewakili kadar peralihan antara sub-populasi. Model ini juga menggambarkan kepelbagaian kerosakan sel dan mekanisme pembaikan di antara dua dos yang berturut-turut. Dalam model kedua, kita mengkaji dinamik populasi sel kanser payudara yang dirawat dengan radioterapi dengan menggunakan sistem persamaan pembezaan stokastik. Mengikut kitaran sel, setiap sel tergolong dalam salah satu daripada tiga sub-populasi G, S atau M, yang mewakili jurang, sintesis dan sub-populasi mitosis. Sel dalam sub-populasi M sangat radio-sensitif, manakala sel-sel dalam sub-populasi S sangat radio-tahan. Oleh itu, dalam proses radioterapi, kadar kematian sel sub-populasi adalah tidak sama. Di samping itu, memandangkan proses aliran cytometry gagal mengesan sel apoptotic dengan tepat, maka pe-

rubahan kecil dalam kadar kematian sel dalam setiap sub-populasi semasa rawatan akan dipertimbangkan. Oleh itu, takrif baru untuk jangka hayat tumor berdasarkan saiz populasi diperkenalkan. Jangka hayat tumor ditakrifkan sebagai bilangan minimum dos yang diperlukan untuk mengeluarkan keseluruhan tumor. Kestabilan model pertama dikaji dalam tiga kes. Untuk kes pertama dan kedua, kita andaikan setiap sel mempunyai dua dan tiga sasaran ($m = 2$ dan $m = 3$). Menggunakan criteria Routh-Hurwitz, terbukti sistem itu adalah stabil apabila kebarangkalian bahawa satu sasaran dinyahaktifkan apabila dos (q) adalah lebih besar daripada atau sama dengan 0.5. Akhirnya, kestabilan sistem untuk kes ketiga disiasat secara analitik apabila setiap sel mempunyai m sasaran. Dengan menggunakan teorem Gershgorin, didapati sistem adalah stabil bila $q > 0.5$. Untuk model kedua, kewujudan dan keunikan penyelesaian ditunjukkan dan penyelesaian tepat untuk model SDE itu dikemukakan. Selain itu, kestabilan sistem disiasat melalui syarat perlu dan mencukupi k eats parameter model. Kadar peralihan dianggarkan dalam keadaan mantap. Selepas itu model ini diselesaikan secara berangka menggunakan kaedah Euler-Murayama dan Milstein dan parameter lain dianggarkan dengan menggunakan kaedah kemungkinan simulasi berparameter dan tak berparameter. Akhirnya kita lakukan beberapa eksperimen pada MCF-7 garis sel kanser payudara. Kitaran sel analisis assay telah digunakan untuk menganalisis data eksperimen. Kemudian data yang diperolehi digunakan untuk mengesahkan model yang telah dibina.

Keywords: Pemodelan Matematik, Tumor Sels Dinamik Populasi, Talian Sel Kanker Payudara MCF-7, umor jangka hayat, Teori Sasaran, Flowcytometry, Analisis Analisis Kitaran Sel

ACKNOWLEDGEMENTS

I would like to express my sincere gratitude to my supervisors Professor Mohd Omar, Dr. Ivy Chung and Dr. Shantia Yarhamadian for the continuous support of my Ph.D. study and research, for their patience, motivation, enthusiasm and immense knowledge. Their patience and support helped me overcome many crisis situations and this thesis.

I am also grateful to the following former and current staff at the University of Malaya, for their various forms of supports during my graduate study. My friends have helped me stay sane through these years. Their support and care helped me overcome setbacks and stay focused on my graduate study. I greatly value their friendship and I deeply appreciate their belief in me.

Very special thanks to all professors during my bachelor and master and more specially **Dr. Farid Bahrami** who thought me the right way of thinking and living.

Most importantly, none of this would have been possible without the love and patience of my wife. I would like to express my genuine gratitude to my lovely wife and daughter, Elena, and to my parents and siblings for supporting me spiritually throughout my life and study.

Finally, I appreciate the financial support from Prof. Mohd Omar (**FRGS** grant number **FP015-2015A**) to support this research.

TABLE OF CONTENTS

ABSTRACT ii

ABSTRAK iv

ACKNOWLEDGEMENTS vi

TABLE OF CONTENTS vii

LIST OF FIGURES x

LIST OF TABLES xvi

LIST OF APPENDICES xvii

CHAPTER 1: INTRODUCTION 1

1.1 Research problem 2
1.2 Research Questions 2
1.3 Objectives 2
1.4 Thesis Outline 3

CHAPTER 2: LITERATURE REVIEW 6

2.1 Biological Background 6
2.1.1 Cell Cycle Progression and Apoptosis 6
2.1.2 Radiation Therapy 9
2.1.3 Cell Death definition in Radiobiology 10
2.1.4 Radiation and Cell Arrest 12
2.1.5 Target Theory 17
2.2 Mathematical Background 18
2.2.1 Routh-Hurwitz Criterion 18
2.2.2 Gershgorin Discs and Gershgorin Theorem 20
2.2.3 Markov Chain 21
2.2.4 Brownian Motion 23
2.2.5 White Noise 24
2.2.6 Ito Stochastic Differential Equations 25
2.2.7 Numerical Solution 29
2.2.8 Parameter Estimation of a SDE model 31
2.3 Mathematical Models 38
2.3.1 Early Models of tumor growth 39
2.3.2 Mathematical models of radiation effect 40
2.3.3 Cell Cycle Models 45

CHAPTER 3: MATHEMATICAL MODELS 48

3.1 Markov chain model for a single cell 49
3.1.1 Treatment Mechanism 49
3.1.2 Repair Mechanism 50

3.1.3 Transition matrix of Z_k 52
3.2 An ODE model for tumor Cells Population Dynamics Based on Target Theory 53
3.2.1 Assumptions 55
3.2.2 Model derivation 56
3.2.3 Model Calibration 58
3.3 The SDE model for the tumor cells population dynamics based on cell cycle position 62
3.3.1 Assumptions 62
3.3.2 Stochastic Differential Equation Model 63
3.3.3 Model Calibration 65
3.3.4 Steady-State Solution 65
3.3.5 Evaluation of the model parameters 68
3.4 Tumor lifespan 69

CHAPTER 4: MATHEMATICAL RESULTS 71

4.1 Single-Strand Break (SSB) and Double-Strand Breaks (DSBs) as one subpopulations 71
4.1.1 Stability Analysis 72
4.1.2 Bifurcation Analysis 78
4.2 Single-Strand Break (SSB) and Double-Strand Breaks (DSBs) as two subpopulations 83
4.2.1 Stability Analysis 86
4.2.2 Numerical simulation: Lifespan and bifurcation analysis 93
4.2.3 Bifurcation analysis 95
4.3 The general case of m targets 98
4.4 SDE Model 103
4.4.1 Existence and Uniqueness of the solutions 104
4.4.2 Explicit Solution 104
4.4.3 Linear Moment Stability Analysis 104
4.4.4 Simulation Results 106

CHAPTER 5: EXPERIMENTAL RESULTS 119

5.1 Methodology 119
5.1.1 Chemical and reagent 119
5.1.2 Cell Cultures 119
5.1.3 Seeding and Radiation 119
5.1.4 Cell Cycle Assay 120
5.2 Result 122
5.3 Simulation and Parameter Estimation 123

CHAPTER 6: DISCUSSION 133

6.1 Remind the purpose of this study 133
6.2 A summary of results 134
6.2.1 The ODE model of tumor cells population dynamics 134
6.2.2 The SDE model of tumor cells population dynamics 135
6.3 Future Works 136

CHAPTER 7: CONCLUSION 138

REFERENCES 140

LIST OF PUBLICATIONS 153

APPENDICES 157

LIST OF FIGURES

Figure 2.1 Schematic illustration of the cell cycle progression and checkpoints. 9

Figure 3.1 Different states for a cell with $m = 3$ targets. 49

Figure 3.2 The transition graph of the radiation process before considering the repair mechanism, for the case of $m = 3$. 51

Figure 3.3 The transition graph for (Z_k) after the application of treatment and repair mechanism. 52

Figure 3.4 Schematic illustration of tumor cell population model. 56

Figure 3.5 Schematic illustration of the cell cycle in a tumor treated by radiation 63

Figure 4.1 Stability analysis in case $m = 2$. 74

Figure 4.2 Stability Analysis For $m = 2$. Red area represents the system stability region. 75

Figure 4.3 The Dynamics of The Population Size where m=2, q=0.5, and r=0.1 (Stable Case) 78

Figure 4.4 Trajectories where the system is stable. The number of targets are supposed to be two in each cell. 79

Figure 4.5 The Dynamics of The Population Size where $m = 2$, $q = 0.3$, and $r = 0.1$ (Unstable Case). 79

Figure 4.6 Trajectories where the system is unstable. The number of targets are supposed to be two in each cell. 80

Figure 4.7 Stability Region Where $m = 2$ 82

Figure 4.8 Stability Region Where $m = 5$ 83

Figure 4.9 Stability Region Where $m = 10$ 83

Figure 4.10 Stability Region where $m = 4$ and $m = 10$ 83

Figure 4.11 Stability Region where $m = 20$ and $m = 50$ 84

Figure 4.12 Influence of μ on the tumor lifespan in case $m = 2$. 84

Figure 4.13 Influence of μ on the tumor lifespan in case $q = 0.6$ and $n_0 = 10^7$. 84

Figure 4.14 Compare the lifespan trend for $m = 2$ and $m = 3$, where $q = 0.8$ and $n_0 = 10^3$. 85

Figure 4.15 Compare the lifespan trend for $m = 6$ and $m = 7$, where $q = 0.9$ and $n_0 = 10^3$. 86

Figure 4.16 The influence of the repair mechanism probability (r) on the tumor lifespan where $m = 2$ and $n_0 = 10^3$. 87

Figure 4.17 The influence of the treatment probability (q) on the tumor lifespan where $m = 2$ and $n_0 = 10^3$. 88

Figure 4.18 The tumor Lifespan where $m = 2$, $n_0 = 10^3$, $0.6 \leq q \leq 1$, and $0 \leq r \leq 1$. 89

Figure 4.19 The tumor Lifespan where $m = 6$, $n_0 = 10^3$, $0.6 \leq q \leq 1$, and $0 \leq r \leq 1$. 90

Figure 4.20 Comparing the tumor lifespan where $m = 2$ and $m = 6$. 91

Figure 4.21 3-D stability region. 91

Figure 4.22 3-D stability region. 92

Figure 4.23 Stability analysis. 92

Figure 4.24 The influence of parameter μ on tumor lifespan for $q = 0.6$ and $r = 0.2$. (a) $n_0 = 100$, (b) $n_0 = 1000$. 94

Figure 4.25 Influence of μ on tumor lifespan where n_0 changes from 10^3 to 10^{10} when $q = 0.6$ and $0 < r < 1$. 94

Figure 4.26 (a) Influence of inactivation probability (q) on tumor lifespan (L). The blue and red solid lines represent the tumor lifespan values corresponding to $r = 0.3$ and $r = 0.4$, respectively. (b) Influence of the reactivation probability of a target after a dose fraction (r) on tumor lifespan (L). The blue and red solid lines represent the tumor lifespan values corresponding to $r = 0.3$ and $r = 0.4$, respectively 95

Figure 4.27 Variations in tumor lifespan (L) with respect to changes in the initial number of tumor cells (n_0) for $r = 0.1$ and $q = 0.5$. 96

Figure 4.28 Dynamics of all tumor cells ($N(t)$) and subpopulations $x_0(t)$, $x_1(t)$ and $x_2(t)$, for $q = 0.6$ and $r = 0.2$. 97

Figure 4.29 Dynamics of all tumor cells ($N(t)$) and subpopulations $x_0(t)$, $x_1(t)$ and $x_2(t)$, for $q = 0.2$ and $r = 0.4$. 97

Figure 4.30 System phase diagram where (a) $(0,0,0)$ is stable for $q = 0.6$ and $r = 0.4$ (b) $(0,0,0)$ is unstable for $q = 0.2$ and $r = 0.4$. 98

Figure 4.31 Stability region of the system(4.2.1) with respect to the values of $\mu = 0.1$, $\mu = 0.5$ and $\mu = 1$. 98

Figure 4.32 3-D diagram of the population dynamics of subpopulations x_0, x_1 and x_2. $n_0 = 1000$, and q varies from 0.4 to 0.6 with step size 0.05. Here, r changes: (a) $r = 0.4$, (b) $r = 0.5$, (c) $r = 0.6$. 98

Figure 4.33 3-D diagram of the population dynamics of subpopulations x_0, x_1 and x_2. $n_0 = 1000$, and q varies from 0.4 to 0.6 with step size 0.05. Here, r changes: (a) $r = 0.7$, (b) $r = 0.8$, (c) $r = 0.9$. 99

Figure 4.34 System bifurcation analysis, where q varies between 0.4 and 0.6 and $r = 0.9$. The system is stable when $q \geq 0.5$ 99

Figure 4.35 3-D plot for $|a_1(q,r)|$, $|a_1(q,r)a_2(q,r) - a_3(q,r)|$ and $|a_3(q,r)|$. The system(4.2.1) is stable if and only if these functions are positive. 99

Figure 4.36 Intersection of the area in which functions $a_1(q,r)$ and $a_3(q,r)$ are positive and $a_1(q,r)\ a_2(q,r) > a_3(q,r)$. The Routh-Hurwitz Criterion is satisfied for all values of q and r in the blue region. 100

Figure 4.37 Gershgorin disc $B(A_{tt}, R_t)$. 103

Figure 4.38 Stability region of the system. 106

Figure 4.39 Cell population dynamics for subpopulation G over 100 trajectories by solving Equation(3.3.5). Here, the black circles are the trajectories corresponding to the observed numbers of cells (parametric method). The blue lines represent the first and third quartiles of the simulated trajectories and the red lines illustrate 95% confidence interval areas obtained by taking, at each time, the 2.5^{th} and 97.5^{th} percentiles of the simulated trajectories. The green line is the empirical mean of the process. 109

Figure 4.40 Cell population dynamics for the subpopulation S over 100 trajectories by solving Equation (3.3.5). Here, the black circles are the trajectories corresponding to the observed numbers of cells (parametric method). The blue lines represent the first and third quartiles of the simulated trajectories and the red lines illustrate 95% confidence interval areas obtained by taking, at each time, the 2.5^{th} and 97.5^{th} percentiles of the simulated trajectories. The green line is the empirical mean of the process. 110

Figure 4.41 Cell population dynamics for the subpopulation M over 100 trajectories by solving Equation (3.3.5). Here, the black circles are the trajectories corresponding to the observed numbers of cells (parametric method). The blue lines represent the first and third quartiles of the simulated trajectories and the red lines illustrate 95% confidence interval areas obtained by taking, at each time, the 2.5^{th} and 97.5^{th} percentiles of the simulated trajectories. The green line is the empirical mean of the process. 110

Figure 4.42 Histogram of the observed number of cells in each subpopulation at time T=40 over 100 trajectories with Euler-Maruyama approximation. 111

Figure 4.43 Cell population dynamics for subpopulation G. The black circles show the trajectories corresponding to the observed data (nonparametric method). The blue lines represent the first and third quartiles of the simulated trajectories and the red lines illustrate the 95% confidence interval areas obtained by taking, at each time, the 2.5^{th} and 97.5^{th} percentiles of the simulated trajectories. The green line is the empirical mean of the process. 112

Figure 4.44 Cell population dynamics for subpopulation S. The black circles show the trajectories corresponding to the observed data (nonparametric method). The blue lines represent the first and third quartiles of the simulated trajectories and the red lines illustrate the 95% confidence interval areas obtained by taking, at each time, the 2.5^{th} and 97.5^{th} percentiles of the simulated trajectories. The green line is the empirical mean of the process. 112

Figure 4.45 Cell population dynamics for subpopulation M. The black circles show the trajectories corresponding to the observed data (nonparametric method). The blue lines represent the first and third quartiles of the simulated trajectories and the red lines illustrate the 95% confidence interval areas obtained by taking, at each time, the 2.5^{th} and 97.5^{th} percentiles of the simulated trajectories. The green line is the empirical mean of the process. 113

Figure 4.46 Histogram of the observed number of cells in each subpopulation at time T=40 over 100 trajectories with Euler-Maruyama approximation. 114

Figure 4.47 Cell population dynamics for subpopulation G. The black circles show the trajectories corresponding to the observed data (nonparametric method). The blue lines represent the first and third quartiles of the simulated trajectories and the red lines illustrate the 95% confidence interval areas obtained by taking, at each time, the 2.5^{th} and 97.5^{th} percentiles of the simulated trajectories. The green line is the empirical mean of the process. 115

Figure 4.48 Cell population dynamics for subpopulation S. The black circles show the trajectories corresponding to the observed data (nonparametric method). The blue lines represent the first and third quartiles of the simulated trajectories and the red lines illustrate the 95% confidence interval areas obtained by taking, at each time, the 2.5^{th} and 97.5^{th} percentiles of the simulated trajectories. The green line is the empirical mean of the process. 115

Figure 4.49 Cell population dynamics for subpopulation M. The black circles show the trajectories corresponding to the observed data (nonparametric method). The blue lines represent the first and third quartiles of the simulated trajectories and the red lines illustrate the 95% confidence interval areas obtained by taking, at each time, the 2.5^{th} and 97.5^{th} percentiles of the simulated trajectories. The green line is the empirical mean of the process. 116

Figure 4.50 Histogram of the observed number of cells in each subpopulation at time T=40 over 100 trajectories with Milstein approximation. 117

Figure 4.51 (a) Cell population dynamics in the whole tumor over 20 trajectories, where the system of SDEs (3.3.5) is solved by Euler-Maruyama algorithm and the parameters are estimated by a parametric method; (b) Cell population dynamics in the whole tumor over 20 trajectories, where the system of SDEs (3.3.5) is solved by Euler-Maruyama or Milstein algorithm and the parameters are estimated by nonparametric method. 117

Figure 4.52 Lifespan diagrams. 118

Figure 5.1 Cell counting by using hemocytometer. 121

Figure 5.2 Cell cycle analysis for cells at time points zero, 24, 48 and 72 hours after radiation in two cases control and irradiated cells. 123

Figure 5.3 The proportion of cells in G_1, S and G_2/M phase for cells at the time of radiation (time 0) and 24, 48 and 72 hours after radiation in two cases control and irradiated cells. The blue and red colors are for control and irradiated cells, respectively. 124

Figure 5.4 Cells viability for cells 24, 48 and 72 hours after radiation in two cases control and irradiated cells. The blue and red color show the control and irradiated cells, respectively. 124

Figure 5.5 Cell population dynamics for subpopulation G over 100 trajectories by solving Equation(3.3.5). Here, the black circles are the trajectories corresponding to the observed numbers of cells (parametric method). The blue lines represent the first and third quartiles of the simulated trajectories and the red lines illustrate 95% confidence interval areas obtained by taking, at each time, the 2.5^{th} and 97.5^{th} percentiles of the simulated trajectories. The green line is the empirical mean of the process. 127

Figure 5.6 Cell population dynamics for the subpopulation S over 100 trajectories by solving Equation(3.3.5). Here, the black circles are the trajectories corresponding to the observed numbers of cells (parametric method). The blue lines represent the first and third quartiles of the simulated trajectories and the red lines illustrate 95% confidence interval areas obtained by taking, at each time, the 2.5^{th} and 97.5^{th} percentiles of the simulated trajectories. The green line is the empirical mean of the process. 127

Figure 5.7 Cell population dynamics for the subpopulation M over 100 trajectories by solving Equation(3.3.5). Here, the black circles are the trajectories corresponding to the observed numbers of cells (parametric method). The blue lines represent the first and third quartiles of the simulated trajectories and the red lines illustrate 95% confidence interval areas obtained by taking, at each time, the 2.5^{th} and 97.5^{th} percentiles of the simulated trajectories. The green line is the empirical mean of the process. 128

Figure 5.8 Cell population dynamics for subpopulation G. The black circles show the trajectories corresponding to the observed data (nonparametric method). The blue lines represent the first and third quartiles of the simulated trajectories and the red lines illustrate the 95% confidence interval areas obtained by taking, at each time, the 2.5^{th} and 97.5^{th} percentiles of the simulated trajectories. The green line is the empirical mean of the process. 129

Figure 5.9 Cell population dynamics for subpopulation S. The black circles show the trajectories corresponding to the observed data (nonparametric method). The blue lines represent the first and third quartiles of the simulated trajectories and the red lines illustrate the 95% confidence interval areas obtained by taking, at each time, the 2.5^{th} and 97.5^{th} percentiles of the simulated trajectories. The green line is the empirical mean of the process. 129

Figure 5.10 Cell population dynamics for subpopulation M. The black circles show the trajectories corresponding to the observed data (nonparametric method). The blue lines represent the first and third quartiles of the simulated trajectories and the red lines illustrate the 95% confidence interval areas obtained by taking, at each time, the 2.5^{th} and 97.5^{th} percentiles of the simulated trajectories. The green line is the empirical mean of the process. 130

Figure 5.11 Cell population dynamics for subpopulation G. The black circles show the trajectories corresponding to the observed data (nonparametric method). The blue lines represent the first and third quartiles of the simulated trajectories and the red lines illustrate the 95% confidence interval areas obtained by taking, at each time, the 2.5^{th} and 97.5^{th} percentiles of the simulated trajectories. The green line is the empirical mean of the process. 131

Figure 5.12 Cell population dynamics for subpopulation S. The black circles show the trajectories corresponding to the observed data (nonparametric method). The blue lines represent the first and third quartiles of the simulated trajectories and the red lines illustrate the 95% confidence interval areas obtained by taking, at each time, the 2.5^{th} and 97.5^{th} percentiles of the simulated trajectories. The green line is the empirical mean of the process. 131

Figure 5.13 Cell population dynamics for subpopulation M. The black circles show the trajectories corresponding to the observed data (nonparametric method). The blue lines represent the first and third quartiles of the simulated trajectories and the red lines illustrate the 95% confidence interval areas obtained by taking, at each time, the 2.5^{th} and 97.5^{th} percentiles of the simulated trajectories. The green line is the empirical mean of the process. 132

Figure 1 Five most common cancer in the world based on incidence and mortality rates in 2012. 159

Figure 2 Five most common cancer in men in 2012 based on incidence and mortality rates in 2012. 160

Figure 3 Five most common cancer in women in 2012 based on incidence and mortality rates in 2012. 160

Figure 4 Cell cycle analysis irradiated dish 4 and 8 hours after radiation. 164

Figure 5	Cell cycle analysis irradiated dish 16 and 24 hours after radiation.	164
Figure 6	Cell cycle analysis irradiated and control dish 48 hours after radiation.	164
Figure 7	Proportion of cells in G_1, S and G_2/M phase for cells at the time points 4, 8, 16, 24 and 48 hours after radiation and control cells harvested at 48 hours after radiation.	165
Figure 8	Cell cycle analysis irradiated dish 24 and 48 hours after radiation.	166
Figure 9	Cell cycle analysis irradiated and control dish 72 hours after radiation.	166
Figure 10	Proportion of cells in G_1, S and G_2/M phase for cells at the time points 24, 48 and 72 hours after radiation and control cells harvested at 72 hours after radiation.	167
Figure 11	Cell cycle analysis of irradiated and control dish 24 hours after radiation.	168
Figure 12	Cell cycle analysis of irradiated and control dish 48 hours after radiation.	168
Figure 13	Cell cycle analysis irradiated and control dish 72 hours after radiation.	168
Figure 14	Proportion of cells in G_1, S and G_2/M phase for cells at the time of radiation (time 0) and 24, 48 and 72 hours after radiation in two cases control and irradiated cells. The blue and red colors are for control and irradiated cells, respectively.	169
Figure 15	Top countries based on the number of publications.	170
Figure 16	Top universities based on the number of publications.	171
Figure 17	Top ten authors based on the number of publications.	171
Figure 18	The number of publications based on the year of publication.	172
Figure 19	Top research areas based on the number of publications.	172
Figure 20	Top journals based on the number of publications.	173

LIST OF TABLES

Table 3.1	Estimated parameter values in steady-state condition	69
Table 4.1	Influence of the parameters q, m on the Tumor Lifespan L, where $n_0 = 10^3$ and $r = 0.3$.	85
Table 4.2	Influence of the parameters q, m on the Tumor Lifespan L, where $n_0 = 10^3$ and $r = 0.9$.	86
Table 4.3	Influence of parameters (q) and (r) on the tumor lifespan (L) for $n_0 = 100$.	95
Table 4.4	Tumor lifespan for $q = 0.9$ when n_0 varies between 10^2 and 10^5.	95
Table 4.5	Experiment-dependent parameters	107
Table 4.6	Initial Values of model parameters.	108
Table 4.7	Estimated parameter values with 95% confidence intervals for the transition rates using the parametric method	108
Table 4.8	Monte Carlo Statistics for the G, S and M subpopulations at time T=40 hours.	111
Table 4.9	Estimated parameter values and 95% confidence intervals of the movement rates using the nonparametric method.	113
Table 4.10	Monte Carlo Statistics for the G, S and M subpopulations at time T=40 hours.	113
Table 4.11	Estimated parameter values and 95% confidence intervals of the movement rates using the nonparametric method	114
Table 4.12	Monte Carlo Statistics for the G, S and M subpopulations at time T=40 hours.	116
Table 5.1	Proportion of cells in G_1, S and G_2/M phase corresponding to the fourth experiment.	125
Table 5.2	The population size in G_1, S and G_2/M phase.	126
Table 5.3	Estimated parameter values with 95% confidence intervals for the death rates using the parametric method	126
Table 5.4	Estimated parameter values and 95% confidence intervals of the death rates using the nonparametric method.	128
Table 5.5	Estimated parameter values and 95% confidence intervals of the death rates using the nonparametric method	130
Table 1	Proportion of cells in G_1, S and G_2/M phase corresponding to the first experiment.	163
Table 2	Proportion of cells in G_1, S and G_2/M phase corresponding to the second experiment.	166
Table 3	Proportion of cells in G_1, S and G_2/M phase corresponding to the third experiment.	169

LIST OF APPENDICES

Cancer Incidence	158
Breast Cancer Incidence	161
Optimization	163
Scientometric Analysis	170

CHAPTER 1

INTRODUCTION

Cancer affected millions of people in the world and Radiation Therapy (XRT) is one of the common methods of cancer treatment. There are many obstacles in In Vivo and In Vitro conditions. For instance, experiments are usually expensive. Another limitation in experiments is time. In these cases In Silico condition can be very useful.

The role of mathematics in cancer research has steadily increased over time and the future of this discipline is both exciting and critical as new patients are diagnosed with cancer every day. Multidisciplinary collaboration in cancer research is essential and mathematical applications can contribute significantly to many areas of cancer research.

Mathematical models can provide insight and establish a framework for understanding properties of cancer cells, e.g., by modeling the biochemical behavior within a single cancer cell or by modeling a tumor growth.

In this thesis two mathematical models are proposed to explain the population dynamics of tumor cells which are treated with external beam radiation therapy.

The first system is modeled the tumor cells population dynamics by using a system of ordinary differential equations (ODE). The model is also based on target theory and hit theory.

Then we model the tumor cells population dynamics via a multidimensional stochastic differential equation (SDE). In this model subpopulations show the number of cells in each phase of cell cycle.

1.1 Research problem

The majority of existing models assume that the cell sensitivity will be constant during the radiation. The same assumption is also taken into account for the cell population, i.e., a surviving cell is expected to be viably considered as an irradiated cell.

In such circumstances, all cells are believed to have similar survival probability. While, there are strong evidences that damaged cells would be unable to resist the radiation.

According to literature, another common drawback of mathematical models of the domain is the lack of considering the inherent error in death rate caused by the flow cytometry method. This error is rooted in recognizing apoptotic cells as live cells.

Furthermore, in the previous clinical cancer researches only tumors with 10^9 cells have been detectable. However, after resection surgeries, small tumors may still remain. Hence, clinicians irradiate the tissue to kill the rest of tumor cells.

It may causes side effects in normal tissues. Therefore, it is important to predict how many dose fractions are needed to remove the tumor. In other words, it is crucial to know what will be the tumor lifespan.

1.2 Research Questions

Research Questions of this research are:

1. How to model tumor cells population dynamics where the treatment heterogeneity and cell cycle position are taking accounted for?

2. Under which conditions on the model parameters the system is stable?

3. What is the tumor lifespan?

1.3 Objectives

The objectives of this study are listed as following:

I ODE Model

a) Tumor Cells population size is modeled by using a system of Ordinary Differential Equations(ODE) and based on target theory and hit theory.

b) The system stability is probed based on Routh-Hurwitz theorem. This shows under which condition treatment is beneficial.

c) The effects of each parameter(so called Bifurcation Analysis) is studied.

d) The tumor lifespan is defined based one the tumor cells population size.

II SDE Model

a) Tumor cells population size is modeled by applying a multi-dimensional Stochastic Differential Equations(SDE).

b) Stability analysis of the system is studied.

c) The model is calibrated and verified by using experimental data.

1.4 Thesis Outline

This thesis is organized as follows:

Chapter 2 is divided into three sections. In the first section, biological terms such as cell cycle, apoptosis, radiation therapy as one of the most common cancer therapies, the definition of cell death in radio biology, the effect of radiation on cell cycle arrest and target theory are presented.

The second section is for mathematical background such as Markov chain, Brownian motion and white noise, Ito stochastic differential equations (SDEs), numerical soloutions of SDEs and parametric and non-parametric simulated likelihood estimation parameter methods.

Finally early mathematical models of the tumor growth, mathematical models of the effect of radiation on cells and cell cycle models are listed on the last section.

In chapter 3, two mathematical models are presented to explain the effect of radiation therapy on the population dynamics of tumor cells.

The first model is a system of m ordinary differential equations where the subpopulations are classified according to the effect radiation on cells and m is the number of targets in each cell.

In the second model tumor cells are divided into three subpopulations where each subpopulation shows the cell cycle position. Thereafter, the cells population dynamics is modeled via a multi-dimension Ito stochastic differential equation.

Finally, the tumor lifespan is defined for the models based on the tumor cells population size.

Mathematical results for both models are presented in chapter 4.4.4.

The ODE model is considered in three cases

1. Case $m = 2$:

   Generally it is very difficult to distingush between cells with single-strand break and cells with double strand breaks. Therefore cells are divide into two subpopulations, cells with DNA fragmentation and the cells without DNA break.

2. Case $m = 3$:

   Thereafter, it is supposed that the cells with SSB and DSB be detectable. Subsequently, cells with SSB, cells with DSB and cells without DNA fragmentation.

3. General case: Suppose that each cell has m targets and each target may be deactivated after the application of a dose fraction. Therefore, m subpopulations are cells with zero, one, two, ... and $m-1$ inactive targets.

Using Routh-Hurwits and Gershgorin Theorems, it is shown that the system is stable under some conditions of model parameters. Moreover the effects of different parameters

on the tumor lifespan is studied.

In the subsequent section, the SDE model is studied. Then the existence and uniqueness of solution and the explicit solution of the equation is probed. Subsequently, the stability analysis of the system is investigated and a necessary and sufficient condition of the model stability is proven. The last section of this chapter is presented the simulation results. In this section, the model is solved numerically by using Euler-Maruyama and Milstein Methods. Then the model parameters are estimated applying SLE method and by using the simulated data.

The results obtained from real experiments are shown in chapter 5. According to the data obtained from experiments on MCF-7 breast cancer cells, the model parameters are estimated by using the simulated likelihood estimation method.

Chapter 7 is for conclusion.

CHAPTER 2

LITERATURE REVIEW

2.1 Biological Background

2.1.1 Cell Cycle Progression and Apoptosis

Cell division is an essential procedure in live organisms. During this process, DNA content is duplicated and one mother cell is divided into two daughter cells. All these progressions are a continuous process and take place in a harmonized system to provide proper separation and configuration of daughter cells including whole genomes. This process is called cell cycle progression. Cell cycle consists of four main phases: Gap 1 (G_1), Synthesis (S), Gap 2 (G_2) and Mitosis (M).

2.1.1 (a) Cell Cycle Progression

The duration of cell cycle in vivo is approximately 24 hours (Bernard & Herzel, 2006). However, some factors may affect the cell cycle duration such as cell type and the organism. For example, in only 90 minutes yeast cells can complete their cell cycle. In general, the cell cycle is divided into two main parts:

(i) Mitosis

(ii) Interphase

Mitosis (M) is referring to the phase in which a mother cell divides into two daughter cells and it is the most remarkable phase of the cell cycle, connecting the main restructuring of almost all parts of the cell. Mitosis happens right after the G_2 phase. In this phase, a mother cell has two copies of DNA and two different nuclei and the mother cell splits

into two new baby cells. Evidence show that a proper cell division takes only about an hour in a human cell (Simms, Bean, & Koerber, 2012).

Mitosis is broken up into the four stages as below:

(i) Prophase

(ii) Metaphase

(iii) Anaphase

(iv) Telophase

The period between two consecutive mitosis is called the interphase. More than 95% of cell cycle duration happens in interphase. The mitosis phase begins when nuclear is separated, in proportion to the daughter chromosomes division (karyokinesis) and frequently finishes at the end of cytoplasm division (cytokinesis).

The time proportion of cell cycle in which cells are organizing for separation is defined as the interphase. During this time cells grow and DNA replicates in proper arrangement. This period of the cell cycle has three different phases:

(i) G_1 phase (Gap 1)

(ii) S phase (Synthesis)

(iii) G_2 phase (Gap 2)

G_1 phase is considered as the first phase of cell cycle progression. This phase initiates after exactly mitosis phase and the finishes right before DNA replication. Therefore, in G_1 phase cells are metabolically dynamic and continuously grow. However, they are not able to reproduce their DNA.

Synthesis or *S* phase is starting after the first gap. During the *S* phase, DNA synthesis or copying happens and the quantity of DNA contains in each cell duplicates. In other words, the number of DNAs is duplicated at the end of the *S* phase.

Note that if a cell contains a certain number of chromosomes at G_1, then the number of chromosomes remains unchanged even after synthesis phase. During the *S* phase, DNA replication begins in the nucleus, and the centriole duplicates in the cytoplasm in animal cells.

G_2 phase or the second gap of cell cycle begins after synthesis. In this phase, the common errors of the synthesis phase are repaired and proteins are preparing to enter into mitosis phase.

In addition to the mentioned phases of cell cycle, a quantity of cells in the mature animals do not divide and some of them divide only infrequently, as wanted to substitute injured or dead cells.

These inactive cells, which are neither separating nor preparing to split are called quiescent cells and G_0 is considered as the phase of cell cycle in which cells are quiescent. Cells in G_0 phase of cell cycle stay metabolically active but do not proliferate except requested to do conditional on the organism.

2.1.1 (b) Apoptosis

Apoptosis, or programmed cell death, is a common part of the progress and healthiness of multicellular organisms. Cells die in because of a number of stimuli. Throughout apoptosis, cells act in a controlled and regulated trend. Therefore apoptosis is distinct from necrosis in which uncontrolled cell death causes serious problems for cells. In contrast, apoptosis is supposed as a normal process of cell death in which cells play an essential role in their own death.

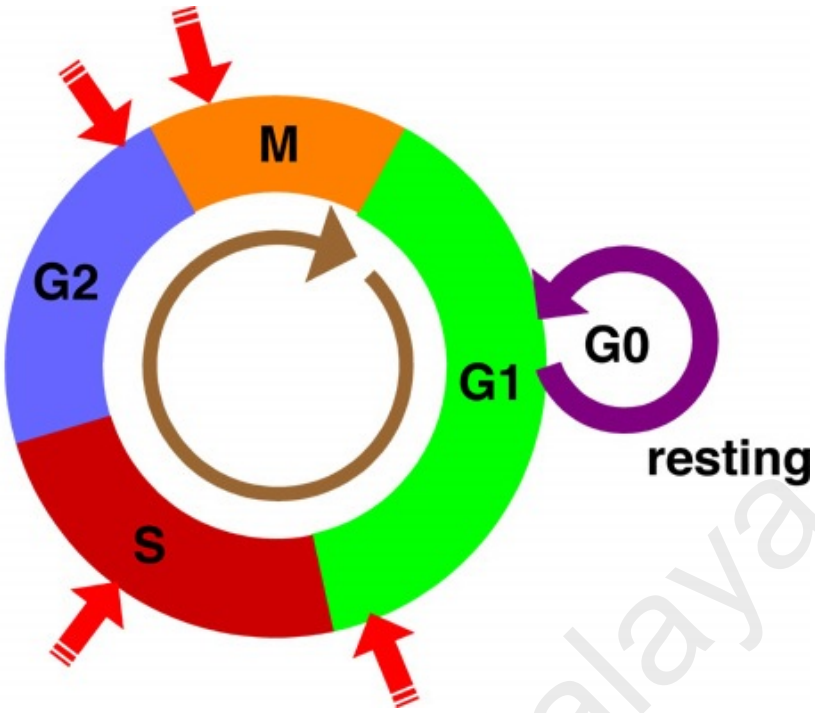

Figure 2.1: Schematic illustration of the cell cycle progression and checkpoints.

2.1.2 Radiation Therapy

In 1896, an important lecture titled **Concerning a New Kind of Ray** was presented by Prof. Wilhelm Conrad Roentgen. He entitled it the **X-ray**, and used the algebraic symbol **X** to illustrate an undefined quantity.

The instantaneous universal keenness was there. During a few months, machines were being developed to apply *X*-rays to detect cancer. Then, radio articles were using as an instrument in cancer treatment after three years. Subsequently, the first Nobel Prize awarded in physics was given to him in 1901. At first, radiotherapy functioned just with radium and relatively low-voltage diagnostic instruments.

In France, it was proven as a crucial discovery that everyday radiation dose fractions during a few weeks considerably increased the chance of patient treatment. The mechanisms and the techniques that dispense radiation particles have developed progressively over the time.

In early 20th century, after applying of radiation as a treatment and diagnosis method, it was presented that radiation parallel with cancer treatment could also cause it. Many

of first radiologists using their radiotherapy equipment, tested radiation power on their own arms skin try to find a dose that would cause a pink response (erythema), which was similar to skin sunburn. They named this **erythema dose**, and this measurement was estimated the proper fraction of daily radiation dose.

Conformal radiation therapy (CRT) applies special computers and CT images in order to very precisely draw the tumor's position in three dimensions. The patient is covered with a plastic cast for irradiating the cancerous tissue through radiation particles and avoiding the normal tissues from the side effects of them.

The radiation beams are matching to the shape of the tumor correspondingly. They are sent to the tumor from many different directions. The IMRT (Intensity-Modulated Radiation Therapy) is similar to CRT in company with targeting photon beams from many different ways, the beams' power has a probability to change. This makes additional control in decreasing the radiation particles to hit healthy tissue when sending a high dose to the tumor.

An associated methodology, conformal proton beam radiation therapy, applies a similar method to concentrate radiation on the tumor cells. Besides, another alternate of using X-rays, this methodology applies proton beams. Protons are atoms' portions lead to minor injury to tissues. They go through but are extremely efficacious to destroy the cancerous cells. It shows that proton beam radiation can transfer additional radiation to the tumor when possibly declining injury to the adjoining normal tissues.

2.1.3 Cell Death definition in Radiobiology

The popular utilization of radiation in cancer therapy finishes principally from its ability to justify the death of tumor cells. Pathways inside the DNA Damage Response (DDR) system extremely affects the biological consequences of radiation, comprising cell mortality (Han & Yu, 2009).

The DDR also identifies the class of cell mortality that happens, and in addition to the sensibility of cells death following radiation, DDR identifies the timing of their death.

As the DDR varies in different forms of tumor and normal, the presence of cell mortality can also change among different cell types expansively.

It is so crucial to describe what is predestined by the cell death in cancer therapy and radiobiology. In a few years, it has been less attention the differentiations in the mechanisms or types of cell mortality after applying the radiotherapy or the other treatments. The reason was that some of the pathways which affect cell mortality were not known during that time. Moreover, evaluation of cell death rate is difficult. Cell death occurs frequently at different times of radiation and after passing one or two round of cell cycle, in living cells, which continue to proliferate. So, it is difficult to measure cell mortality rate.

Instead, researchers concentrated on measuring **clonogenic survival**, which is described as the ability of a cell to proliferate for an unlimited time period after irradiation. This is extremely applicable and robust parameter for measuring radiation effect because any cell which keeps proliferative capability can be a reason to fail for controlling the tumor locally. So, in radiobiology, cell death is usually associated with any process leads to the endless conquest of clonogenic ability. This is a too general presence standard of cell death, and clearly does not mean when utilized to critically distinguished cell types that do not proliferate, like muscle and nerve cells.

For these cells, it is reasonable to assess the specific kinds of cell mortality leading to cell damage or to consider how radiation changes the role of them. Nonetheless, loss of proliferating ability is generally a suitable definition for cell death in radiobiology and a very useful to the proliferating cells. Two classifications of cell death made occur by irradiation. They are:

1. **Pre-Mitotic**:

   In lesser of cell types, cell death occurs fast, during some hours after irradiation (Endlich, 2000).

2. **Post-Mitotic**:

   The massive most of proliferating normal and tumor cells die at a pretty long time after irradiation, regularly after trying mitosis one time or more.

2.1.4 Radiation and Cell Arrest

Mammalian cell cycle consists of G_1, S, G_2 and M phases, and the radio-sensitivity are changed in the various phases. It is extensively believed that in cellular radiobiology the subsequent sights of the diverse radio-sensitivities are related to the different stages of the cell cycle (Sinclair, 2012; Su, 2006).

- Cells are highly radio-sensitive in the G_2/M phase of the cell cycle.
- If G_1 has a significant interval, there is typically a time period with a resistance, which decreases towards the S phase.
- the resistance is enhanced in the S phase, with the maximum enhancement occurs in the last portion of the phase.

Advancement from one phase to the other happens by phosphorylation or dephosphorylation of Cyclin-dependent kinases (Cdks).

Arrest at cell cycle checkpoints are frequently caused by DNA injuries, which are termed DNA integrity checkpoints. There are more checkpoints at the margins between nearby phases. Also there is an S phase checkpoint which distinguishes a delayed replication fork.

The checkpoint reactions are preserved between organisms, though the various phases

and mechanisms are fewer amongst mammalian cells (Durocher & Jackson, 2001; Rouse & Jackson, 2002). In mammalian cells, PI3-K related protein kinases (PIKK kinases), ATM (ataxia telangiectasia mutated protein)/ATR (ataxia telangiectasia and Rad3-related protein) are among main regulatory checkpoint responses.

(I) G_1/S arrest:

Two dominant forms of G_1/S arrest are prolonged arrest and a more transient response which was detected in mammalian cells explicitly (Di Leonardo, Linke, Clarkin, & Wahl, 1994; Little, 1968). The earlier is a p53- dependent reaction and the second one is similar to the G_1/S response observed in yeast. Observations show that p53 null cell lines or transformed fibroblasts (usually lack this arrest according to p53 inactivation) exposed higher radio-resistance compared to p53 wild cells (Lee & Bernstein, 1993). Therefore, G_1/S arrest after irradiation is not useful for the survival of cells.

(II) *S* phase arrest:

Cell cycle arrest in the *S* phase permits changes of the radiation-induced lesions before being repaired by DNA replication into permanent chromosomal breakdowns. The *S*-phase checkpoint is the most complicated one among the cellular checkpoints. Evidence shows that initial *S* phase arrest in next radiation are ATM-dependent but future *S* phase arrest are related to ATR (ataxia telangiectasia and Rad3-related protein) (Zhou et al., 2002).

Cells are lacking in genes of NBS and ATM and show a phenotype which is called radio-resistant DNA synthesis. *S* phase arrest cannot be detected without fixing the injuries (Jackson, 2002).

(III) G_2/M arrest:

The influence of G_2/M arrest on cells after generation of damages by irradiation is not clear, even though it is largely approved that the arrest increases cell survival and decreases the chance of genomic modifications.

Protein kinases Chk1 and Chk2 control the G_2/M checkpoint. As a consequence of the induced injuries, both of the Phosphorylation of Chk and its motivation are ATM-dependent.

According to evidence, ATM phosphorylates Cds1 and/or Chk1, which in turn phosphorylates and inactivates Cdc25. After γ- irradiation several diversities in the G_2/M arrest were identified among the normal and ATM lacking cells. After one irradiation, the normal cells show a postponement in going to the M phase from the G_2 phase, and A-T cells presented a shorter delay in comparison with the normal cells. This shows that the G_2/M arrest is partially ATM-dependent (Beamish & Lavin, 1994).

2.1.4 (a) Single-Strand Breaks (SSB) & Double-Strand Breaks (DSB)

From the evidence of radiobiological research, it is recommended that DNA is used as the standard aim for the radiations' biologic effects. Today, it is well-known that radiation creates an extensive range of DNA damages, which contain lesions to nucleotide bases (base damages), DNA single-strand breaks (SSBs) and double-strand breaks (DSBs) (Han & Yu, 2010).

Radiation-caused DNA damages are essential in understanding radiation-caused cell death, cell alteration and carcinogenesis, over initiation of gene alteration and chromosome deviation (Lehnert, 2007; Valentin, 2006).

Ionizing-radiation- caused base lesions have been detected widely in vitro in radiation of free bases, oligonucleotides, nucleosides or DNA in hydrous dilutions or in the solid-

state (von Sonntag, 1987; Nicoloff & Hoekstra, 1996). Even though special sorts of DNA base lesions such as 8-hydroxydeoxyguanosine have substantial biological importance in some research areas, existing information indicates that such insulated base damages are playing an insignificant role in the radiation mutagenesis (Ward, 1998).

The base excision repair trail can fix the damaged bases. Researches on radiation damages to different positions in the DNA proposes that SSB is also not significant in mammalian cells. An SSB is produced by the response of any of deoxyribose hydrogens (Ward, 1998). In the existence of oxygen, radiation will enhance the making of alkali-labile sites (Hutchinson, 1985). DNA ligation can mend the maximum number of the SSBs made by ionizing radiation (von Sonntag, 1987). However, DSBs produced by ionizing radiation or other carcinogenesis substances are supposed to be most related damage to carcinogenesis and mutations.

Unrepaired DSBs are important dangers to the genomic integrity (Hoeijmakers, 2001). DSBs can cause chromosomal abnormalities, which instantaneously affect a lot of genes to cause failure and cells death (Rich, Allen, & Wyllie, 2000). It is proven that DSBs can be created in some of the natural procedures such as counting replication, oxidative metabolisms, meiosis, and production or formation of antibodies (Dahm-Daphi, 2000). Genome protection involves in the ability to overhaul DSBs and to validate that fixation is completed with enough reliability.

Two central DSB repair ways are mentioned which one homologous recombination (HR) and non-homologous end joining (NHEJ).

HR controls DSB conservations in yeast and NHEJ controls it in mammalian cells, correspondingly. There are several excellent review articles discussing the DSB repair's mechanisms in the literature (Jeggo, 1998; Karran, 2000; Khanna & Jackson, 2001; Kurz & Lees-Miller, 2004; Sancar, Lindsey-Boltz, Ünsal-Kaçmaz, & Linn, 2004; Collis, DeWeese, Jeggo, & Parker, 2005).

HR is a useful DSB repair's trail. The genetic data missing at the broken ends of the homologous chromosome or unspoiled sister chromatid is saved by HR. In the HR development, the injured DNA physically associates with an unspoiled DNA with a homologous order and considers it as a model for repair.

Single-strand annealing (SSA) is an additional procedure for repairing DSBs by using the homology amongst two end points of the linked orders. The progression depends on homologous areas to arrange the DNA constituents to be joined again. Areas with SSBs have formed nearby the damage, which extends to the consecutive orders. When this progression has completed sufficiently to disclose the supplementary orders, both DNAs are strengthened and then they ligated.

DNA repair mechanism through the NHEJ trail is emergent and uneven procedure rejoins both ends of a double-strand break whenever there is not necessity of order homology between both ends.

Even though DSB repair is fairly popular, not as much of it is understood on how can different ends join in DSBs. Tumorigenic chromosome translocations can be created by Links between ends from diverse DSBs.

Two theories for the connection of DSBs in translocations are named the dynamic **breakage-first** theory and the static **contact-first** theory, change basically in their constraint for DSB mobility.

The **breakage-first** theory considers that breaks happened at far enough positions which can consequently be taken together to form translocations (Sax, 1941). This theory expects that DSBs should travel over huge areas in the nucleus before their interaction.

Whether such wide immigration and consequent interaction of DSBs can essentially happen is imprecise. In order to assess DSB including chromosome domains are movable and can act with each other or not, (Aten et al., 2004) presented near-horizontal linear tracks of DSBs in nuclei by means of illustrating cells to α particles from a radiation

source which is located beside the cells.

DSBs are visualized by immunofluorescence of γ-H2AX. Variations in the 3-D circulations of DSBs are calculated by examining the morphology trial at many intervals after radiation. The alterations in the track morphology are observed only in few minutes after DSB initiation, representing the domains' movement.

2.1.5 Target Theory

In the 1920s, target theory and hit theory were introduced for the first time. During this decade, biologists were starting to improve quantum methods to deactivate phenomena when biological tissue was irradiated (Dessauer, 1922; Crowther, 1924).

Other researchers continued the radiation's modeling affects the alive cells experimentally and theoretically (Atwood & Norman, 1949; E. C. Pollard, Guild, Hutchinson, & Setlow, 1955; D. E. Lea, 1955; E. Pollard, 1959)).

After these influential models, several mathematical models have been proposed to show the relation between cells and radiation particles (J. F. Fowler, 1989; Sy & Han, 1982; Ditlov, 2009; Satow & Kawai, 2006; Chapman, 2007; Ditlov, 2009).

In target theory, it is supposed that each cell has a certain number of dynamic sites called **targets**. Targets are radiosensitive, i.e., they may be deactivated by radiation particles and a cell dies if all its targets become deactivated. For instance, it is recognized that the chromosomes are very sensitive targets (Dertinger & Jung, 2013). However, additional evidences show that nuclear membrane or some other cell organelles, which are closed to the nuclear membrane can be considered as targets as well (Datta, Cole, & Robinson, 1976). When each target is hit by a number of radiation particles, it will be deactivated. Several classes of hit models are categorized by the number of hits and targets.

1. Single target–single hit

2. Single target–multi hit

3. Multi target–single hit

4. Multi target–Multi hit

In above-mentioned models, it is common to assume that all cells have homogeneous behavior. In fact, there are at least three focal causes to question this theory. The first reason is that heterogeneity comes from the non-uniform 3-D dose of radiation distribution. The second issue is the alterations among the cell types (proliferating, necrotic, quiescent, stem cells, etc.) and the non-uniform concentration of nutrients and oxygen. The third reason is associated to a cell-to- cell injuries inconsistency and also to the diversity of the radiation effects on cells.

2.2 Mathematical Background

2.2.1 Routh-Hurwitz Criterion

Suppose that

$$\dot{\mathrm{x}} = A \,.\, \mathrm{x} \tag{2.2.1}$$

illustrates the dynamics of cells population and

$$A(i+1, j+1) = \begin{cases} \Pi(i,j) + \mu(1-q)^m - 1 & i, j = 0 \\ \Pi(j,i) & i \neq j \\ \Pi(i,j) - 1 & Others \end{cases} \tag{2.2.2}$$

is the matrix associated with Equation (2.2.1), where $i, j = 0, ..., (m-1)$ and

$$\mathrm{x} = (x_0, x_1, ..., x_{m-1})^\top$$

Therefore:

Theorem 2.2.1. *Let $A \in \mathbb{M}^{m\times m}$. The system (2.2.1) is stable at equilibrium point $x^* = 0$ if and only if all the eigenvalues of the matrix A have negative real part.*

Proof. See (Sideris, 2013) □

Theorem 2.2.2. ***(Routh-Hurwitz Criterion)*** *Suppose that $P(\lambda) = a_m x^m + a_{m-1}x^{m-1} + a_1 x + a_0$ is the characteristic polynomial of a matrix $A \in \mathbb{M}^{m\times m}$. Let*

$$D_k = \det \begin{bmatrix} a_1 & a_3 & a_5 & \dots & a_{2k-1} \\ 1 & a_2 & a_4 & \dots & a_{2k-2} \\ 0 & a_1 & a_3 & \dots & a_{2k-3} \\ 0 & 1 & a_2 & \dots & a_{2k-4} \\ \vdots & \vdots & \vdots & \vdots & \vdots \\ 0 & 0 & 0 & \dots & a_k \end{bmatrix} \tag{2.2.3}$$

where $a_j = 0$ if $j > m$. Then roots of $P(\lambda)$ have negative real part if and only if $D_k > 0$ for all $k = 1, ..., m$.

Proof. (Teschl, 2012) □

Following theorem is a straightforward result of combination Theorem (2.2.1) and Theorem (2.2.2) in case $m = 2$.

Theorem 2.2.3. *Let $A \in \mathbb{M}^{2\times 2}$. If λ_1, and λ_2 are the eigenvalues of the matrix A, then the system (2.2.1) is stable at equilibrium point x^* if and only if*

$$a_1 = -(\lambda_1 + \lambda_2) > 0$$

and

$$a_2 = \lambda_1\ \lambda_2 > 0$$

where

$$P(\lambda) = \lambda^2 + a_1\lambda + a_2$$

is the characteristic polynomial of matrix A.

2.2.2 Gershgorin Discs and Gershgorin Theorem

Let A be a complex $(m \times m)$ matrix, with entries (A_{tk}). For $t \in \{1,...,m\}$ let $R_t = \sum_{k\neq t} |A_{tk}|$ be the sum of the absolute values of the non-diagonal entries in the t-th row. Let $D(A_{tt}, R_t)$ be the closed disc centered at A_{tt} with radius R_t. Such a disc is called a Gershgorin disc (Varga, 2010).

Theorem 2.2.4. *Every eigenvalue of A lies within at least one of the Gershgorin discs $D(A_{tt}, R_t)$.*

Proof. Let λ be an arbitrary eigenvalue of A and let $x = (x_k)$ be the corresponding eigenvector. Let $t \in \{1,\ldots,m\}$ be chosen such that $|x_t| = \max_k |x_k|$ (That is to say, choose t so that x_t is the largest (in absolute value) number in the vector x). Then $|x_t| > 0$, otherwise $x = 0$. Since x is an eigenvector, $Ax = \lambda x$, and thus:

$$\sum_k A_{tk}x_k = \lambda x_t \quad \forall t \in \{1,\ldots,m\}$$

So, splitting the sum, we get

$$\sum_{k\neq t} A_{tk}x_k = \lambda x_t - A_{tt}x_t$$

Dividing both sides by x_t ($x_t \neq 0$ for this choice of t) and take the absolute value to obtain

$$\begin{aligned} |\lambda - A_{tt}| &= \left|\frac{\sum_{k\neq t} A_{tk}x_k}{x_t}\right| \\ &\leq \sum_{j\neq i}\left|\frac{A_{tk}x_k}{x_t}\right| \\ &\leq \sum_{k\neq t}|A_{tk}| = R_t \end{aligned} \tag{2.2.4}$$

where the last inequality is valid because

$$\left|\frac{x_k}{x_t}\right| \leq 1 \quad \text{for } j \neq t$$

□

2.2.3 Markov Chain

Present probability theory deals with chance processes where the information of prior results effects predictions for upcoming trials. Theoretically, once a series of accidental trials is observed, all of the previous results might affect the forecasts of the following trial. For instance, predicting the grades of a student on a series of assessments in a specific course.

A. A. Markov started the study of a vital novel classification of the chance process in 1907 in which the result of a certain test can influence the result of the subsequent test.

This kind of process is named a Markov chain.

Assume that I is a countable set, i.e., $I = \{i, j, k, \dots\}$. Therefore, each $i \in I$ is called a **state** and I is the **state-space**.

Now suppose that $(\Omega, \mathbf{F}, \mathbf{P})$ is a **probability space**. Ω is a set of outcomes, $\mathbf{F}$ is a set of subsets of Ω, and for any $A \in \mathbf{F}$, $\mathbf{P}(A)$ is the probability of A. In this part, we will focus on a sequence of random variables $X_0, X_1, \dots, X_n$, in which a number of simple rules determine the corresponding joint distribution.

A random variable X with values in I is considered as a function $X : \Omega \to I$.

In addition, the vector $\lambda = (\lambda_i : i \in I)$ is named a measure if $\lambda_i \geq 0$ for all i. A measure is called a distribution when $\sum_{i \in I} \lambda_i = 1$.

Now, suppose that $\{\lambda_i : i \in I\}$ such that $0 \leq \lambda_i \leq 1$ for all i and $\sum_i \lambda_i = 1$ is a distribution over I. More specially, suppose that $\lambda = \sigma_i = (0, \dots, 1, \dots, 0)$. Moreover, $P = (p_{ij} : i, j \in I)$ with $p_{ij} \geq 0$ for all i, j and $\sum_j p_{ij} = 1$ is called the transition matrix. Subsequently, each row of a transition matrix is a distribution over I.

Definition 2.2.1. *Suppose that $(X_n)_{n \geq 1}$ is a sequence of random variables. (X_n) is called a Markov chain with transition matrix P and primary distribution λ if for any $n \geq 0$ and $i_0, \dots, i_{n+1} \in I$,*

1. $P(X_0 = i_0) = \lambda_{i_0}$
2. $P(X_{n+1} = i_{n+1} | X_0 = i_0, \dots, X_n = i_n) = P(X_{n+1} = i_{n+1} | X_n = i_n) = p_{i_n i_{n+1}}$

(X_n) is called a Markov (λ, P).

2.2.4 Brownian Motion

Robert Brown discovered Brownian motion for the first time when he observed the tiny motion of microscopic particles moved in water in a random directions. Caused by the disordered movement of separate water particles, each such molecule is squeezing in all directions.

In 1905, Albert Einstein mentioned a diffusive movement of mesoscopic particles (i.e., macroscopically very small, but still visible through a microscope) suspended in a liquid, by accepting Boltzmann's view of atomism.

Once the particles in the liquid experience heat movement and push the mesoscopic particle in an arbitrary way, the particle is forced to move in any direction irregularly, which is called a **Brownian motion**.

Assume that $(\Omega, \mathbf{F}, \mathbf{P})$ is a probability space. A stochastic process is a measurable function $\mathbf{X}(t, \omega)$ defined on the product space $[0, +\infty) \times \Omega$. Especially:

(a) for $t \in [0, +\infty)$, $\mathbf{X}(t, \cdot)$ is a random variable,

(b) The pathway $\mathbf{X}(\cdot, \omega)$ is a measurable function for any $\omega \in \Omega$,.

Definition 2.2.2. *A stochastic process* $\mathbf{W}(t, \omega)$ *is entitled a* ***Brownian Motion*** *(BM) if:*

1. $\mathbf{P}\{\omega \ : \ \mathbf{W}(0, \omega) = 0\} = 1$.

2. *For any* $0 \leq s < t$*, the random variable* $\mathbf{W}(t) - \mathbf{W}(s)$ *has a normal distribution with mean* 0 *and variance* $(t - s)$*. Therefore, for any* $a < b$*,*

$$\mathbf{P}(a \leq W(t) - W(s) \leq b) = \frac{1}{\sqrt{2\pi(t-s)}} \int_a^b e^{\frac{x^2}{2(t-s)}} \, dx. \tag{2.2.5}$$

3. *For any* $0 \leq t_1 < t_2 < \cdots < t_n$*, the random variables* $\{\mathbf{W}(t_1), (\mathbf{W}(t_2) - \mathbf{W}(t_1)), \ldots, (\mathbf{W}(t_n) -$

$\mathbf{W}(t_{n-1}))\}$, *are independent. Under this condition we say* $\mathbf{W}(t,\omega)$ *has independent increments.*

4. *Almost all sample paths of* $\mathbf{W}(t,\omega)$ *are continuous functions, i.e.,*

$$\mathbf{P}\{\omega \ : \ \mathbf{W}(\cdot,\omega) \ \ is \ \ continuous\} = 1. \tag{2.2.6}$$

2.2.5 White Noise

Brownian motion is considered as the fundamental structure to build a large group of Markov processes with continuous sample paths, named diffusion processes.

A special form of diffusion processes will be discussed in this section with similar **noise** as typical Brownian motion, and different **drift**.

Stochastic Differential Equations (SDEs) are useful method to define these forms of processes. A stochastic differential equation is written as:

$$\dot{\mathbf{X}} = b(\mathbf{X}) + \mathscr{E}(t) \tag{2.2.7}$$

where $b : \mathbb{R} \to \mathbb{R}$ is a particular smooth function and $\mathscr{E}(t) = \dot{W}(t)$ shows the derivative of Brownian motion with respect to time, or **white noise**.

Equation (2.2.7) can be interpreted in two ways:

1. A Brownian motion $\dot{X} = \mathscr{E}$ perturbed by a **drift** term $b(X)$, or

2. An ordinary differential equation $\dot{X} = b(X)$ perturbed by an **additive** noise.

Pointwise derivations of Brownian motions are not defined, but it is possible to explain them in a distributional sense to obtain a general form of a stochastic process named white

noise represented by:

$$\mathscr{E}(t,\omega) = \dot{W}(t,\omega) \tag{2.2.8}$$

White noises can also be shown by $\mathscr{E}\ dt = dW$. The word white noise comes from the **spectral theory of stationary random processes**. According to Definition. (2.2.2), the Brownian motion has Gaussian independent increments property with mean zero. Hence, its derivation with respect to time is also a Gaussian stochastic process with mean and its values at different times are independent.

2.2.6 Ito Stochastic Differential Equations

Notation. Suppose that $\mathbf{W}(\cdot)$, and X_0 are an m-dimensional Brownian motion, and an n-dimensional random variable which is independent of $\mathbf{W}(\cdot)$, respectively. Then

$$\mathscr{F}(t) := \mathscr{U}(X_0, \mathbf{W}(s)(0 \leq s \leq t)) \qquad t \geq 0 \tag{2.2.9}$$

is called the σ-algebra made by X_0 describing the history of the Wiener process until (and including) time t.

Definition 2.2.3. *Let $X(\cdot)$ is a real-valued stochastic process such that*

$$X(r) = X(s) + \int_s^r F\ dt + \int_s^r G\ dW$$

where $F \in \mathbb{L}^1(0,T)$, $G \in \mathbb{L}^2(0,T)$ and $0 \leq s \leq r \leq T$. Then for $0 \leq t \leq T$, $X(\cdot)$ is said to have the stochastic differential for $0 \leq t \leq T$, which is written as:

$$dX = F\ dt + G\ dW \tag{2.2.10}$$

Theorem 2.2.5. *(Ito's Formula). Let $X(\cdot)$ has a stochastic differential*

$$dX = F\ dt + G\ dW$$

where $F \in \mathbb{L}^1(0,T)$ and $G \in \mathbb{L}^2(0,T)$. Assume $u : \mathbb{R} \times [0,T] \to \mathbb{R}$ is continuous and its partial derivatives $\frac{\partial u}{\partial t}$, $\frac{\partial u}{\partial x}$ and $\frac{\partial^2 u}{\partial x^2}$ are continuous. If

$$Y(t) := u(X(t),t)$$

then Y has the stochastic differential

$$\begin{aligned} dY &= \frac{\partial u}{\partial t}\ dt + \frac{\partial u}{\partial x} dX + \frac{1}{2}\frac{\partial^2 u}{\partial x^2}\ G^2\ dt && (2.2.11) \\ &= (\frac{\partial u}{\partial t} + \frac{\partial u}{\partial x}\ F + \frac{1}{2}\frac{\partial^2 u}{\partial x^2}\ G^2)\ dt + \frac{\partial u}{\partial x}\ G\ dW && (2.2.12) \end{aligned}$$

Equation (2.2.11) is called Ito's formula or Ito's chain rule.

Hence,

Definition 2.2.4. *According to the notation, an Ito stochastic differential equation (SDE) is defined as a differential equation of the form:*

$$\begin{cases} d\mathbf{X} = \mathbf{b}(\mathbf{X},t)\ dt + \mathbf{B}(\mathbf{X},t)\ d\mathbf{W} \\ \mathbf{X}(0) = \mathbf{X}_0 \end{cases} \qquad (2.2.13)$$

Definition 2.2.5. *An $\mathbb{R}^n$-valued stochastic process $\mathbf{X}()$ is called a solution of the Ito SDE (2.2.13) for $0 \le t \le T$ when it provides the subsequent conditions:*

1. *$\mathbf{X}(\cdot)$ is progressively measurable with respect to $\mathscr{F}(\cdot)$*
2. *$\mathbf{F} := \mathbf{b}(\mathbf{X},t) \in \mathbb{L}_n^1(0,T)$*

3. $\mathbf{G} := \mathbf{B}(\mathbf{X},t) \in \mathbb{L}^2_{n\times m}(0,T)$

4. $\mathbf{X}(t) = \mathbf{X}_0 + \int_0^t \mathbf{b}(\mathbf{X}(s),s)ds + \int_0^t \mathbf{B}(\mathbf{X}(s),s)d\mathbf{W}$ *a.s.* *for all* $0 \le t \le T$

Following are some well-known examples of SDEs.

Example 2.2.1. *Suppose that* $m = n = 1$ *and* g *be a continuous function (not a random variable). Then the SDE equation*

$$\begin{cases} dX = gXdW \\ X(0) = 1 \end{cases} \tag{2.2.14}$$

has the unique solution as:

$$X(t) = e^{-\frac{1}{2}\int_0^t g^2 ds + \int_0^t g dW} \tag{2.2.15}$$

for all $0 \le t \le T$.

Next example is called one-dimensional Geometric Brownian Motion (GMB).

Example 2.2.2. *Suppose* $P(t)$ *is the stock price at time* t. *Therefore, the growth of* $P(t)$ *in time can be modeled by assuming that* $\frac{dP}{P}$ *, the relative change of price, is changing according to the following SDE*

$$\frac{dP}{P} = \mu dt + \sigma dW \tag{2.2.16}$$

when μ *and* σ *show drift and stock volatility, respectively. Hence, the equation* (2.2.16) *can be written as:*

$$dP = \mu P dt + \sigma P dW \tag{2.2.17}$$

Using Ito formula, we have:

$$P(t) = P(0)\, e^{\sigma W + (\mu - \frac{\sigma^2}{2})t} \tag{2.2.18}$$

Definition 2.2.6. *Let*

$$\mathbf{b}(X,t) = \mathbf{c}(t) + \mathbf{d}(\mathbf{t})X$$

and

$$\mathbf{B}(X,t) = \mathbf{C}(t) + \mathbf{D}(\mathbf{t})X$$

where

$$\mathbf{c} : [0,T] \to \mathbb{R}^n$$

$$\mathbf{d} : [0,T] \to \mathbb{M}^{n\times n}$$

$$\mathbf{C} : [0,T] \to \mathbb{M}^{n\times m}$$

$$\mathbf{D} : [0,T] \to \mathbf{L}(\mathbb{R}^n, \mathbb{M}^{n\times m})$$

Then, equation (2.2.13) is called a ***linear stochastic differential equation*** *(linear SDE).*

Definition 2.2.7. *A linear SDE is* ***homogeneous*** *if* $c \equiv C \equiv 0$ *for all values of* $0 \leq t \leq T$.

Moreover a linear SDE is called ***linear in the narrow sense*** *if* $D \equiv 0$.

Remark 2.2.1. $\mathbf{b}$ *and* $\mathbf{B}$ *fulfil the conditions of the existence and uniqueness theorem when*

$$\sup_t [|\mathbf{c}(t)| + |\mathbf{D}(t)| + |\mathbf{E}(t)| + |\mathbf{F}(t)|] < 1 \tag{2.2.19}$$

Moreover, the linear SDE

$$\begin{cases} d\mathbf{X} = (\mathbf{c}(t) + \mathbf{D}(t)\mathbf{X})dt + (\mathbf{E}(t) + \mathbf{F}(t)\mathbf{X})d\mathbf{W} \\ \mathbf{X}(0) = \mathbf{X}_0 \end{cases} \tag{2.2.20}$$

has a unique solution with $\mathbb{E}(|\mathbf{X}_0|^2) < 1$.

2.2.7 Numerical Solution

In most cases, it is not easy to find the exact solution for SDEs. Hence, it is important to solve them by using numerical methods. In this part, two standard numerical methods to solve SDEs are reviewed.

Consider the one-dimensional Ito SDE Suppose that

$$\begin{cases} dX = f(X_t, \theta)\, dt + g(X_t, \theta)\, dW \\ X(0) = \mathrm{x}_0 \end{cases} \tag{2.2.21}$$

be an Ito stochastic differential equation, where W is an m-dimensional Brownian motion. In addition, assume that $f : \mathbb{R} \times \Theta \to \mathbb{R}$ and $g : \mathbb{R} \times \Theta \to \mathbb{R}^{1\times m}$ are given functions of $\theta \in \Theta$, where θ is an unknown finite-dimensional parameter. For more convenience, we use $f(X_t)$ in place of $f(X_t, \theta)$.

2.2.7 (a) Euler-Maruyama Method

Euler-Maruyama method is known as one of the most popular numerical methods for solving SDEs. First, consider the Ito SDE (2.2.21) on interval of $[t_0, T]$. Now let $t_0 < t_1 < < t_n < < t_N = T$ be a discretization of the interval $[t_0, T]$. Thus, the Euler-Maruyama approximation is defined as a continuous time stochastic process satisfying:

$$\begin{cases} y_{n+1} = y_n + h_n f(y_n) + g(y_n)\Delta W_n \\ y_0 = \mathrm{x}_0 \end{cases} \tag{2.2.22}$$

where $y_n = y(t_n)$ and $h_n = t_{n+1} - t_n$ is the step-size and $n = 0, 1, \ldots, N-1$. In addition

$$\Delta W_n = W(t_{n+1}) - W(t_n) \sim \mathcal{N}(0, h_n) \tag{2.2.23}$$

in which $W(t_0) = 0$, and $\mathcal{N}$ has normal distribution.

The multi-dimensional Euler-Maruyama method is defined as:

$$\begin{cases} y_{n+1}^k = y_n^k + hf^k + g^{(k,k)}\Delta \mathbf{W}_n^k \\ \mathrm{y}_0^k = \mathrm{x}_0^k \end{cases} \tag{2.2.24}$$

The Euler-Maruyama method has strong order of convergence $\frac{1}{2}$ (and weak order of convergence 1). We refer the reader to (Kloden & Platen, 1992) for more details.

It should be noted that the accuracy order of a numerical scheme may equals p in general, but this order may change for SDEs in individual form. For example, the strong order of accuracy in Euler-Maruyama process with additive noise is one.

As the Euler-Maruyama method has a lower order of accuracy, the numerical outcomes are less accurate. To solve this issue it is possible to use a small step-size , or more efficient methods such as **Milstein** method.

2.2.7 (b) Milstein Method

In 1-dimentional SDEs, the Milstein scheme is defined as:

$$y_{n+1} = y_n + hf(y_n) + g(y_n)\Delta \mathbf{W}_n + \frac{1}{2}g(y_n)g'(y_n)((\Delta \mathbf{W}_n)^2 - h) \tag{2.2.25}$$

Here, the term "$\prime$" demonstrates differentiation with respect to X.

This scheme has the strong order 1 of convergence, where $\mathbb{E}(\mathrm{x}_0^2) < \infty$. f and g are twice continuously differentiable, and f, f', g, g' and g'' satisfy a uniform Lipschitz condition.

Note that in case of SDEs with additive noise, both the Euler-Maruyama and the Milstien method show same outcomes.

Now consider a d-dimensional system of (Ito) SDEs:

$$d\mathbf{X}_t = f(\mathbf{X}_t;\theta)dt + g(\mathbf{X}_t;\theta)d\mathbf{W}_t, \quad \mathbf{X}(0) = \mathrm{x}_0 \tag{2.2.26}$$

where $\mathbf{W}$ is m-dimensional Wiener process, $f : \mathbb{R}^d \times \theta \to \mathbb{R}^d$ and $g : \mathbb{R}^d \times \theta \to \mathbb{R}^{d\times m}$. Let $m = d$. Therefore g is a diagonal matrix and the SDE has diagonal noise. In this case, the multi-dimensional Milstein method for the k^{th} element $(k = 1,\ldots,d)$ of the Ito SDEs is written as:

$$\begin{cases} y_{n+1}^k = y_n^k + hf^k + g^{(k,k)})\Delta\mathbf{W}_n^k + \frac{1}{2}g^{(k,k)}\frac{\partial g^{(k,k)}}{\partial \mathbf{X}^k}((\Delta\mathbf{W}_n^k)^2 - h) \\ \mathrm{y}_0^k = \mathrm{x}_0^k \end{cases} \tag{2.2.27}$$

where f^k denote the k^{th} element in f, and $g^{(k,k)}$ denotes the $(k,k)^{th}$ element in g. Readers are referred to (Kloden & Platen, 1992) for more details in general form.

2.2.8 Parameter Estimation of a SDE model

Stochastic differential equations are powerful and useful methods to model the progression of dynamics phenomena, e.g. population dynamics of tumor cells, over the time. In these models, parameters play a critical role in characterizing the dynamics of the system. It frequently happens that the model parameters are not identified precisely, though sample data for the individual dynamic phenomena are accessible.

The main interest is to find improved approximations for the model parameters by means of the observed data. Practically, the most important problem in parameter estimation arises when the data is available only in discrete time points in a time interval, while SDEs are continuous processes.

There have been many research articles which have addressed new methods of parameter estimation in diffusion processes in the literature. Among these, we refer readers to (Durham & Gallant, 2002; Ait-Sahalia, 2002; Aït-Sahalia, 2002; Alcock & Burrage, 2004; Bibby, Jacobsen, & Sørensen, 2004; Brandt & Santa-Clara, 2002b; Hurn, Lindsay, & Martin, 2003; Nicolau, 2002).

The overall structure is specified by the subsequent n-dimensional system of (Ito) SDEs

$$\begin{aligned} dX_t &= f(t, X_t; \theta)dt + g(t, X_t; \theta)dW_t \\ X_0 &= x_0 \end{aligned} \tag{2.2.28}$$

where $t > 0$ and W is an m-dimensional standard Brownian motions, $f : [0, +\infty) \times \mathbb{R}^n \times \Theta \to \mathbb{R}^n$ and $g : [0, +\infty) \times \mathbb{R}^n \times \Theta \to \mathbb{R}^{n \times n}$ are identified functions conditional on parameter $\theta \in \Theta$.

In addition, suppose that x_0 is a deterministic initial value and $x_0, x_1, \ldots, x_n$ are series of past observations from the diffusion process X obtained from non-stochastic discrete time-points $t_0 < t_1 < \cdots < t_n$. As X is Markovian, the maximum likelihood estimator (MLE) of θ can be determined when the transition densities $p(x_t; x_s, \theta)$ of X are identified, for $s < t$. In this case, the log-likelihood function of θ is given by

$$l_n(\theta) = \sum_{i=1}^{n} \log p(x_i; x_{i-1}, \theta) \tag{2.2.29}$$

By maximizing the function in equation (2.2.29) with respect to the parameter θ, the maximum likelihood estimator $\hat{\theta}$ can be estimated. Under mild regularity conditions, $\hat{\theta}$ is reliable, i.e., it is asymptotically normally distributed and asymptotically efficient, when n goes to infinity (Dacunha-Castelle & Florens-Zmirou, 1986).

The difficulty with the MLE is that the transition density function of the underlying diffusion process is often unknown. One response to this problem is to compute an approximate transition density function numerically by:

1. solving numerically the Kolmogorov partial differential equations, which is satisfied by the transition density (Lo, 1986);

2. deriving a closed-form Hermite expansion to the transition density (Aït-Sahalia et

al., 2008; Aït-Sahalia, 2002);

3. simulating R times the process to Monte-Carlo integrate the transition density (e.g. (Hurn et al., 2003; Nicolau, 2002; Pedersen, 1995)): this method is known as simulated maximum likelihood (SML).

Recently a novel method using exact simulation was proposed (Beskos, Papaspiliopoulos, Roberts, & Fearnhead, 2006). Each of these techniques has been successfully implemented by the aforementioned authors, but each one has limitations (Ait-Sahalia, 2002). Note that methods 1 and 3 which are mentioned above are computationally intense and poorly accurate. Durham and Gallant (Durham & Gallant, 2002) developed their important sampling ideas in order to improve the performance of Brandt and Santa-Clara's (Brandt & Santa-Clara, 2002b, 2002a) method. Our opinion is that a method should be not only accurate and fast but also practical. The simulation-based method 3 which is mentioned above, is highly time-consuming and has proved that it is less accurate than e.g. method 2 (Jensen & Poulsen, 2002).

On the other hand, they are very general and have proved to be applicable over a wide range of SDE models. In general, method 2 should be the choice (but see (Stramer & Yan, 2012) for some limitations), but computing the Hermite expansion of the transition density could be a very difficult task, especially if the SDE is multivariate and non-linear. Parameter estimation methods have some limitations. For instance, achieving a good estimation is highly depending on some elements such as the number of available observations (n) (the larger the better), the number of simulations (R) (the larger the better), the step-size (h) (the smaller the better), the suitability of the initial value of θ in the optimization process.

Remark 2.2.2. *To solve the above mentioned problems, it is highly recommended to plot*

SDE trajectories with different parameter values and perceive how the trajectories perform with respect to the real data, before the parameter estimation. When a proper value for parameters is establishing, it can be considered as an initial value in the parameter estimation process.

2.2.8 (a) A Non-Parametric Method

In the case of one-dimensional Ito SDE, a non-parametric simulated maximum likelihood method is proposed in (Hurn et al., 2003). Here, we propose some improvement compare with the original method and apply to the multidimensional SDEs.

Suppose that $p(t_i, x_i; (t_{i-1}, x_{i-1}), \theta)$ is the transition density of x_i from x_{i-1} to x_i. Then the maximum likelihood estimation for θ is known by maximizing the value of the following function:

$$L(\theta) = \sum_{i=1}^{n} p(t_i, x_i; (t_{i-1}, x_{i-1}), \theta) \tag{2.2.30}$$

with respect to θ.

Practically, $L(\theta)$ is estimated by means of the Monte Carlo simulations as it is described by the subsequent method:

1. Take the time interval $[t_{i-1}, t_i]$ and split it into M subintervals of size $h = (t_i - t_{i-1})/M$. Therefore, equation (2.2.28) is applied to these partitions by applying the procedure (e.g. Euler-Maruyama, Milstein) in which x_{i-1} at time t_{i-1} is taken as the initial point and consequently an approximation of X at t_i is obtained.

   Repeating this procedure R times, R estimations of the X procedure at time t_i beginning from x_{i-1} at t_{i-1} are generated. We demonstrate these values with $X^1{}_{t_i}, \ldots, X^R{}_{t_i}$, i.e. $X^r{}_{t_i}$ is the obtained value of (2.2.28) at t_i beginning from x_{i-1} at t_{i-1} in the r^{th} simulation $(r = 1, \ldots, R)$;

2. We use the simulated values $X^1{}_{t_i}, \ldots, X^R{}_{t_i}$ to make a non-parametric kernel density

estimate of the transition density $p(t_i, x_i; (t_{i-1}, x_{i-1}), \theta)$

$$p^R(t_i, x_i; t_{i-1}, x_{i-1}, \theta) = \frac{1}{Rh_i} \sum_{r=1}^{R} K(\frac{x_i X^r{}_{t_i}}{h_i}) \tag{2.2.31}$$

Here, h_i is the kernel bandwidth at time t_i and $K(\cdot)$ is an appropriate symmetric, non-negative kernel function with the unit mass;

3. The previous process is iterated for each x_i and the obtained $p^R(t_i, x_i; t_{i-1}, x_{i-1}, \theta)$ values are used to produce

$$L^R(\theta) = \Pi_{i=1}^{n} p^R(t_i, x_i; t_{i-1}, x_{i-1}, \theta) \tag{2.2.32}$$

4. $L^R(\theta)$ is maximized with respect to θ to get the estimation MLE θ^R of θ.

Remind that the precise structure of L^R necessitates that the Wiener increments, after the generation, are kept stable for the subsequent optimization process. A proper choice of $K(\cdot)$ is given by the normal kernel

$$K(u) = \frac{1}{\sqrt{2\pi}} \exp(-u^2/2) \tag{2.2.33}$$

with bandwidth given by (Scott, 2015)

$$h_i = (4/3)^{1/5} s_i R^{1/5}, i = 1, \ldots, n \tag{2.2.34}$$

where s_i's show the standard deviation of the sample data presented to the kernel at time t_i, i.e. s_i which is calculated in $X^1{}_{t_i}, \ldots, X^R{}_{t_i}$.

Note that, for numerical limitations, it is more appropriate to minimize the negative log-likelihood function

$$\log L^R(\theta) = \sum_{i=1}^{n} \log p^R(t_i, x_i; (t_{i-1}, x_{i-1}), \theta) \tag{2.2.35}$$

and the estimated MLE is obtained by $\theta^R = arg\min_\theta \log(L^R(\theta))$. In the case of multi-dimensional SDEs, the method can be directly developed, for example, by considering pairwise independence of system variables in the method. Here, the multidimensional kernel density estimator can be demonstrated as the result of the kernels of each variable and the bandwidth for the generic dimension k of the SDE denoted by

$$h_{i,k} = (4/(d+2))^{1/(d+4)} s_{i,k} R^{1/(d+4)} \tag{2.2.36}$$

where $i = 1, \ldots, n$ and $k = 1, \ldots, d$ (Scott, 2015).

Remark 2.2.3. *In statistics* ***regularity conditions*** *typically refer to necessities that cause function or groups of functions (usually probability density functions)* ***behave well*** *in numerous senses. These assumptions are considered in proofs of statements that are believed to hold in most practical cases and frequently not clearly stated in the theorem statement.* ***Mild*** *or* ***weak*** *term fundamentally state that* ***it is considered to observe these regularity conditions nearly all the time in practice****.*

2.2.8 (b) A Parametric Method

In the prior subsection, a non-parametric method has been presented to estimate the parameters of an SDE model. This scheme is applicable to approximate both Ito and Stratonovich SDEs by means of either the Euler-Maruyama or the Milstein methods, while the parametric method described here is only applicable to Ito SDEs by means

of only the Euler-Maruyama separation.

The simulated maximum likelihood method introduced in this section was originally presented in (Pedersen, 1995) and was developed in (Durham & Gallant, 2002) using **importance sampling** methods. For simplicity, we only take the original form. For a d-dimensional fully observed SDE, $L(\theta)$ is estimated by means of Monte Carlo simulations based on the following procedure:

1. Consider interval $\mathbf{I} = [t_{i-1}, t_i]$ with the partitions of length $h = (t_i - t_{i-1})/M$, then equation (2.2.28) is applicable on the mentioned subinterval by means of a normal scheme such as Euler-Murayama or Milstein.

   Here, x_{i-1} at time t_{i-1} is taken as the initial value and consequently an estimation of X at $t_{i-1} + (M-1)h$ is achieved. This process is repeated R times, thus producing R estimations of the X at time $t_{i-1} + (M-1)h$ beginning from x_{i-1} at t_{i-1}.

   Remember that the X values ${X^1}_{t_i}, \ldots, {X^R}_{t_i}$ are the integrated value of (2.2.28) at t_i beginning from x_{i-1} at t_{i-1} in the r^{th} iteration$(r = 1, \ldots, R)$;

2. The simulated values ${X^1}_{t_i}, \ldots, {X^R}_{t_i}$ are applied to build a non-parametric kernel density estimate of the transition density $p(t_i, x_i; (t_{i-1}, x_{i-1}), \theta)$

$$p^R(t_i, x_i; t_{i-1}, x_{i-1}, \theta) = \frac{1}{R} \sum_{r=1}^{R} \Phi(x_i; {mean^R}_i, {Var^R}_i) \tag{2.2.37}$$

   in which

$${mean^R}_i = {X^r}_{t_{i-1}} + h \;\; f(t_{i-1} + (M-1)h, {X^r}_{ti-1}; \theta), \tag{2.2.38}$$

   and

$${Var^R}_i = h \;\; \sum_{r=1}^{R} (t_{i-1} + (M-1)h, {X^r}_{t_{i-1}}; \theta), \tag{2.2.39}$$

   Here, $\Phi(x; \cdot, \cdot)$ representing the multivariate normal density at x and $\sum(t, x; \theta) =$

$g(t,x;\theta)g(t,x;\theta)^{\top}$, where $\top$ indicates transposition;

3. The prior technique is iterated for each x_i and the $p^R(t_i,x_i;t_{i-1},x_{i-1},\theta)$ are obtained values to be used in

$$L^R(\theta) = \Pi_{i=1}^{n} p^R(t_i,x_i;t_{i-1},x_{i-1},\theta) \tag{2.2.40}$$

4. $\log L^R(\theta)$ is minimized with respect to θ to obtain the MLE estimation θ^R of θ.

The convergence of θ^R to the MLE of θ when $M \to \infty$ and $R \to \infty$, with $\frac{R^{\frac{1}{2}}}{M} \to 0$ is proven under mild regularity conditions (Brandt & Santa-Clara, 2002b).

2.3 Mathematical Models

There are a large number of mathematical models proposed for the population dynamics of tumors and the tumor growth. We refer reader to review articles (Araujo & McElwain, 2004; Bellomo & Preziosi, 2000; Bellomo, Li, & Maini, 2008; Byrne, Alarcon, Owen, Webb, & Maini, 2006; Martins, Ferreira, & Vilela, 2007; Nagy, 2005; Roose, Chapman, & Maini, 2007; Chaplain, 2008).

Partial differential equations (PDEs) are one of the most popular methods to describe the spatial models. Different PDE models are proposed for tumor growth. Among that, we refer the reader to (Araujo & McElwain, 2004; Roose et al., 2007; Chaplain, 2008)).

Mathematical models based on kinetic theory are also known as the second class of mathematical models for tumor growth (Bellomo & Delitala, 2008).

The other important class of models for the population dynamics of tumor cells and the tumor growth are Ordinary Differential Equations (ODEs) models.

These forms of models are called non-spatial models (Adam & Bellomo, 2012; Dullens,

Van Der Tol, De Weger, & Den Otter, 1986; Bajzer, Marušić, & Vuk-Pavlović, 1996; Sachs, Hlatky, & Hahnfeldt, 2001a; Nagy, 2005).

With a simple and intuitive structure, ODE models are able to explain the interaction between tumor cells with each other, tumor cells and normal tissues and the response of tumor cells to the different treatments (Bajzer et al., 1996; Sachs et al., 2001a).

ODE models can be classified based on the compartments of the model (e.g. one (Gompertz, 1825), two (Sachs et al., 2001a), three (Bajzer et al., 1996), six (Piantadosi, Hazelrig, & Turner, 1983) or more ((Piantadosi et al., 1983)) compartments. The other models focus on the practical features of the tumor growth (Nagy, 2005).

2.3.1 Early Models of tumor growth

The first mathematical models for the tumor growth were focused on the dynamics of tumor growth. Many researchers considered diffusion processes as the most remarkable part of tumor growth models. For instance, the effects of X-rays on the Jensen's rat sarcoma growth conducted by Mayneord, in 1932.

They found that the tumor's growth changed linearly with respect to time in the last period of their growth (Mayneord, 1932)). Same findings were achieved by Haddow in 1938 (Haddow, 1938) during the study of mouse carcinomas.

As reported in (Mayneord, 1932), researchers were highly interested in the tumor growth rate since the tumor disappearance or is continued growth after radiation was an insufficient criterion to evaluate the impact of radiation on tumor growth.

After histological investigation discovered that dynamic growth was limited to a thin covering at the tumor's margin, a mathematical model was developed by Mayneord (Mayneord, 1932) in which the influence of different distributions of dynamically separating cells was investigated.

Many researchers continued experimental studies to investigate how hypoxic tumor cell

affected the tumor's radio-sensitivity (Cramer, 1934; Mottram, 1936; Gray, Conger, Ebert, Hornsey, & Scott, 1953).

A mathematical framework was proposed by (Thomlinson & Gray, 1955) to model the oxygen diffusion and utilize it to complete an experimental study of some forms of bronchial carcinoma, which grow in the solid rods. These rods are capillaries free. Cells are fed by diffusion of metabolites obtained from the adjacent stroma. In big tumors, necrotic centers enclosed by whole tumor cell are detectable.

According to the facts, a declining trend in oxygen pressure must exist between the margin and the center of each tumor cord. Using the different damages caused by X- or γ-radiation in anoxic cells with well-oxygenated cells, researchers tried to estimate the critical value of the tumor cord's outer radius where the oxygen concentration goes to zero at the center of tumor, by using the theory developed by (A. Hill, 1928).

In 1825, Gompertz proposed an actuarial model (Gompertz, 1825). Later, the model was used to study the population growth in biological and economical events (Winsor, 1932). Gompertzian model is widely used for examining the growth in both normal (Laird, Tyler, Barton, et al., 1965) and tumor cells.

(Laird, 1964) showed that many of primary tumors in rabbit, rat, and mouse could be modeled by Gompertzian equations. (Burton, 1966) developed a model to examine not only the oxygen distribution in spherical tumors in which the blood supply is entirely restricted to the surface but also the resulting relative radius of the central zone to the total radius. These results were used to show that growth curve could be described by a Gompertzian equation.

2.3.2 Mathematical models of radiation effect

The earliest models for the fractionated radiation therapy was developed based on some theories such as target theory and hit theory (Cohen, 1971) and Power Law equation of

the Nominal Standard Dose theory of fractionated cell kill (Ellis, 1969).

However, the Linear Quadratic (LQ) model was widely used by many researchers from the beginning of the 1980s. This model was used to predict the relationship between cell mortality caused by radiation and radiated dose fractions, where the magnitude of each dose fraction was around 2 Gray.

LQ model was formed based on the prominent work (D. Lea & Catcheside, 1942) by Lea and Catcheside or the DNA Single-Strand Break (SSB) and Double-Strand Breaks (DSBs).

In the middle of 1980s, using LQ model became very popular and some researchers modified the model. For instance, (Withers, Taylor, & Maciejewski, 1988) considered the time-factor for the tumors with rapid response.

Moreover, (Alper, 1979) modified the model based on the oxygenation enhancement ratio (OER) for the tumors, which were radio-resistant in hypoxia condition.

Later, some other mathematical models were proposed (e.g. the binary misrepair model and models of repair capacity saturation). In a research by (Brenner, Hlatky, Hahnfeldt, Huang, & Sachs, 1998), similar outcomes were shown in a comparison between LQ model and these models under specific condition (e.g. 2 Gray in each dose fraction).

A comprehensive review article in the history of mathematical modeling of fractionated radiation therapy has been provided by (Dale, Jones, et al., 2007). This article and some other works such as (J. F. Fowler, 1989; J. Fowler, 2014; Bentzen, 1993) are recommended as a key reference for all tumor growth mathematical modelers.

In the last two decades of the 20th century, along with the development and extensive applications of LQ model in clinical research, other models has been developed.

In the first step, these models had a mathematical framework. However, some researchers utilized the stochastic modeling methods to explain the influence and action of ionizing radiation on alive cells. The models became more complex over the time, so it was re-

quired to propose more accurate models and to model on smaller scales.

Macroscopic tumors modeling is the most relevant mod for comparisons to human data and eventual translation into clinical use, consequently, the modeling of the tumors vascular system became of interest.

In massive clinical data for specific tumors such as head and neck (Dunst et al., 2003); (Nordsmark & Overgaard, 2004; Rischin et al., 2006), hypoxic condition is very important. Subsequently, some mathematical modelers considered oxygenation parameters in their models.

As a consequence, modelers applied diffusion theory to model the carrying of oxygen through tissue (S. E. Hill, 1928). Such a mentioned theories were used to develop new complex stochastic and hybrid mathematical models (Tannock, 1972; McElwain, Callcott, & Morris, 1979).

In the 1980s, using a personal computer was very popular in some parts of the world like US, Germany, and Norway. Therefore, tumor growth and treatment modeling were improved in this period. CELLSIM (later called 2D CELLGROW) (Donaghey, 1980, 1983) is one of the earliest stochastic models for the growth of vascular tumors.

(O'Donoghue, 1997) proposed a mathematical model based on the Linear Quadratic (LQ) model to show the tumor growth changes. He examined a type of tumor cell proliferation that is exponential at small tumor sizes and Gompertzian at larger sizes. Moreover, by using deterministic equations, tumor mass curves and cell survival fraction were plotted as a function of time.

Duchting et al. in the 1980s and 1990s developed mathematical stochastic models of the tumor growth treated by radiation. They were pioneer to consider cell by cell modeling of the tumor cells population dynamic by considering the cellular oxygenation parameters, cellular kinetics and radiation schedule parameters (Düchting & Vogelsaenger, 1985; Duechting, Ginsberg, & Ulmer, 1995; Duechting, Lehrig, Ginsberg, Dedeleit, & Ulmer,

1992; Düchting & Vogelsaenger, 1981).

Seminal models has been proposed by Kocher et al in 1990s (Kocher, Treuer, & Müller, 1997; Kocher et al., 2000). In their study, oxygenation was considered via modeling a 3D regular vessels array inside the tumor mass.

In the late 1990s, Wouters group proposed a new mathematical model in which the tumor oxygenation and reoxygenation processes have been considered (B. G. Wouters & Brown, 1997; B. Wouters et al., 2002).

A stochastic modeling of tumor growth was developed in the next few years. The model considered cells with different ranges of proliferative capacity. It also described the kinetics of fast repopulation and radiation therapy and chemotherapy as a treatment (Marcu, Van Doorn, & Olver, 2004; Marcu, Van Doorn, Zavgorodni, & Olver, 2002; Marcu, Bezak, & Olver, 2006).

The model showed that the asymmetry loss in stem cells division (for a small percentage of stem cells population) could be the essential mechanism in tumor repopulation while cells movement from G_0 phase to G_1 phase of the cell cycle does not play an important role in tumor regrowth.

Two mathematical models of tumor treatment including stochastic parameter distribution were proposed in 2002.

In the first model, microvascular density and 2D tumor heterogeneity were modeled and clinically verified (Nilsson, Lind, & Brahme, 2002).

In the second study, the model accounted for the transporting different doses to different cells according to the oxygen status (Popple, Ove, & Shen, 2002).

In this model, both chronic (permanent) and acute (temporal) hypoxia was considered. It is verified that 20% to 50% increase in dose in the hypoxic condition required the same dose to control the tumor growth in the oxic condition.

In 2006, a spatial mathematical model was developed by Sovik group to **dose-paint** radio-

resistant tumors sub-volumes with higher than normal doses (Søvik, Malinen, Bruland, Bentzen, & Olsen, 2006).

Considering reoxygenation, the model was verified by applying clinically appropriate oxygenation distribution. They showed that applying different doses to different parts of the tumor can notably boost Tumor Control Probability (TCP). Moreover, they found that the reoxygenation rate is an important parameter in the model.

Tumors without reoxygenation had the most benefit of dose redistribution. In addition, the level of the temporal hypoxia influenced results less than that of permanent one.

In the models proposed by Dasu et al. (Daşu & Denekamp, 1999; Toma-Daşu, Daşu, & Karlsson, 2006; Toma-Daşu, Daşuu, & Brahmeu, 2009) the influence of hypofractionation, acute and chronic hypoxia on tumor control has been explored via a probabilistic model (Toma-Daşu et al., 2006; Daşu, Toma-Daşu, & Karlsson, 2005). After that, the most important model parameter was measured.

Model outcomes verified that a complete explanation is needed for tumor oxygenation to predict the treatment results. Moreover, results showed that the existence of permanent oxygenation is more important than the changes of acute hypoxia between fractions of treatment.

Lastly, many stochastic models are developed to model the relation between vascularized tumor growth and radiation therapy in the past decades.

For example, Stamatakos et al have proposed several studies to model the effects of radiation on tumor growth for brain and lung cancers.

Early works started with a 3D discrete model (Starnatakos et al., 2001) using in vitro small lung cancer cells. In this work, they improved the models proposed by Duechting et al. in the 1980s.

Since 2004, they concentrated on glioblastoma multiform. The models has been calibrated and verified by using experimental and clinical data (G. Stamatakos et al., 2010;

G. Stamatakos, Antipas, Uzunoglu, & Dale, 2014; D. Dionysiou, Stamatakos, Gintides, Uzunoglu, & Kyriaki, 2008; Antipas, Stamatakos, Uzunoglu, Dionysiou, & Dale, 2004; D. D. Dionysiou & Stamatakos, 2006; G. S. Stamatakos, Georgiadi, Graf, Kolokotroni, & Dionysiou, 2011).

Considering angiogenesis, Borkenstein et al. (Borkenstein, Levegrün, & Peschke, 2004) introduced a spatial model for tumor growth treated by radiation in which each tumor cell was considered individually. Capillaries are located in a 3D lattice.

Cells were oxygenated according to the distance to the nearby capillary cell. It was shown that cells in a hypoxic condition secrete an angiogenesis factor comparing to the proportion of hypoxic tumor cells.

HYP-RT is a temporal stochastic model (Harriss-Phillips, Bezak, & Yeoh, 2014; Tuckwell, Bezak, Yeoh, & Marcu, 2008) simulating individual tumor cell division and the effects of fractionated radiotherapy, with assumed randomized spatial cell placement in the tumor.

The model is based on the proliferative hierarchy of epithelial cells, simulating head and neck squamous cell carcinoma growth and radiotherapy, with hypoxia modeled by using realistic oxygen distributions and a dose per fraction dependent OER curve.

The model is capable of simulating the effects of reoxygenation of hypoxic tumors as well as the accelerated repopulation. Results show that accelerated repopulation and the percentage of stem cells are the two most important parameters controlling growth rate and radiotherapy outcome.

2.3.3 Cell Cycle Models

Investigating the effects of treatments on breast cancer cell lines involves determining how they influence cell proliferation rate.

As cells proliferate, they progress through a series of distinct phases. In the first phase,

the G_1 (gap phase), cells are only receptive to environmental signals. This phase is named so as it appears as a gap between the previous cell division stage and subsequent DNA synthesis phase (Uzman, 2003).

If a cell decides to divide, it makes an irreversible decision to progress into the S phase, or the synthesis phase, during which DNA synthesis occurs.

Upon DNA synthesis completion, the cell moves into the G_2 phase (the second gap phase), when accumulated errors in the replicated DNA are reviewed and corrected.

The cell then moves into the M phase (mitosis phase), where the duplicated chromosomes are separated into two sets of nuclei. At the end of the M phase, the cell splits into two identical cells via a process called cytokinesis. Both daughter cells begin their cycle again in the G_1 phase (Uzman, 2003).

Several mathematical models for cell cycle progression have been developed (Sible & Tyson, 2007). For instance, Piantadosi et al.'s cell cycle model contains five compartments: G_0, G_1, S, G_2 and M (Piantadosi et al., 1983). It uses a system of six nonlinear ODEs to model the tumor growth.

Similar approaches have been presented in (Pena, 2004) and (Sachs, Hlatky, & Hahnfeldt, 2001b), by considering two compartments. According to (Pena, 2004), cells are divided into quiescent and active compartments. (Sachs et al., 2001b) considers hypoxic and normoxic tumor cells in the subpopulation.

Basse et al. studied tumor growth populations in human cell lines through a multi-compartment model of cell cycles (Basse, Baguley, Marshall, Wake, & Wall, 2004).

Using an age structure model, Albano and Giorno developed a mathematical model of cell population dynamics for colorectal cancer (Albano & Giorno, 2006). Simms et al.,(Simms et al., 2012), applied a three-compartment cell cycle model to the MCF-breast cancer cell line.

It introduced a cell population dynamic based on three main subpopulations, namely G,

S and M, each of which is divided into three, two, and two subpopulations, respectively. This approach resulted in a system of seven nonlinear delay ODEs describing cell population dynamics.

One common drawback among above mentioned mathematical models is that they all suffer from lack of considering the inherent error in the death rate caused by the flow cytometry method. This error is rooted in recognizing apoptotic cells as live cells (Daukste, 2012).

CHAPTER 3

MATHEMATICAL MODELS

In this chapter, first, we introduce a discrete model which describes the effect of radiation as the treatment and included DNA repair mechanism in cells based on the **Target Theory** and **Hit Theory** in section (3.1). Thereafter two mathematical models will propose to study the population dynamics of tumor cells which are treated by radiation.

According to the Target Theory, the tumor population is divided into m different sub-populations based on the different effects of ionizing radiations on human cells in the first model in section (3.2).

A hybrid model consists of a system of ordinary differential equations with random variable coefficients representing the transition rates between sub-populations, is used to model the dynamics of cell sub-populations within the tumor.

Moreover, a new mathematical model is proposed for studying the population dynamics of breast cancer cells treated with radiotherapy by using a system of stochastic differential equations (SDEs) through the second model in section (3.3).

According to the cell cycle, each cell belongs to one of three subpopulations G, S, or M, representing gap, synthesis, and mitosis subpopulations.

Cells in the M subpopulation are highly radio-sensitive, whereas cells in the S subpopulation are highly radio-resistant. Subsequently, the proposed model is calibrated by using experimental data from previous experiments involving the MCF-7 breast cancer cell line.

Finally, we will propose a new definition for the tumor lifespan based on the tumor cell population size in section (3.4).

3.1 Markov chain model for a single cell

According to the target theory and hit theory, each cell has a certain number m of radio-sensitive sites so-called targets. These targets may be deactivated by radiation particles and a cell dies if all of its targets become deactivated. Therefore, after the application of one dose fraction of radiation, one cell may have $m+1$ possible states.

1. The cell has i deactivated target(s) where $i \in \{0,1,...,m-1\}$.

2. The cell has m deactivated targets. This cell is considered to be dead.

For example, different states for a cell with $m = 3$ targets is shown in Figure (3.1).

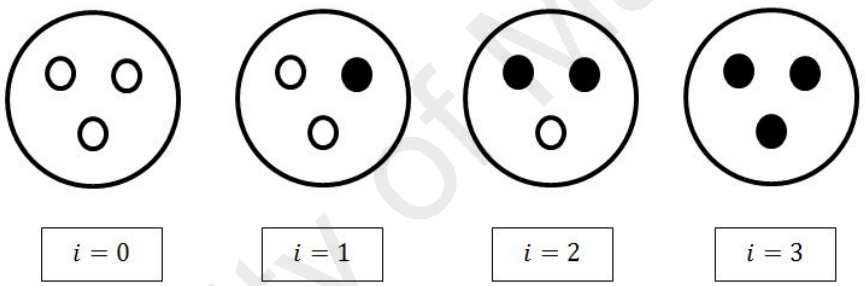

Figure 3.1: Different states for a cell with $m = 3$ targets.

Now let Z_k be the random variable describing the state of the cell at time k and $Z_k = i \in \{0,1,...,m\}$ is the number of deactivated targets at time k. We suppose that Z_k is a discrete-time Markov chain. Hence, the cell state at time $k+1$ only depends on the current state at time k.

In the next subsection we evaluate the transition matrix Π, which models both the effect of radiation and repair Mechanism

3.1.1 Treatment Mechanism

Denote $\mathbf{P}(i,j)$ the probability to deactivate j targets at time $k+1$ when i targets are disabled at time k. Let q be the probability of inactivating a target after applying a dose fraction u_0. Moreover, we suppose that disabling targets in the cell are independent events.

Thus after applying a fraction dose, the possible states at time $k+1$ of a cell which was in state i at time k are {i, i+1, ..., m}. The cell may switch at time $k+1$ to the state j by the deactivation of $j-i$ target(s) among the $m-i$ active ones. Consequently,

$$\mathbf{P}(i,j) = \begin{cases} \binom{m-i}{j-i} q^{j-i}(1-q)^{m-j} & i \leq j \\ 0 & j < i \end{cases} \tag{3.1.1}$$

and the explicit expression is:

$$P = \begin{bmatrix} [(1-q)^m & \binom{m}{1} q\,(1-q)^{m-1} & \ldots & q^m \\ 0 & (1-q)^{m-1} & \ldots & q^{m-1} \\ . & . & . & . \\ . & . & . & . \\ . & . & . & . \\ 0 & 0 & \ldots & q \\ 0 & 0 & \ldots & 1 \end{bmatrix} \tag{3.1.2}$$

Figure (3.2) shows the transition graph of the radiation process before taking the repair of inactive targets into account, for the case of a 3-target cell, i.e. $m = 3$.

3.1.2 Repair Mechanism

We introduce now repair mechanisms of deactivated targets, which occur between the application of two consecutive dose fractions. Let r be the probability of an inactive target in a living cell to revive during the period that separates two consecutive dose fractions. We assume that any target can be repaired independently from each other. The possible states at time $k+1$ of a cell which was in state i at time k are $\{0,1,...,i\}$. Denote $\mathbf{R}(i,j)$ the probability that the cell switches at time $k+1$ to the state j. Since $i-j$ targets among

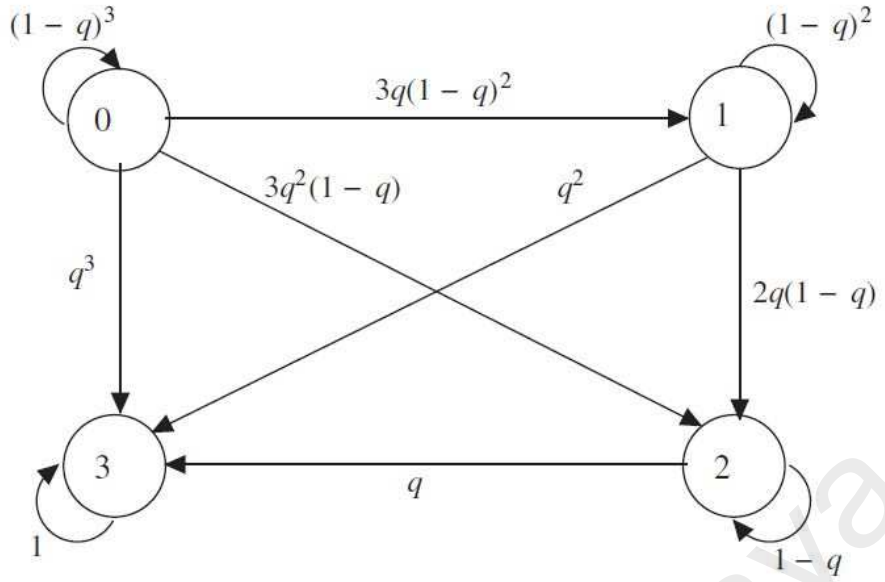

Figure 3.2: The transition graph of the radiation process before considering the repair mechanism, for the case of $m = 3$.

the i inactive targets are repaired, then

$$\mathbf{R}(i,j) = \begin{cases} \binom{i}{j} r^{i-j}(1-r)^j & j \le i < m \\ 0 & i < j \end{cases} \tag{3.1.3}$$

where $\mathbf{R}(m,m) = 1$ and $\mathbf{R}(m,j) = 0$ for $m \neq j$.

and the explicit expression is:

$$R = \begin{bmatrix} [1 & 0 & \dots & 0 \\ r & 1-r & \dots & 0 \\ r^2 & \binom{2}{1} r\,(1-r) & . & 0 \\ . & . & . & . \\ . & . & . & . \\ r^{m-1} & \binom{m-1}{1} r^{m-2}\,(1-r) & \dots & 0 \\ 0 & 0 & \dots & 1 \end{bmatrix} \tag{3.1.4}$$

3.1.3 Transition matrix of Z_k

We model the dynamics of the Markov chain Z_k first by taking the effects of dose fractions and second by taking the repair mechanisms into account as follows:

$$\Pi = \mathbf{P}\,\mathbf{R} \tag{3.1.5}$$

where **P** models the effects of dose fractions and **R** describes repair mechanisms.
In the case of a 3-target cell,

$$R = \begin{bmatrix} [(rq+q')^3-(rq)^3 & 3\,r'q\,q'^2+6rr'q^2q' & 3r'^2q^2q' & q^3 \\ rq'^2 & r'q'^2+4rr'qq' & 2r'^2qq' & q^2 \\ r^2q' & 2rr'q' & r'^2q' & q \\ 0 & 0 & \ldots & 1 \end{bmatrix} \tag{3.1.6}$$

where $q' = 1-q$ and $r' = 1-r$.

Figure (3.3) shows the transition graph corresponding to the Markov chain (Z_k) after taking the repair of inactive targets into account.

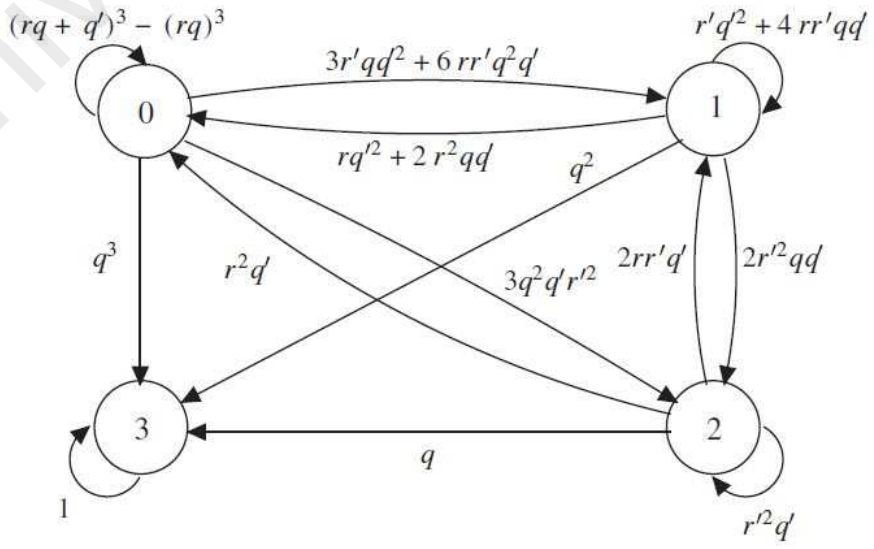

Figure 3.3: The transition graph for (Z_k) after the application of treatment and repair mechanism.

3.2 An ODE model for tumor Cells Population Dynamics Based on Target Theory

One of the typical methods to treat cancer is External Beam Radiation Therapy (XRT). It has been verified that the ionization the process initiated through radiating particles leads to lesions in the cells (Curtis, 1986). The lesions negatively affect the DNA structure, which is considered one of the most harmful kinds of radiotherapy damage (Wyman & Kanaar, 2006), (Hoeijmakers, 2001). In this regard, probabilistic models such as Tumor Control Probability (TCP) (Zaider & Minerbo, 2000; Dawson & Hillen, 2006; Gay & Niemierko, 2007) and Normal Tissue Complication Probability (NTCP) (Lyman, 1985; Källman, Ågren, & Brahme, 1992) can be utilized in the classification and evaluation of radiation treatment planning.

Numerous stochastic models have been developed to predict tumor response to radiation treatment (e.g. linear quadratic model (Zaider & Minerbo, 2000; J. F. Fowler, 1989), cell population dynamics models (Quinn & Sinkala, 2009; Sachs et al., 2001b; Gámez, López, Garay, & Varga, 2009), mixed-effects behavioral models (Bastogne et al., 2010) and cell cycle models (Kirkby, Burnet, & Faraday, 2002).) Most of these models do not incorporate biological tumor damage heterogeneity, which is the focus of our study. We refer the reader to Michelson and Leith (Adam & Bellomo, 1997) for information on different types of heterogeneity.

The Target Theory is an essential concept for understanding radiation biology (Rédei, 2008). The target is assumed to be a radio-sensitive site within cells. Each cell contains a certain number of targets, each of which may be deactivated after being hit by radiation particles. Moreover, between two consecutive dose fractions, each target may become active again the following immune system reaction (Turner, 1975). Even though many complex interpretations of the target theory have been developed, the basic principle entails the death of the organism on account of the target(s) inactivation within the organ-

ism. Despite the target being considered a unit of biological function (Nomiya, 2013), the number of targets and their locations in an organism are sometimes vague. Regarding cell sensitivity, a large part of models usually assumes that cell sensitivity is constant during radiation (Keinj, Bastogne, & Vallois, 2011, 2012; O'Rourke, McAneney, & Hillen, 2009). The same assumption is also made for cell populations, i.e., a surviving cell is expected to be viably considered an irradiated cell. Therefore, all cells are supposed to have similar survival probabilities. However, there is strong evidence that damaged cells are unable to resist radiation (Keinj et al., 2011, 2012).

The clinical significance of the intra-tumor heterogeneity of cell phenotypes and cell damage is discussed in (Gupta et al., 2011; Durrett, Foo, Leder, Mayberry, & Michor, 2011). As such, providing a definition for the suitable duration of treatment is rather a clinical challenge, especially when therapeutic response variability is considered. In this regard, Kienj et al. developed a discrete-time Markov chain multinomial model for tumor response (Keinj et al., 2011). This model employs the Target Theory.

As described in (Keinj et al., 2011), this multinomial model can be generalized to incorporate the heterogeneity of cell damage as a result of treatment. However, the model merely enumerates the surviving cells in the tumor rather than the tumor's lifespan. This model inspects the number of surviving cells in the tumor and not the tumor lifespan as seen in the majority of models utilized to measure tumor response to treatment.

In this section, a new mathematical model is proposed for the population dynamics of heterogeneous tumor cells following external beam radiation treatment.

According to the Target Theory, the tumor population is divided into m different subpopulations based on the diverse effects of ionizing radiation on human cells.

A hybrid model consists of a system of differential equations with random variable coefficients representing the transition rates between subpopulations.

Such model is utilized to model the dynamics of cell subpopulations within a tumor. The

model also describes the cell damage heterogeneity and the repair mechanism between two consecutive dose fractions.

3.2.1 Assumptions

We adopted the following assumptions in our modeling framework:

1. Cells have the same phenotype but act independently.

2. In the radiotherapy process, the magnitude of each dose fraction (u_0) is constant during treatment (i.e. $u_0 = 2\ Gy$). The time lag between two consecutive dose fractions is 24 hours.

3. Each cell consists of m targets, which may be deactivated with probability q after each dose fraction. As described earlier, $\mathbf{P}(i,j)$ represents the treatment probability matrix in the transition from i to j inactive targets, i.e., deactivating j targets when i targets were disabled before. This probability is written as:

$$\mathbf{P}(i,j) = \begin{cases} \binom{m-i}{j-i} q^{j-i}(1-q)^{m-j} & i \leq j \\ 0 & j < i \end{cases} \tag{3.2.1}$$

4. Each target may be revived with probability r. As described previously, $\mathbf{R}(i,j)$ represents the repair probability matrix in the transition from i to j, as given by:

$$\mathbf{R}(i,j) = \begin{cases} \binom{i}{j} r^{i-j}(1-r)^{j} & j \leq i < m \\ 0 & i < j \end{cases} \tag{3.2.2}$$

   where $\mathbf{R}(m,m) = 1$ and $\mathbf{R}(m,j) = 0$ for $m \neq j$.

5. x_i indicates the cell subpopulation with i deactivated target(s), where $i = 0, ..., (m-1)$. For $i \neq j$, each cell can move from x_i to x_j with the constant time-independent transition rate of $\alpha(i,j)$.

6. A cell is considered as a dead cell if all targets are deactivated. The cell death rate in subpopulation x_i is considered constant, D_i.

7. Cells can reproduce if all targets become active. For simplicity, we assume that just before the repair mechanism acts, cells in subpopulation x_0 can give birth to new cells proportional to subpopulation x_0 with a constant rate of (β). As such, each cell in subpopulation x_0 can divide into exactly two daughter cells with probability μ or it can remain unchanged with probability $(1-\mu)$ between two consecutive dose fractions.

Therefore, we can divide the tumor cells population into m subpopulations $\{x_0, x_1, \ldots, x_{(m-1)}\}$ according to the effect of radiation particles on cells. The schematic illustration of tumor cells population is shown in Figure. (3.4).

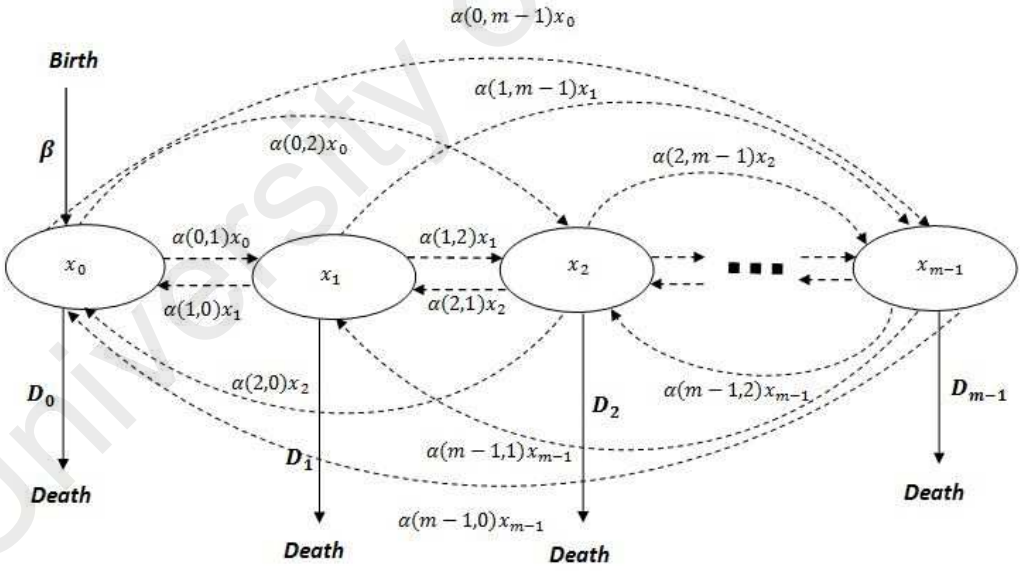

Figure 3.4: Schematic illustration of tumor cell population model.

3.2.2 Model derivation

As indicated in Fig. (3.4), tumor dynamics is generally described as the effect of radiotherapy on the different tumor cell subpopulations.

Based on the conservation low

$$\frac{dx_i(t)}{dt} = In(t) - Out(t) \tag{3.2.3}$$

Subsequently, the conservation law for subpopulation x_i's, $i = 0, \ldots, m-1$ is written as follows.

For $i = 0$:

$$\frac{dx_0(t)}{dt} = \underbrace{\beta\, x_0(t)}_{\text{Birth due to mitosis}} + \underbrace{\sum_{j=1}^{m-1} \alpha(j,0) x_j(t)}_{\text{transition to } x_0} - \overbrace{\Big[\sum_{k=1}^{m-1} \alpha(0,k)\Big]\, x_0(t)}^{\text{transition from } x_0} - \overbrace{D_0\, x_0(t)}^{\text{Death}} \tag{3.2.4}$$

and for $i \neq 0$:

$$\frac{dx_i(t)}{dt} = \underbrace{\sum_{\substack{j=0 \\ j\neq i}}^{m-1} \alpha(j,i)\, x_j(t)}_{\text{transition to } x_i} - \overbrace{\Big[\sum_{\substack{k=0 \\ k\neq 1}}^{m-1} \alpha(i,k)\Big]\, x_i(t)}^{\text{transition from } x_i} - \overbrace{D_i\, x_i(t)}^{\text{Death}} \tag{3.2.5}$$

These equations produce the following ODE system:

$$\begin{aligned}
\frac{dx_0(t)}{dt} &= \beta\, x_0(t) + \sum_{j=1}^{m-1} \alpha(j,0)\, x_j(t) - \Big[\sum_{k=1}^{m-1} \alpha(0,k) + D_0\Big]\, x_0(t) \qquad (3.2.6)\\
\frac{dx_1(t)}{dt} &= \sum_{\substack{j=0 \\ j\neq 1}}^{m-1} \alpha(j,1)\, x_j(t) - \Big[\sum_{\substack{k=0 \\ k\neq 1}}^{m-1} \alpha(1,k) + D_1\Big]\, x_1(t)\\
&\vdots\\
\frac{dx_{m-1}(t)}{dt} &= \sum_{j=0}^{m-2} \alpha(j,m-1)\, x_j(t) - \Big[\sum_{k=0}^{m-2} \alpha(m-1,k) + D_{m-1}\Big]\, x_{m-1}(t)
\end{aligned}$$

3.2.3 Model Calibration

The probability that a cell will remain in x_0 after radiation is $\mathbf{P}(0,0)$. Therefore, the average number of births in one day after applying the k^{th} dose fraction and just before the $(k+1)^{th}$ dose fraction is equal to:

$$\begin{aligned} n(k) &= x_0(k)\ \mu\ \mathbf{P}(0,0) \\ &= x_0(k)\ \mu(1-q)^m \end{aligned} \tag{3.2.7}$$

As seen in Eq. (3.2.7), the newborn cells population size is proportional to x_0. Therefore, the birth rate can be taken as:

$$\beta = \mu(1-q)^m \tag{3.2.8}$$

Lemma 3.2.1. *Suppose that a cell has i deactivated target(s) just before the application of a dose fraction and* $\Pi = \boldsymbol{PR}$. *After treatment and repair,*

1. $\Pi(i,j)$ *represents the probability that a cell with i deactivated target(s) has j deactivated target(s) right before the application of the next dose fraction.*

2. *An average number of* $x_i\Pi(i,j)$ *cells move from* x_i *into* x_j.

3. *For fixed m and* $k \geq 1$, *map* $i \to \Pi^k(i,m)$ *is an increasing map.*

Proof. 1. Suppose that $\Pi = \mathbf{PR}$. Therefore:

$$\Pi(i,j) = \sum_{k=0}^{m} \mathbf{P}(i,k)\mathbf{R}(k,j) \tag{3.2.9}$$

Eq. (3.1.3) shows that $\mathbf{R}(m,j) = 0$ for $j < m$. Therefore:

$$\Pi(i,j) = \sum_{k=0}^{m-1} \mathbf{P}(i,k)\mathbf{R}(k,j) \tag{3.2.10}$$

Now assume that a cell has i deactivated targets just before applying a dose fraction. After radiation and right before the repair mechanism, this cell may remain in subpopulation x_i with probability $\mathbf{P}(i,i)$, or it may move to subpopulation x_k, $k = i+1,...,(m-1)$, with probability $\mathbf{P}(i,k)$.

Following the repair, this cell may move from subpopulation x_k to subpopulation x_j with probability $\mathbf{R}(k,j)$. Therefore, the probability of transitioning from subpopulation x_i into subpopulation x_j after treatment and repair (one day) is $\Pi(i,j)$.

2. The effect of treatment and repair on one cell is independent of the rest of the cells. Therefore, the average number of cells moving from subpopulation x_i into subpopulation x_j is equal to $x_i\Pi(i,j)$.

3. See (Keinj et al., 2012).

□

The following corollary is a direct consequence of lemma (3.2.1).

Corollary 3.2.1. *With the same assumptions in Lemma (3.2.1):*

1. *The cells' transition rate from subpopulation x_i into subpopulation x_j is equal to*

$$\alpha(i,j) = \Pi(i,j) \ \ (Day^{-1}) \tag{3.2.11}$$

2. *The death rate of subpopulation x_i is*

$$D_i = \Pi(i,m) \ \ (Day^{-1}) \tag{3.2.12}$$

Remark 3.2.1. *According to lemma 3.2.1, we can separate the tumor cells into different sub-populations according to their sensitivities to radiation. Therefore, the death rate in a subpopulation with more deactivated targets is higher than a subpopulation with fewer deactivated targets, which can be interpreted as treatment heterogeneity in the model.*

Now, starting with subpopulation x_0, cells give birth at a constant rate of $\mu(1-q)^m \ \ (Day^{-1})$. In addition, cells move from subpopulation x_i into subpopulation x_0 at a rate of $\Pi(i,0) \ \ (Day^{-1})$. Conversely, cells move from subpopulation x_0 into subpopulation x_i at a rate of $\Pi(0,i) \ \ (Day^{-1})$ or may die at a rate of $\Pi(0,m) \ \ (Day^{-1})$ where Π is the transition matrix. Hence, for any $i = 0,...,(m-1)$:

$$\sum_{k=0}^{m} \Pi(k,i) = 1 \tag{3.2.13}$$

and

$$\sum_{\substack{k=0 \\ k\neq i}}^{m} \Pi(i,k) = 1 - \Pi(i,i) \tag{3.2.14}$$

By substituting Equations (3.2.8), (3.2.11), (3.2.12) and (3.2.13) in equation (3.2.4) we have:

$$\begin{aligned} \frac{dx_0(t)}{dt} &= (\mu(1-q)^m)\, x_0(t) + \Big[\sum_{j=1}^{m-1} \Pi(i,j)\, x_j(t)\Big] - \Big[\sum_{k=1}^{m} \Pi(0,k)\Big]\, x_0(t) \\ &= (\mu(1-q)^m)\, x_0(t) + \Big[\sum_{j=1}^{m-1} \Pi(i,j)\, x_j(t)\Big] - \Big[1 - \Pi(0,0)\Big] x_0(t) \end{aligned} \tag{3.2.15}$$

Therefore:

$$\frac{dx_0(t)}{dt} = [\Pi(0,0) + \mu(1-q)^m - 1]\, x_0(t) + \sum_{j=1}^{m-1} \Pi(j,0) x_j(t) \tag{3.2.16}$$

For $i = 1, ..., (m-1)$, the same analysis shows that:

$$\frac{dx_i(t)}{dt} = \sum_{\substack{j=0 \\ j\neq i}}^{m-1} \Pi(j,i)\, x_j(t) - x_i(t) \sum_{\substack{k=0 \\ k\neq i}}^{m} \Pi(i,k) \tag{3.2.17}$$

therefore we get:

$$\frac{dx_i(t)}{dt} = \sum_{\substack{j=0 \\ j\neq i}}^{m-1} \Pi(j,i)\, x_j(t) - x_i\, [1 - \Pi(i,i)] \tag{3.2.18}$$

Finally, by substituting Equation (3.2.16) and Equation (3.2.18) in Equation (3.2.6), the tumor growth model is described by:

$$\begin{aligned}
\frac{dx_0(t)}{dt} &= [\Pi(0,0) + \mu(1-q)^m - 1]\, x_0(t) + \sum_{k=1}^{m-1} \Pi(k,0) x_k(t) \qquad (3.2.19)\\
\frac{dx_1(t)}{dt} &= [\Pi(1,1) - 1]\, x_1(t) + \sum_{\substack{k=0 \\ k\neq 1}}^{m-1} \Pi(k,1) x_l(t).\\
&\vdots\\
\frac{dx_{m-1}(t)}{dt} &= [\Pi(m-1,m-1) - 1]\, x_{m-1}(t) + \sum_{k=0}^{m-2} \Pi(k,m-1) x_k(t).
\end{aligned}$$

with initial conditions $\mathrm{x}(0) = (n_0, 0, ..., 0)^\top$.

3.3 The SDE model for the tumor cells population dynamics based on cell cycle position

According to experimental results, cells radio-sensitivity are changing based on the cell cycle stage (Valenzuela, Mateos, de Almodóvar, & McMillan, 2000). The experiments has verified that a cell is more radio-sensitive during the $G2/M$-phase (Quiet, Weichselbaum, & Grdina, 1991; Tell et al., 1998) and more radio-resistant in the S-phase (Howard & Pelc, 1986; Nagasawa, Keng, Harley, Dahlberg, & Little, 1994).

In the proposed model, the tumor cell population is divided into three subpopulations according to radio-sensitivity (Simms et al., 2012; Wake & Byrne, 2013; Falcetta, Lupi, Colombo, & Ubezio, 2013; Weber, Jaehnert, Schichor, Or-Guil, & Carneiro, 2014; Gurkan-Cavusoglu, Schupp, Kinsella, & Loparo, 2011), i.e., gap (G), synthesis (S), and mitosis (M), with the possibility of cell death in each subpopulation. These represent a concise formulation of the cell cycle.

3.3.1 Assumptions

1. The magnitude of radiation is constant (2Gy) during treatment.

2. Cells population consists of three time-dependent subpopulations $G(t)$, $S(t)$ and $M(t)$, which in turn representing Gap, Synthesis and Mitosis.

3. The transition rate of cells moving from subpopulation G into subpopulation S is the time-dependent rate $\alpha(t)$; the transition from subpopulation S into subpopulation M is the constant rate β and subpopulation M to subpopulation G is the constant rate γ, which can be considered the birth rate.

4. All cells are at risk of dying, but at different rates. The death rate of cells in subpopulation G is a constant rate q_1, whereas cells in subpopulations S and M have q_2 and q_3 rates respectively.

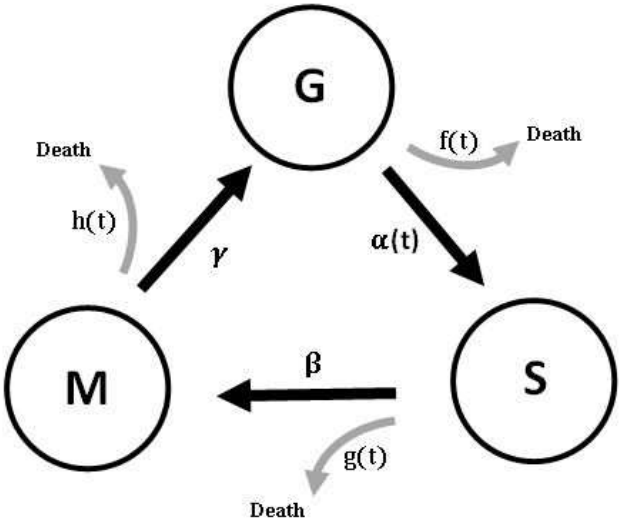

Figure 3.5: Schematic illustration of the cell cycle in a tumor treated by radiation

5. Due to environmental noise effects such as inaccuracy of the cytometry method in counting cells in the apoptosis stage, a noise in the death rate is deemed to capture these effects. Therefore, cell death rates are given by:

$$f(t) = q_1 + r_1(t) \tag{3.3.1}$$

$$g(t) = q_2 + r_2(t)$$

$$h(t) = q_3 + r_3(t)$$

where $r_1(t)$, $r_2(t)$, and $r_3(t)$ are stochastic noise terms, and $q_2 < q_1 < q_3$.

3.3.2 Stochastic Differential Equation Model

When cells are proliferating, they move from one subpopulation into another (Bernard & Herzel, 2006; Johnston, Edwards, Bodmer, Maini, & Chapman, 2007).

During the radiotherapy with gamma rays ($2-4$ Gy), the transition rates of cell movement change at checkpoints G_1 and G_2. As illustrated in Figure (3.5), using transition rates

between subpopulations, the population dynamic is described by:

$$\begin{cases} \dfrac{dG_T(t)}{dt} = -(\alpha(t)+f(t))G_T(t)+2\gamma M_T(t) \\ \dfrac{dS_T(t)}{dt} = \alpha(t)G_T(t)-(\beta+g(t))S_T(t) \\ \dfrac{dM_T(t)}{dt} = \beta S_T(t)-(\gamma+h(t)))M_T(t) \end{cases} \tag{3.3.2}$$

By applying (3.3.1), (3.3.2) can be written as:

$$\begin{cases} \dfrac{dG_T(t)}{dt} = -[\alpha(t)+(q_1+r_1(t))]G_T(t)+2\gamma M_T(t) \\ \dfrac{dS_T(t)}{dt} = \alpha(t)G_T(t)-[\beta+(q_2+r_2(t))]S_T(t) \\ \dfrac{dM_T(t)}{dt} = \beta S_T(t)-[\gamma+(q_3+r_3(t))]M_T(t) \end{cases} \tag{3.3.3}$$

Assuming that $r_i(t)dt = \sigma_i dW^i$ for $i = 1,2,3$ (Evans, 2012), the stochastic differential equation system describing the population dynamics of cells is written as:

$$\begin{cases} dG_T(t) = [-(\alpha(t)+q_1)G_T(t)+2\gamma M_T(t)]dt-[\sigma_1 G_T(t)]dW^1(t) \\ dS_T(t) = [\alpha(t)G_T(t)-(\beta+q_2)S_T(t)]dt-[\sigma_2 S_T(t)]dW^2(t) \\ dM_T(t) = [\beta S_T(t)-(\gamma+q_3)M_T(t)]dt-[\sigma_3 M_T(t)]dW^3(t) \end{cases} \tag{3.3.4}$$

with initial conditions $G_T(0) = 0.49n_0$, $S_T(0) = 0.39n_0$, and $M_T(0) = 0.12n_0$, where n_0 is the initial number of cells (Sutherland, Hall, & Taylor, 1983).

We are assuming:

$$\mathbf{X}(t) = (G_T(t), S_T(t), M_T(t))^\top$$

(3.3.4) can be written in matrix form as:

$$d\mathbf{X} = A\mathbf{X}dt - \sigma\mathbf{X}d\mathbf{W} \tag{3.3.5}$$

where A and σ are the following matrices:

$$A = \begin{bmatrix} -(\alpha+q_1) & 0 & 2\gamma \\ \alpha & -(\beta+q_2) & 0 \\ 0 & \beta & -(\gamma+q_3) \end{bmatrix} \quad \sigma = \begin{bmatrix} \sigma_1 & 0 & 0 \\ 0 & \sigma_2 & 0 \\ 0 & 0 & \sigma_3 \end{bmatrix} \tag{3.3.6}$$

3.3.3 Model Calibration

Loss of reproductive capacity is a widely accepted definition for cell death in radiobiology and is highly applicable to the proliferating cells, including tumor cells for radiotherapy. Cell death quantification is complicated by the fact that cells die at various times after irradiation, often after one or two trips around the cell cycle, and among surviving cells that continue to proliferate.

In the context of radiobiology, cell death rate is generally equated with any process that leads to the permanent loss of clonogenic capacity (Joiner & van der Kogel, 2009).

3.3.4 Steady-State Solution

To evaluate the main model parameters α, β, and γ, it is first assumed that $q_1 = q_2 = q_3 = 0$ and $r_1 = r_2 = r_3 = 0$. If α is constant (which is hereby called unchanging environmental conditions), then our system will eventually reach a certain steady-state behavior that we call steady-state phase.

System (3.3.5) is in a steady state phase, when the proportion of cells across the model phases is constant over time. Note that, as it is experimentally observed, the actual cell populations do not reach a steady-state and instead grow exponentially.

Other mathematical models such as Begg et al.'s (2010) (Begg, Wall, & Wake, 2010) take these steady-state conditions into account by incorporating the terms balancing exponential growth. Throughout this paper, we refer to this condition as a *steady-state phase*, or an *unchanging environmental conditions*.

As it is seen below, parameter α as well as constants of proportions of the model phase could be expressed in terms of experimentally determined parameters.

The cell cycle can be modeled as:

$$\begin{cases} \dfrac{dG_T(t)}{dt} = -\alpha G_T(t) + 2\gamma M_T(t) \\ \dfrac{dS_T(t)}{dt} = \alpha G_T(t) - \beta S_T(t) \\ \dfrac{dM_T(t)}{dt} = \beta S_T(t) - \gamma M_T(t) \end{cases} \tag{3.3.7}$$

Now, consider that

$$\begin{cases} \hat{G}(t) = \dfrac{G_T(t)}{N_T(t)} \\ \hat{S}(t) = \dfrac{S_T(t)}{N_T(t)} \\ \hat{M}(t) = \dfrac{M_T(t)}{N_T(t)} \end{cases} \tag{3.3.8}$$

are the ratios of cells in each subpopulation. Then by using (3.4.3) and (3.3.7) we have:

$$\frac{dN_T(t)}{dt} = \gamma M_T(t) = \gamma \hat{M}(t) N_T(t) \tag{3.3.9}$$

The proliferation rate is defined as:

$$\rho = \gamma \hat{M} \tag{3.3.10}$$

Differentiating (3.3.7) and using (3.3.9) and (3.3.10) will result in:

$$\begin{aligned}\frac{d\hat{G}(t)}{dt} &= \frac{d\frac{G_T(t)}{N_T(t)}}{dt} \\ &= \frac{1}{N_T(t)}.\frac{dG_T(t)}{dt} - \frac{G_T(t)}{N_T^2(t)}.\frac{dN_T(t)}{dt} \\ &= \frac{1}{N_T(t)}.(-\alpha G_T(t) + 2\gamma M_T(t)) - \rho\hat{G}(t) \\ &= -(\alpha+\rho)\hat{G}(t) + 2\gamma\hat{M}(t) \end{aligned} \tag{3.3.11}$$

Therefore the system (3.3.7) is converted to:

$$\begin{cases} \frac{d\hat{G}(t)}{dt} = -(\alpha+\rho)\hat{G}(t) + 2\gamma\hat{M}(t) \\ \frac{d\hat{S}(t)}{dt} = \alpha\hat{G}(t) - (\beta+\rho)\hat{S}(t) \\ \frac{d\hat{M}(t)}{dt} = \beta\hat{S}(t) - (\gamma+\rho)\hat{M}(t) \end{cases} \tag{3.3.12}$$

In the steady-state,

$$\begin{cases} \frac{d\hat{G}(t)}{dt} = 0 \\ \frac{d\hat{S}(t)}{dt} = 0 \\ \frac{d\hat{M}(t)}{dt} = 0 \end{cases} \tag{3.3.13}$$

Therefore,

$$\begin{cases} -(\alpha+\rho)\hat{G} + 2\gamma\hat{M} = 0 \\ \alpha\hat{G} - (\beta+\rho)\hat{S} = 0 \\ \beta\hat{S} - (\gamma+\rho)\hat{M} = 0 \end{cases} \tag{3.3.14}$$

In the steady-state this problem is equivalent to the following eigenvalue and eigenvector

problem.

$$\begin{pmatrix} -\alpha & 0 & 2\gamma \\ \alpha & -\beta & 0 \\ 0 & \beta & -\gamma \end{pmatrix} \begin{pmatrix} \hat{G} \\ \hat{S} \\ \hat{M} \end{pmatrix} = \rho \begin{pmatrix} \hat{G} \\ \hat{S} \\ \hat{M} \end{pmatrix} \tag{3.3.15}$$

Now, according to the Perron-Frobenius theorem (Varga, 2009), $\hat{G}$, $\hat{M}$, $\hat{S}$ and ρ can be explicitly stated as the solution to (3.3.15) in terms of α, β, γ.

There are three different solutions for $\hat{G}$, $\hat{M}$, $\hat{S}$ and ρ possible but positivity of the matrix selects the Perron solution.

$$\begin{cases} \alpha = \dfrac{(\gamma+\rho)\hat{M}+\rho\hat{S}}{\hat{G}} \\ \beta = \dfrac{(\gamma+\rho)\hat{M}}{\hat{S}} \\ \gamma = \dfrac{\rho}{\hat{M}} \end{cases} \tag{3.3.16}$$

3.3.5 Evaluation of the model parameters

In this section experimental data is engaged to numerically evaluate the main model parameters. Here by combining equations (3.3.9) and (3.3.10) we get:

$$\frac{dN_T(t)}{dt} = \rho N_T(t) \tag{3.3.17}$$

Therefore

$$N_T(t) = N_T(0)e^{\rho t} \tag{3.3.18}$$

Assuming that K is the doubling time, we will have

$$\rho = \frac{\ln(2)}{K} \tag{3.3.19}$$

Table 3.1: Estimated parameter values in steady-state condition

Parameter	Estimated Value
ρ	$0.0289(hr^{-1})$
α	$0.0892(hr^{-1})$
β	$0.0819(hr^{-1})$
γ	$0.2468(hr^{-1})$

In (Sutherland et al., 1983), multiple experiments were performed to determine the average steady-state values of G, S and M under the same growth conditions.

The results are reported as $48.9 \pm 0.6\%$, $39.4 \pm 0.6\%$ and $11.6 \pm 0.3\%$, for G, S and M respectively. The doubling time is reported to be 24 hours and thus $\rho = 0.0289$. The data does not provide any particular margin of error for the observed doubling time.

Yet, the large enough number of repetition of the experiment guaranties a reasonably accurate value for the doubling time. Replacing ρ by its numerical value in (3.3.16), yields to the values of main model parameters listed in Table (3.1).

3.4 Tumor lifespan

What dose of radiation is required to remove the tumor completely? A small number of cells may still remain after resection, that is not visible and detectable by MRI.

Therefore, it is crucial to know how many dose fractions must be applied to eliminate remaining cancerous cells.

In this section, we are going to answer this question by using the tumor lifespan concept. Subsequently, tumor lifespan is defined in terms of population dynamics.

Now, suppose that $N_T(t)$ shows the tumor population size at time t.

Definition 3.4.1. *The tumor lifespan is defined as the minimum necessary dose fractions needed for the tumor removal. As such, the tumor lifespan is defined as:*

$$L = \min\{t : \lfloor N_T(t) \rfloor = 0\} \tag{3.4.1}$$

in which $\lfloor N_T(t) \rfloor$ represents the integer part (or floor) of $N_T(t)$ and the tumor population size at time t in the first and second models is defined as:

$$N_T(t) = \sum_{l=0}^{m-1} x_l(t) + n(\lfloor t \rfloor) \tag{3.4.2}$$

$$N_T(t) = G_T(t) + S_T(t) + M_T(t) \tag{3.4.3}$$

respectively.

CHAPTER 4

MATHEMATICAL RESULTS

Stability Analysis is referring to the terms applied to investigate the stability of solutions of differential equations and of trajectories of dynamical systems under small changes of initial conditions. Suppose that $x^* \in \mathbb{R}^m$ is an equilibrium point for the differential equation $\dot{\mathrm{x}} = f(\mathrm{x})$.

x^* is a stable equilibrium if for every neighborhood U of x^* in $\mathbb{R}^m$ there is a neighborhood U_1 of x^* in U such that every solution $\mathrm{x}(t)$ with $\mathrm{x}(0) = \mathrm{x}_0$ in U_1 is defined and remains in U for all $t > 0$.

A different form of stability is asymptotic stability. If U_1 can be chosen above so that, in addition to the properties for stability, we have $\lim_{t\to\infty} \mathrm{x}(t) = x^*$, then we say that x^* is asymptotically stable.

An equilibrium x^* that is not stable is called unstable. This means there is a neighborhood U of x^* such that for every neighborhood U_1 of x^* in U, there is at least one solution $\mathrm{x}(t)$ starting at $X(0) \in U_1$ that does not lie entirely in U for all $t > 0$ (Hirsch, Smale, & Devaney, 2012).

4.1 Single-Strand Break (SSB) and Double-Strand Breaks (DSBs) as one subpopulations

There are some assay to recognize single-strand break (SSB) and double-strand breaks (DSB) such as PCR (polymerase chain reaction), comet, halo, TUNEL (Terminal deoxyribonucleotidyl transferase-mediated deoxyuridine triphosphate nick end labeling) assay, HPLC-Electrospray tandem mass spectrometry, FISH (Fluorescence in situ hybridization), FCM (Flow cytometry), annexin V labeling, immunological assays including im-

munofluorescent and chemiluminescence thymine dimer detection, immunohistochemical assay, Enzyme-linked immunosorbent assay (ELISA), Radio immunoassay (RIA), Gas chromatography-mass spectrometry and electrochemical methods (Kumari, Rastogi, Singh, Singh, & Sinha, 2008).

The main drawback of these methods is that they are not able to distinguish between SSDs and DSBs. As a result we can take both populations (DSBs and SSBs) as one subpopulation. Therefore we can consider $m = 2$. Subsequently the tumor population is divided into two subpopulations cells without DNA fragmentation and cells with DNA fragmentation (SSBs and DSBs).

4.1.1 Stability Analysis

Based on Equation (2.2.2), the matrix A in the system (2.2.1) is defined as below

$$A(q,r) = \begin{bmatrix} 2(q-1)^2 - 2qr(q-1) - 1 & -r(q-1) \\ 2q(q-1)(r-1) & (q-1)(r-1) - 1 \end{bmatrix} \tag{4.1.1}$$

where $0 \leq q, r \leq 1$.

Theorem 4.1.1. *Suppose that the matrix A is defined as Equation (4.1.1), and $q = 0.5$. Therefore, the system (2.2.1) is stable at equilibrium point $(0,0)^\top$ for all $0 < r < 1$.*

Proof. For $q = 0.5$

$$A = \begin{bmatrix} r/2 - 1/2 & r/2 \\ 1/2 - r/2 & -r/2 - 1/2 \end{bmatrix} \tag{4.1.2}$$

In addition:

$$\lambda_1 + \lambda_2 = -1 \tag{4.1.3}$$

And

$$\lambda_1 \, \lambda_2 = \frac{(1-r)}{4} \tag{4.1.4}$$

Therefore for any $0 < r < 1$, the eigenvalues of the matrix A have negative real part. Hence the system (2.2.1) is stable for all $0 < r < 1$. □

Theorem 4.1.2. *Suppose that $m = 2$ and the system(2.2.1)be stable for the value of $q = q_0$ and $r = r_0$. If $q_1 > q_0$, then, for $q = q_1$ and $r = r_0$ the system(2.2.1) is stable too.*

Proof. Suppose that $a(q,r) = A_{11} + A_{22}$ and $d(q,r) = det(A)$. Base on linear algebra if λ_1 and λ_2 are the eigenvalues of the matrix A then $\lambda_1 + \lambda_2 = a(q,r)$ and $\lambda_1\lambda_2 = d(q,r)$. Both eigenvalues of the matrix A have negative real part if and only if $a(q,r) < 0$ and $d(q,r) > 0$.

To proof the theorem, it is sufficient to show that for fixed value of $0 < r < 1$, the functions $a(q,r)$ and $d(q,r)$ are decreasing and increasing, respectively.

Let

$$a(q,r) = (q-1)(r-1) + 2(q-1)^2 - 2qr(q-1) - 2$$

Now suppose that r is fixed, therefore

$$\frac{da}{dq} = 4q + r - 2qr - 2r(q-1) - 5$$

By direct calculation it is very easy to show that $\frac{da}{dq} < 0$.

Figure(4.1.a) shows that this function is decreasing, where $0 < r < 1$ and $0 < q < 1$.

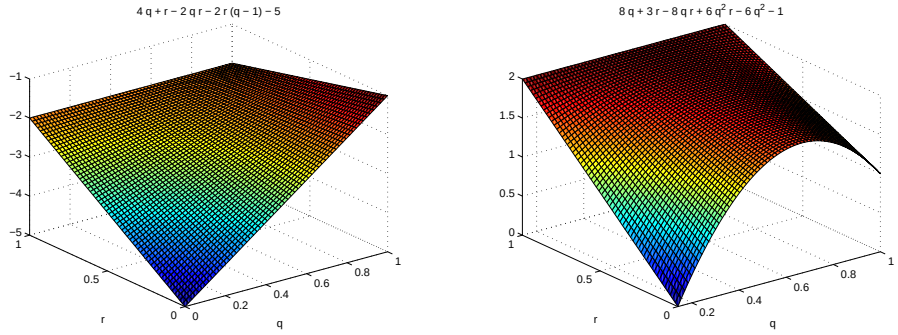

(a) The values of the function $\frac{d}{dq}(a)$ (b) The values of the function $\frac{d}{dq}(d)$.

Figure 4.1: Stability analysis in case $m = 2$.

Now let $d(q,r) = det(A)$. Therefore

$$d(q,r) = 3qr - r - q - 4q^2r + 2q^3r + 4q^2 - 2q^3$$

and

$$\frac{d}{dq}(d) = 8q + 3r - 8qr + 6q^2r - 6q^2 - 1$$

Suppose that

$$f(r) = \frac{d}{dq}(d)$$

for fixed q. therefore

$$\frac{df}{dr} = 6q^2 - 8q + 3$$

is positive for all $0 < q < 1$. So this function is increasing on the interval $[0,1]$. However

$$f = \frac{d}{dq}(d) > 0$$

if and only if $q > 0.1396$.

By plotting it is clear that $\frac{d}{dq}(d) > 0$, whether $q > 0.1396$.

As seen in Figure(4.1.b) this function is positive. Hence the function $d(q,r)$ is increasing.

Now let $q_1 > q_0$ and let the system (2.2.1) be stable for $q = q_0$. The function $a(q,r)$ is decreasing, therefore

$$a(q_1, r_0) < a(q_0, r_0) < 0 \tag{4.1.5}$$

Moreover, the function $d(q,r)$ is increasing. Subsequently,

$$d(q_1, r_0) > d(q_0, r_0) > 0 \tag{4.1.6}$$

Finally, Equations (4.1.5) and (4.1.6) show that the system (2.2.1) is also stable for $q = q_1$ and $r = r_0$. □

As a result of Theorem (4.1.1) and Theorem (4.1.2) it is clear that:

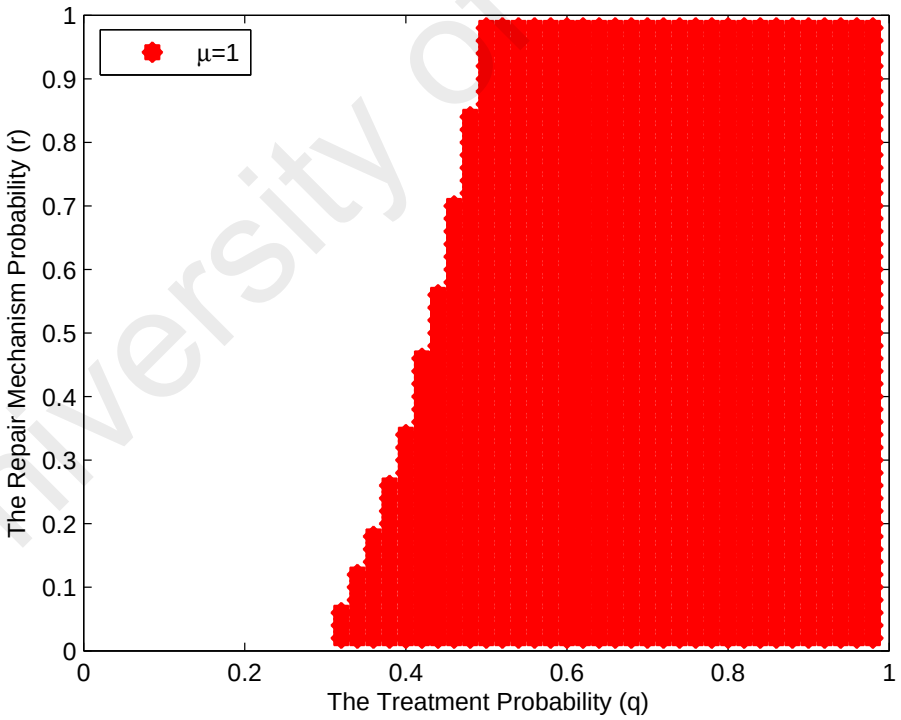

Figure 4.2: Stability Analysis For $m = 2$. Red area represents the system stability region.

Theorem 4.1.3. *For $m = 2$, the system (2.2.1) is stable, where $q \geq 0.5$ and $0 < r < 1$.*

Theorem 4.1.4. *Suppose that S denotes the set of values q such that the system* (2.2.1) *is stable corresponding to all* $0 < r < 1$. *Therefore:*

$$\inf_{q} A = 0.5 \tag{4.1.7}$$

Proof. By Theorem(4.1.3) $S \neq \emptyset$. Suppose that $m = 2$, therefore the matrix A in the system (2.2.1) is defined as in equation (4.1.1).

For small positive h:

$$A(0.5-h,r) = \begin{bmatrix} 2(-h-0.5)^2 - 2r(0.5-h)(-0.5-h) - 1 & -r(-h-0.5) \\ 2(0.5-h)(-h-0.5)(r-1) & (-0.5-h)(r-1) - 1 \end{bmatrix} \tag{4.1.8}$$

if λ_1 and λ_2 are the eigenvalues of matrix A in Equation (4.1.8), therefore:

$$\begin{aligned} \lambda_1 + \lambda_2 &= 3h - hr - 2h^2 r + 2h^2 - 1 \\ &= 2h^2(1-r) + h(1-r) + 2h - 1 \end{aligned} \tag{4.1.9}$$

In addition

$$\begin{aligned} \lambda_1 \lambda_2 &= \det(A) \\ &= (2h^3 + h^2 + 0.5h + 0.25)(1-r) - 2h \end{aligned} \tag{4.1.10}$$

Suppose that $r \to 1^-$. Subsequently,

$$\lambda_1 + \lambda_2 < 0 \tag{4.1.11}$$

and

$$\lambda_1 \lambda_2 < 0 \tag{4.1.12}$$

Therefore eigenvalues have different signs.

As a result the system is unstable at this equilibrium point $(0,0)$. Theorem (4.1.3) completes the proof. □

Corollary 4.1.1. *For any $\varepsilon > 0$ there exist $r_0 = 1 - \varepsilon$ such that the system $\dot{\mathbf{x}} = A(q_0, r_0)\mathbf{x}$ is unstable at equilibrium point $\mathbf{0}$, where $q_0 = 0.5 - \varepsilon$.*

Suppose that $m = 2$, $\mathrm{x} = (x_0, x_1)^\top$ and A is the matrix shown in Equation(4.1.1). As seen in figure (4.2) the system is stable for $q = 0.5$ and $r = 0.1$ and unstable for $q = 0.3$ and $r = 0.1$.

First suppose that $q = 0.5$ and $r = 0.1$. Therefore:

$$A(q,r) = \begin{bmatrix} -0.4500 & 0.0500 \\ 0.4500 & -0.5500 \end{bmatrix} \tag{4.1.13}$$

and the eigenvalues of the matrix A are

$$\lambda_1 = -0.3419$$

and

$$\lambda_2 = -0.6581$$

It is verified by figure (4.3).a that the system is stable at equilibrium point $(0,0)$.

Now let $q = 0.3$ and $r = 0.1$. Here :

$$A(q,r) = \begin{bmatrix} 0.0220 & 0.0700 \\ 0.3780 & -0.3700 \end{bmatrix} \tag{4.1.14}$$

Here

$$\lambda_1 = 0.0807$$

and

$$\lambda_2 = -0.4287$$

are the eigenvalues correspond to the matrix A. Figures (4.5) and (4.6) show that how the system is unstable at equilibrium point $(0,0)$.

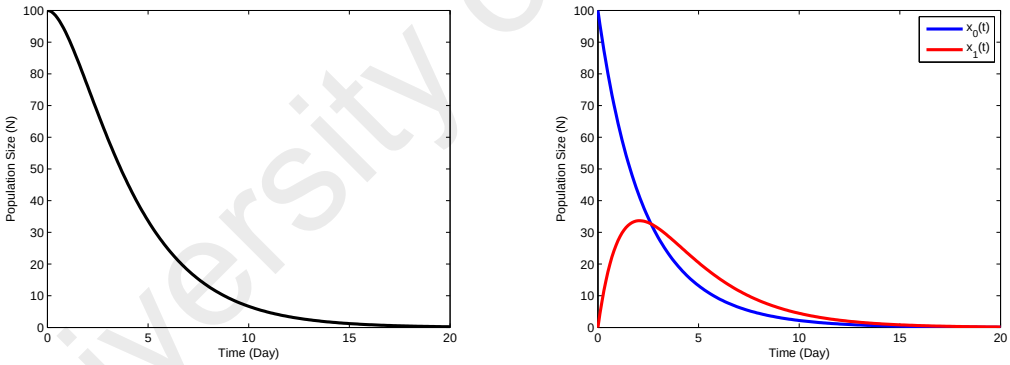

(a) Whole the Tumor (b) Subpopulations

Figure 4.3: The Dynamics of The Population Size where m=2, q=0.5, and r=0.1 (Stable Case)

4.1.2 Bifurcation Analysis

In this section we will show that how the change in the parameters of the model is influencing the lifespan.

1. Figures(4.7 -4.9) show the stability region of the system when the value of parameter μ is changed.

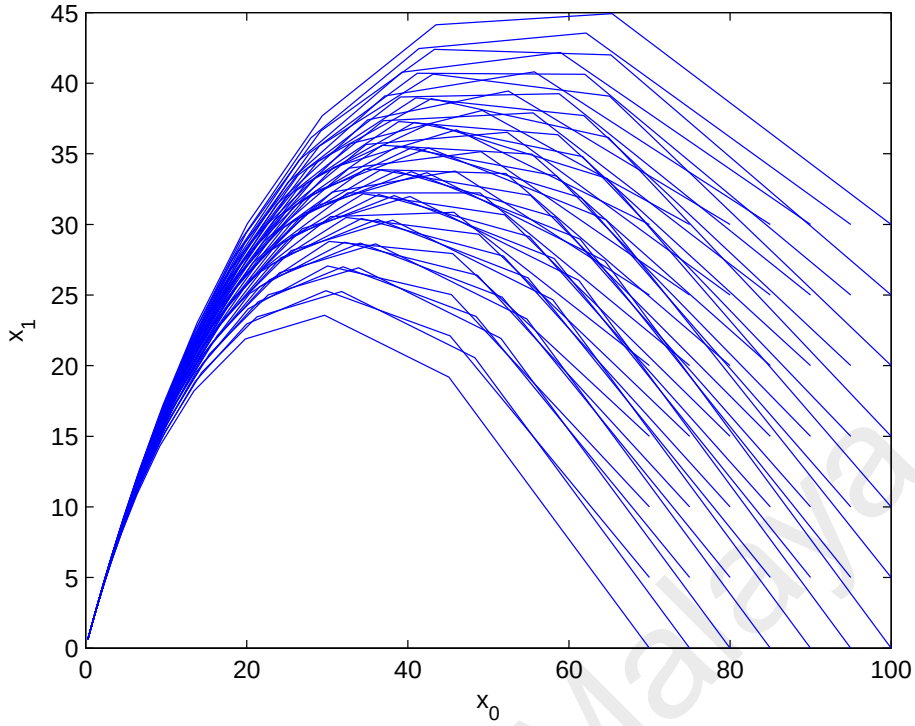

Figure 4.4: Trajectories where the system is stable. The number of targets are supposed to be two in each cell.

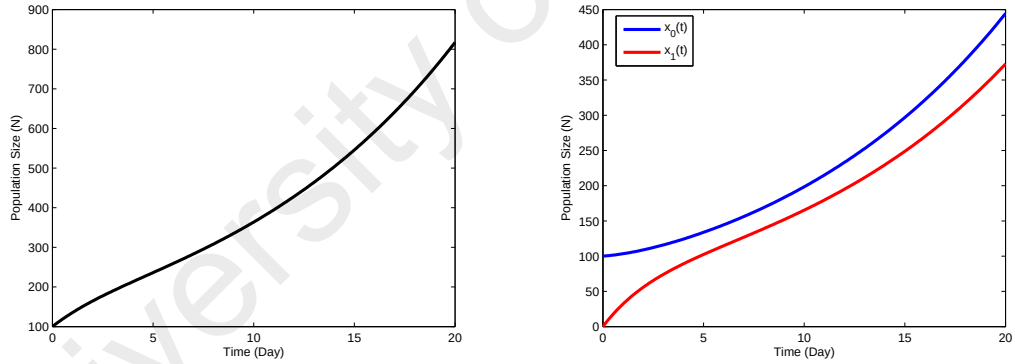

(a) Whole the Tumor (b) Subpopulations

Figure 4.5: The Dynamics of The Population Size where $m = 2$, $q = 0.3$, and $r = 0.1$ (Unstable Case).

a) Figure (4.7) shows a big difference among the stability region of the system, for $m = 2$ where $\mu = 0.1$, $\mu = 0.5$, and $\mu = 1$.

b) The same results are shown where $m = 5$ in Figure (4.8).

c) Despite the cases (1a) and (1b), the difference among stability regions for $m = 10$ is insignificant [Figure(4.9)]. Therefore, it can be inferred that the parameter μ is not an influential parameter when the number of targets are

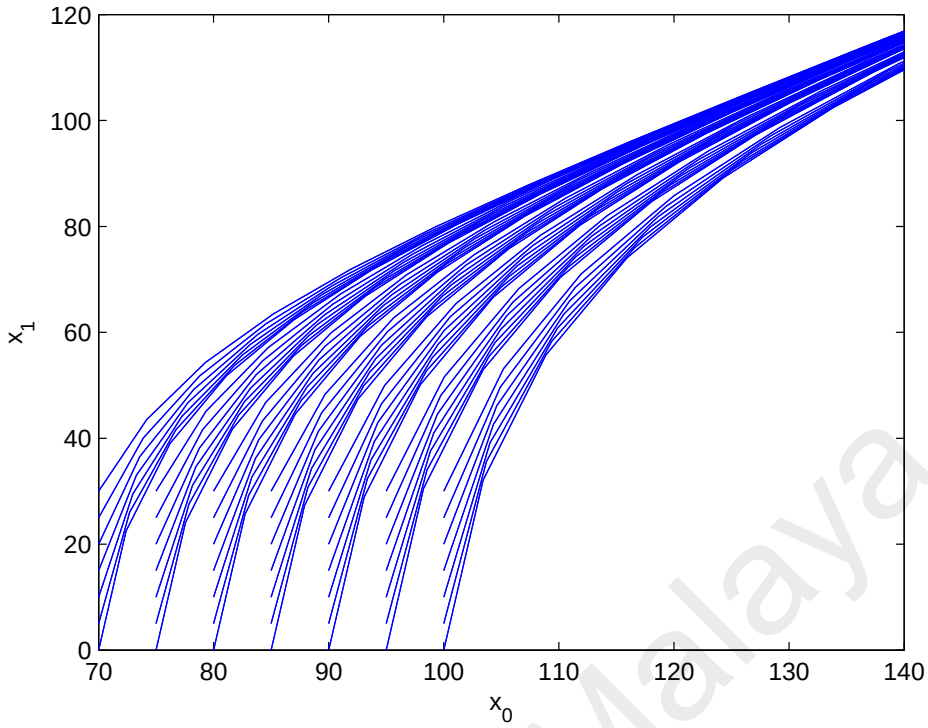

Figure 4.6: Trajectories where the system is unstable. The number of targets are supposed to be two in each cell.

greater than 10.

2. As seen in Figures (4.10) and (4.11), the stability region experiences significant change if the number of targets varies from $m = 4$ to $m = 50$. However, for big values of m, the stability region is changing slightly (Figure(4.11)).

   For instance, stability regions corresponding to $m = 10$ and $m = 20$ are different in only one point. In contrast, the difference in the stability region corresponding to $m = 4$ and $m = 2$ cases are significant.

   As a result we can imply that for low values of m there are quit different stability area, however, for high values m, the stability areas are the same.

3. The next parameter of the model is the probability that a cell gives birth after the application of a dose fraction (μ).

   First, suppose that $m = 2$, $q = 0.6$. The effect of parameter μ on the tumor lifespan (L) are shown in Figure (4.12), in which the initial number of cells varies among

$n_0 = 10^3, 10^7$ and 10^{10}. The blue and red solid lines show the tumor lifespan, when the parameter $0 \leq r \leq 1$ corresponding to $\mu = 0.1$ and $\mu = 1$, respectively.

4. Now suppose that $q = 0.6$, $n_0 = 10^7$ and $\mu = 1$. Figure (4.13) represents the influence of parameter m on the tumor lifespan (L).

   The blue and red solid lines are corresponding to the values $\mu = 0.1$ and $\mu = 1$ in which m changes among 3, 5 and 7. As seen, the tumor lifespan corresponding to different values of μ are almost the same if m if large enough (for instance $m = 7$).

5. For fixed values of $q = 0.8$, and $n_0 = 10^3$, the tumor lifespan remains unchanged for $m = 2$ and $m = 3$. (Figure (4.14)).

   In addition, for $m = 6$, and $m = 7$, the changes in the tumor lifespan is insignificant (Figure (4.15)). However, A big gap in the tumor lifespan is visible, for $m = 2$, and $m = 7$ and $0.3 \leq r \leq 1$.

6. As seen in (Figure (4.14), (4.15)), the lifespan corresponding to the values of $q = 0.8$, and $m = 2$ is fairly similar to the tumor lifespan associated with $q = 0.9$, and $m = 7$. This shows that, although the repair mechanism (r), and the number of a cell's target (m), are important in this model, controlling the parameter (q) is the most important model parameter.

7. Now, suppose that $m = 2$, and $n_0 = 10^3$. For low, middle, and high values of the repair mechanism probability, if $q = 0.5$, the tumor lifespan changes between 30 and 130. However, for $q \geq 0.6$ the changes in the values of repair mechanism parameter (r), affect the tumor lifespan insignificantly(Figure (4.16)).

8. Suppose that $m = 2$, and $n_0 = 10^3$. However the system (2.2.1) is stable, when $q = 0.5$, this value of (q) is not suitable (Figure (4.17)). In addition, the tumor

lifespan stabilizes and it is constant for $q = 0.6$ and $q = 0.8$, respectively.

9. Finally, it is clear that the treatment parameter (q) is more important than the repair mechanism parameter (r), because if we can control the treatment parameter in an acceptance range of $0.8 \leq q \leq 1$ then the tumor lifespan will be stabilized for any value of the repair mechanism value r, and as a result, treatment process will be more effective.

10. Table (4.1) shows the change of tumor lifespan (L) for a fixed value of $n_0 = 10^3$ and a small value of r ($r = 0.3$) corresponding to the different values of parameters q and m. The tumor lifespan clearly stabilizes when $q \geq 0.8$.

11. In contrast, Table (4.2) shows the variation in tumor lifespan for a fixed value of $n_0 = 10^3$ and large value of r ($r = 0.9$) and different values of parameters q and m.

As seen before the $q = 0.5$ is not a suitable value for the treatment parameter. In Figures ((4.18), (4.19)), the 3-D simulation of the tumor lifespan for $q \geq 0.6$, and $0 \leq r < 1$ for two values $m = 2$, $m = 6$ are represented, respectively.

Moreover, we compare the values of L corresponding to different values of $0.6 \leq q \leq 1$ and $0 \leq r \leq 1$ for $m = 2$ and $m = 6$ in Figure (4.20).

Finally, 3-D stability region of the system (2.2.1) where $m = 2,5$ and $m = 10,20$ and $\mu = 1$ in Figures (4.21) and (4.22), respectively.

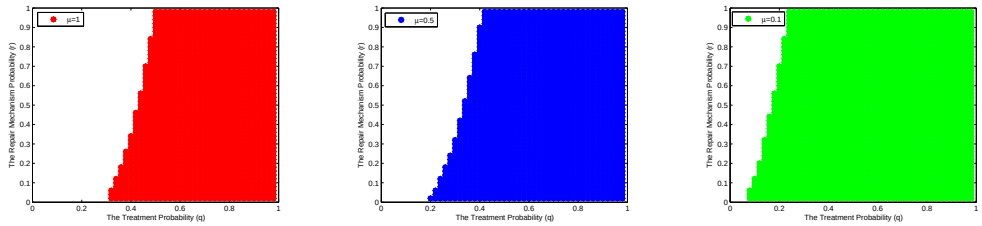

(a) $\mu = 1$ (b) $\mu = 0.5$ (c) $\mu = 0.1$

Figure 4.7: Stability Region Where $m = 2$

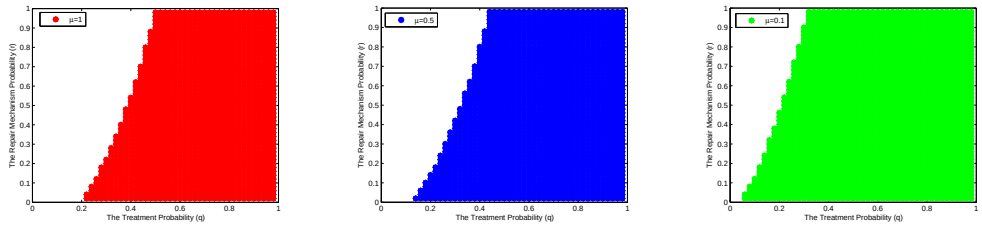

(a) $\mu = 1$ (b) $\mu = 0.5$ (c) $\mu = 0.1$

Figure 4.8: Stability Region Where $m = 5$

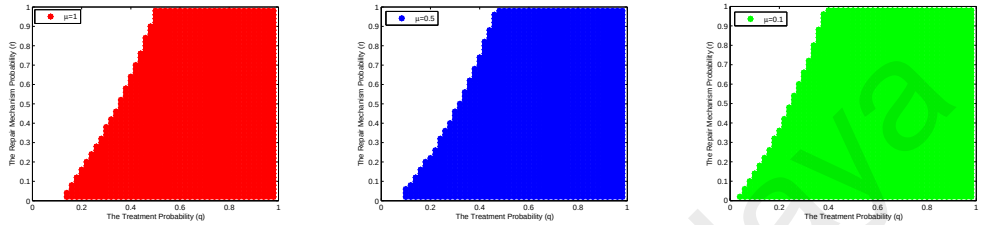

(a) $\mu = 1$ (b) $\mu = 0.5$ (c) $\mu = 0.1$

Figure 4.9: Stability Region Where $m = 10$

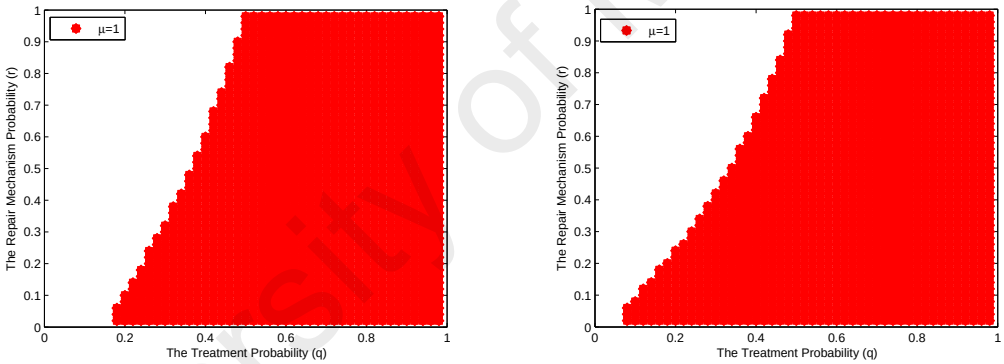

(a) $m = 4$ (b) $m = 10$

Figure 4.10: Stability Region where $m = 4$ and $m = 10$

4.2 Single-Strand Break (SSB) and Double-Strand Breaks (DSBs) as two subpopulations

Ionizing radiation not only causes Double-Strand Breaks (DSBs) but also a substantial extent of DNA base lesions which is called Single-Strand Breaks (SSBs) (Khoronenkova & Dianov, 2015; Vilenchik & Knudson, 2000). One Gray of irradiation will produce roughly 10^5 ionizations, 1000 DNA base damages, 1000 single-strand DNA breaks (SSBs) and 20 to 40 double-strand DNA breaks (DSBs) (Joiner & van der Kogel, 2009).

Specialized repair systems have consequently progressed to detect and repair base dam-

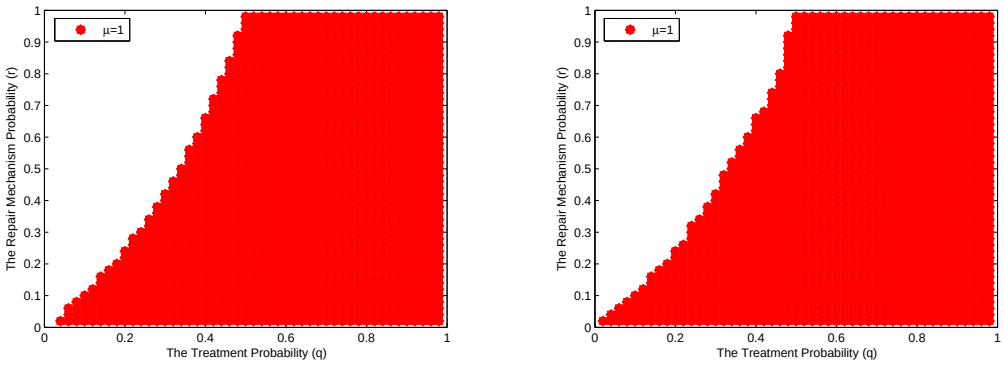

(a) $m = 20$. (b) $m = 50$

Figure 4.11: Stability Region where $m = 20$ and $m = 50$

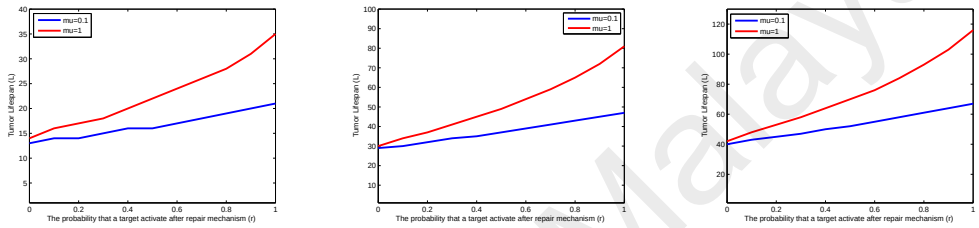

(a) $n_0 = 10^3$ (b) $n_0 = 10^7$ (c) $n_0 = 10^{10}$

Figure 4.12: Influence of μ on the tumor lifespan in case $m = 2$.

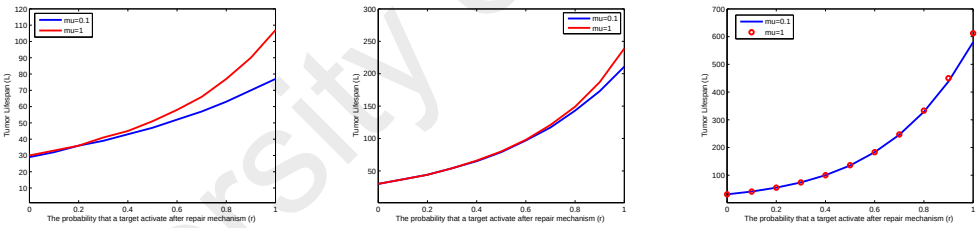

(a) $m = 3$ (b) $m = 5$ (c) $m = 7$

Figure 4.13: Influence of μ on the tumor lifespan in case $q = 0.6$ and $n_0 = 10^7$.

age, i.e. base excision repair (BER), and single-strand breaks, i.e. single-strand break repair (SSBR). SSBR is closely associated with BER. Single-strand breaks can result in DSB development by two means. The first way, ionizing radiation damage frequently takes place in groups, and subsequently, a number of SSBs will also exhibit damage to neighboring DNA bases.

During base damage repair via BER, SSBs form temporarily. Upon the strand opposite a radiation-induced SSB incurring base damage, the break created temporarily during BER may join the radiation break on the opposite strand, resulting in a DSB.

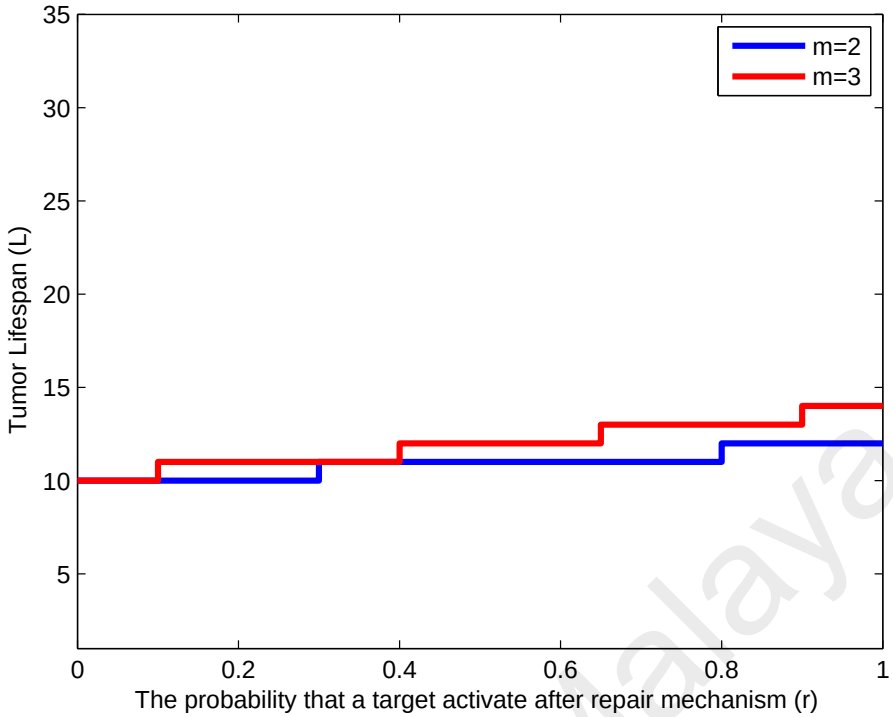

Figure 4.14: Compare the lifespan trend for $m = 2$ and $m = 3$, where $q = 0.8$ and $n_0 = 10^3$.

Table 4.1: Influence of the parameters q, m on the Tumor Lifespan L, where $n_0 = 10^3$ and $r = 0.3$.

q/m	2	3	4	5	6	7
0.6	18	18	21	24	28	33
0.7	13	14	15	17	19	21
0.8	11	11	12	13	14	15
0.9	9	9	10	10	10	11

The second way is if an SSB has come upon a replication fork in the S phase, and if the fork and single-ended DSB will disintegrate (Joiner & van der Kogel, 2009).

Mutations, genomic instability, and cell death can result from failing to mend DNA breaks like DSBs. Due to the critical effects of DSBs, cells have developed homologous recombination (HR) and non-homologous end joining (NHEJ) as two principal repair mechanisms (Ohnishi, Mori, & Takahashi, 2009).

In the course of HR, a double-strand break may transform into a single strand break, because the single-strand DNA production is essential for HR (Joiner & van der Kogel,

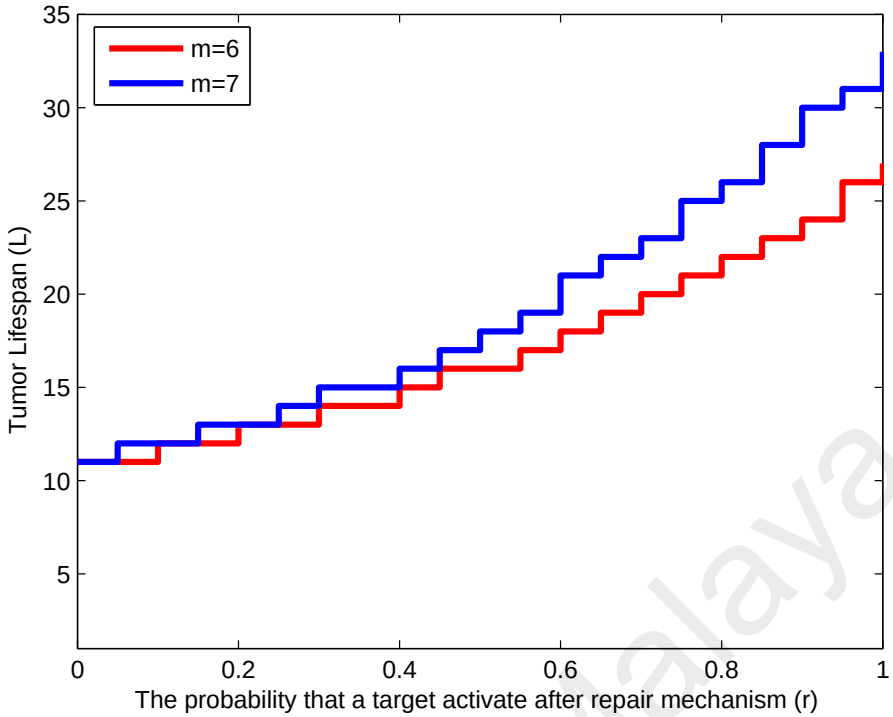

Figure 4.15: Compare the lifespan trend for $m = 6$ and $m = 7$, where $q = 0.9$ and $n_0 = 10^3$.

Table 4.2: Influence of the parameters q, m on the Tumor Lifespan L, where $n_0 = 10^3$ and $r = 0.9$.

q/m	2	3	4	5	6	7
0.6	31	39	54	81	124	193
0.7	17	21	27	54	50	69
0.8	12	14	16	27	24	30
0.9	9	10	11	16	13	14

2009).

4.2.1 Stability Analysis

After applying a dose fraction, a generic, realistic assumption is that cells have only four possibilities of: not being affected by radiation particles (cells in subpopulation x_0), incurring single-strand breaks (cells in subpopulation x_1), incurring double-strand breaks (cells in subpopulation x_2), or dying. In this regard, we study a system with three targets, $m = 3$.

We examine the stability of the system reproduced by Equation (2.2.1) for a parameter

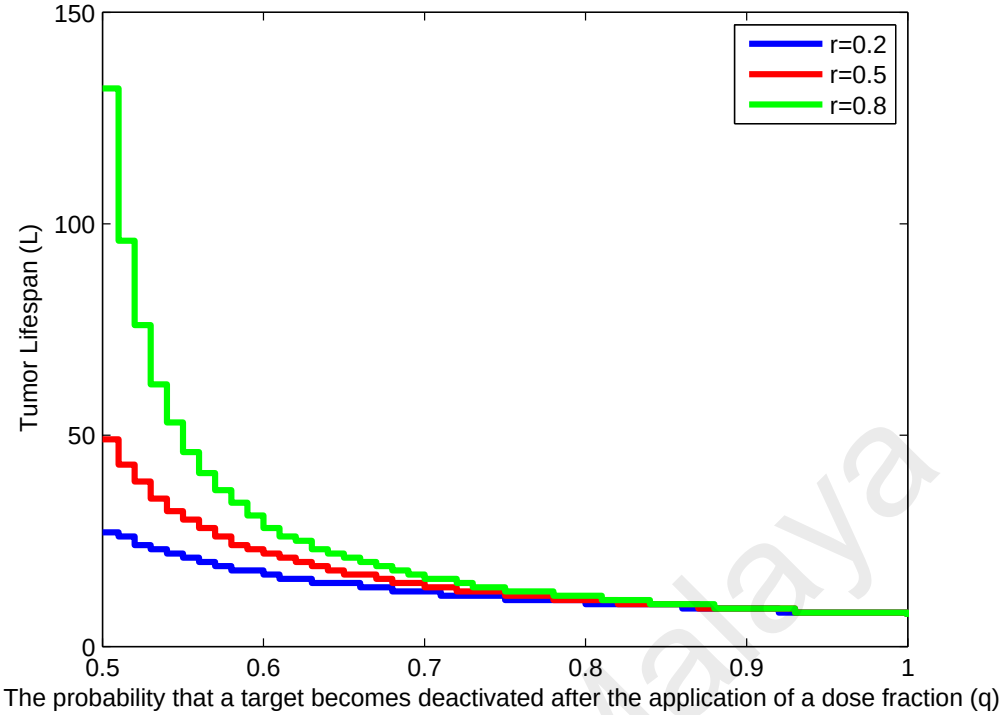

Figure 4.16: The influence of the repair mechanism probability (r) on the tumor lifespan where $m = 2$ and $n_0 = 10^3$.

value of $\mu = 1$, and $m = 3$.

In this case, Equation (2.2.1) is reduced to:

$$\begin{aligned}
\frac{dx_0(t)}{dt} &= [\Pi(0,0) + \mu(1-q)^3 - 1]x_0(t) + \Pi(1,0)x_1(t) + \Pi(2,0)x_2(t) \\
\frac{dx_1(t)}{dt} &= \Pi(0,1)x_0(t) + [\Pi(1,1) - 1]x_1(t) + \Pi(2,1)x_2(t) \\
\frac{dx_2(t)}{dt} &= \Pi(0,2)x_0(t) + \Pi(1,2)x_1(t) + [\Pi(2,2) - 1]x_2(t)
\end{aligned} \tag{4.2.1}$$

with the initial condition $\mathrm{x}(0) = (n_0, 0, 0)$.
Now, suppose that A denotes the coefficient matrix of system (4.2.1) as follows:

$$A(q,r) = \begin{bmatrix}
[3qr(q-1)^2 - 2(q-1)^3 - 3q^2r^2(q-1)] - 1 & r(q-1)^2 - 2qr^2(q-1 & -r^2(q-1) \\
3q^2r(2r-2)(q-1) - 3q(q-1)^2(r-1) & [2qr(2r-2)(q-1) - (q-1)^2(r-1)] - 1 & r(2r-2)(q-1) \\
-3q^2(q-1)(r-1)^2 & -2q(q-1)(r-1)^2 & -[(q-1)(r-1)^2] - 1
\end{bmatrix} \tag{4.2.2}$$

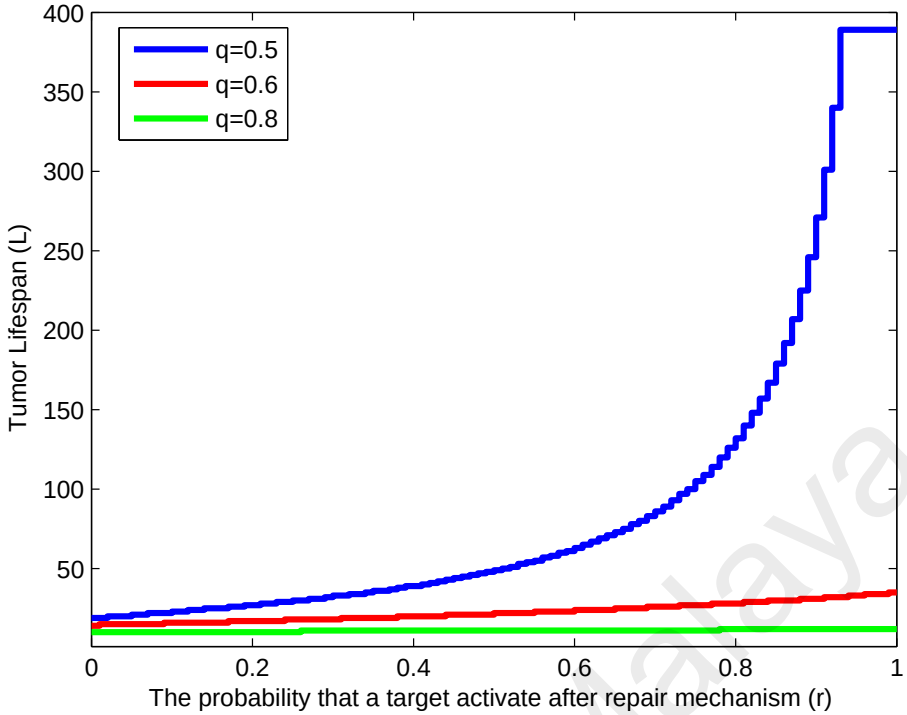

Figure 4.17: The influence of the treatment probability (q) on the tumor lifespan where $m = 2$ and $n_0 = 10^3$.

$$M = \begin{bmatrix} (1-q)^m & \binom{m}{1} q\,(1-q)^{m-1} & \dots & q^m \\ 0 & (1-q)^{m-1} & \dots & q^{m-1} \\ . & . & . & . \\ . & . & . & . \\ . & . & . & . \\ 0 & 0 & \dots & q \\ 0 & 0 & \dots & 1 \end{bmatrix}$$

We use the Routh-Hurwitz criterion for A (which is described in Theorem (2.2.2)) to prove the stability result.

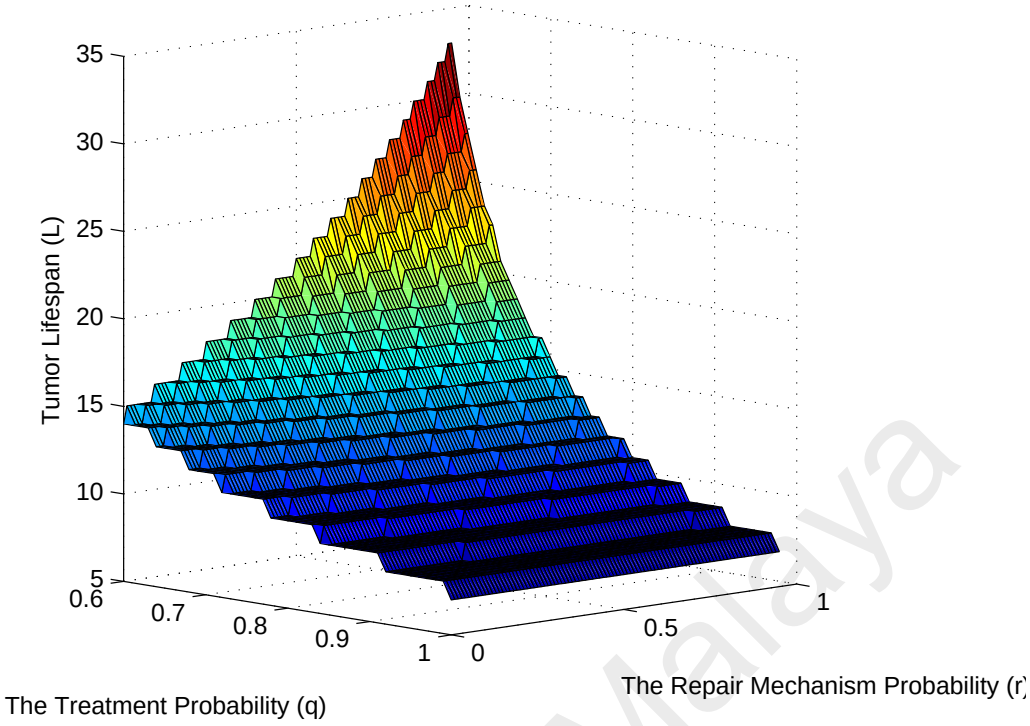

Figure 4.18: The tumor Lifespan where $m = 2$, $n_0 = 10^3$, $0.6 \leq q \leq 1$, and $0 \leq r \leq 1$.

Theorem 4.2.1. *Suppose that*

$$P(\lambda) = \lambda^3 + a_1\,\lambda^2 + a_2\,\lambda + a_3$$

represents the characteristic polynomial of a matrix $A_{3\times 3}$. *The system* $\dot{x} = A\,x$ *is stable if and only if:*

$$a_1 > 0, \quad a_3 > 0, \quad a_1 a_2 > a_3 \tag{4.2.3}$$

Theorem 4.2.2. ***(Stability result)**: System* (4.2.1) *is stable for all values of* $0 < r < 1$ *and* $q = 0.5$.

Proof. Let $P(\lambda)$ be the characteristic polynomial of matrix A. By using the Routh-Hurwitz criterion,, system (4.2.1) is stable if and only if:

$$a_1 > 0, \quad a_3 > 0, \quad a_1 a_2 > a_3 \tag{4.2.4}$$

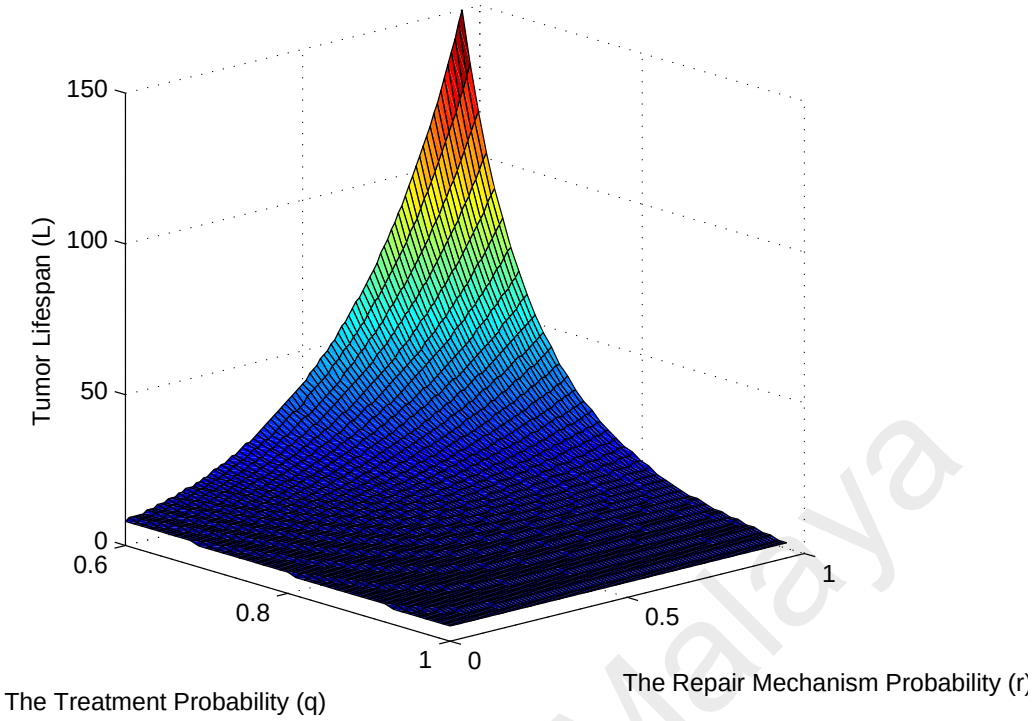

Figure 4.19: The tumor Lifespan where $m = 6$, $n_0 = 10^3$, $0.6 \leq q \leq 1$, and $0 \leq r \leq 1$.

The characteristic polynomial of matrix A for $q = 0.5$ is written as:

$$P(\lambda) = \lambda^3 + \frac{1}{8}(r^2 - r + 4)\lambda^2 + \frac{1}{32}(-r^3 + 7r^2 - 16r + 42)\lambda + \frac{9}{32}(1 - r) \qquad (4.2.5)$$

It is clear that $a_1 > 0$ and $a_3 > 0$. Therefore, it is sufficient to show that $a_1 a_2 > a_3$ for $0 < r < 1$. Considering

$$g(r) = a_1 a_2 - a_3 = \frac{1}{256}(-r^5 + 8r^4 - 39r^3 + 170r^2 - 226r + 600) \qquad (4.2.6)$$

It can be verified that $g(r) > 0$ for $0 < r < 1$ (see Fig. (4.23) (a)). Therefore, the Routh–Hurwitz criterion is satisfied. □

Theorem 4.2.3. *For $q < 0.5$, there exists $0 < r < 1$, such that system (4.2.1) is unstable at the equilibrium point $(0,0,0)$.*

Proof. Suppose that $h > 0$ is an arbitrary real number. Corresponding to $q = 0.5 - h$ and

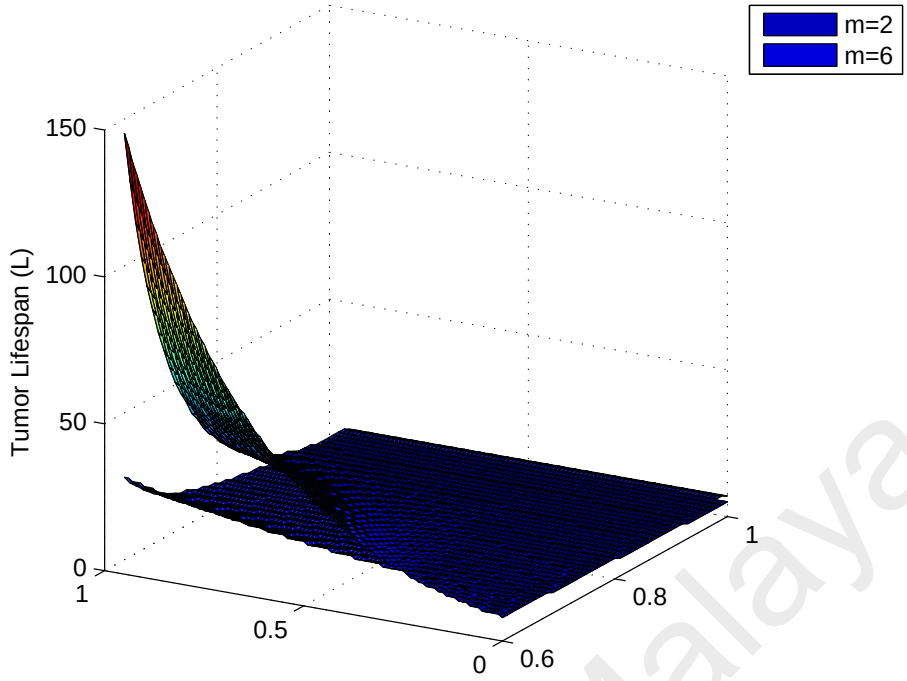

Figure 4.20: Comparing the tumor lifespan where $m = 2$ and $m = 6$.

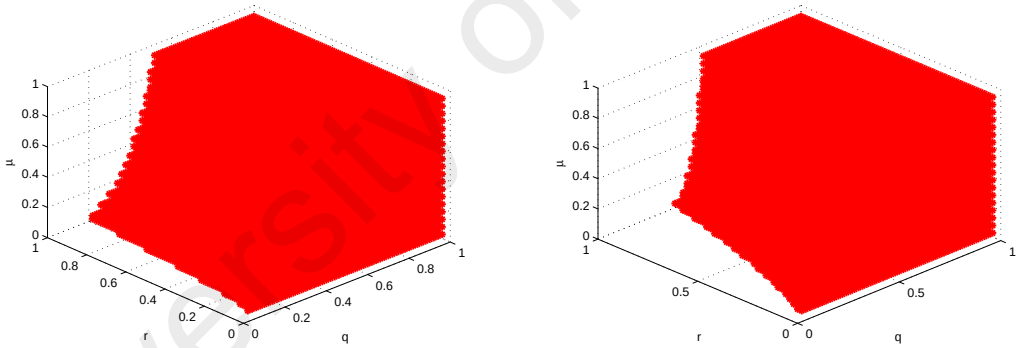

(a) $m = 2$. (b) $m = 5$

Figure 4.21: 3-D stability region.

$r = 1 - h$,

$$P(\lambda) = \lambda^3 + a_1\lambda^2 + a_2\lambda + a_3 \tag{4.2.7}$$

represents the characteristic polynomial of the coefficient matrix in ODE system (4.2.1), where

$$a_3 = -\frac{h}{32}(64h^8 + 96h^7 + 32h^6 - 80h^5 + 52h^4 - 74h^3 + 4h^2 - 18h + 39) \tag{4.2.8}$$

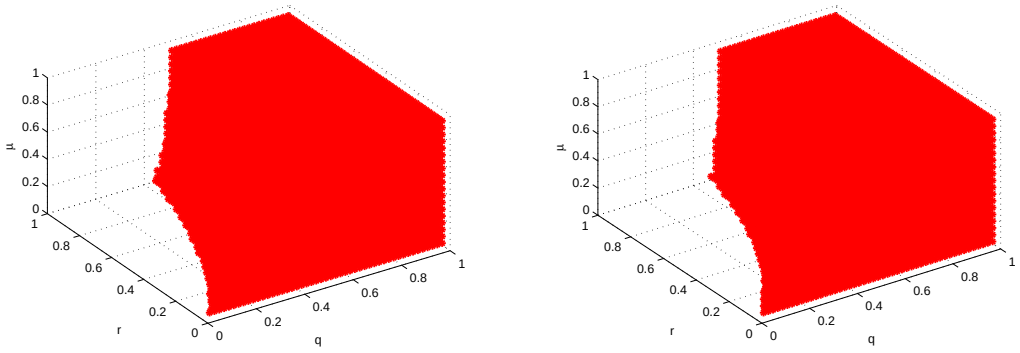

(a) $m = 10$. (b) $m = 20$

Figure 4.22: 3-D stability region.

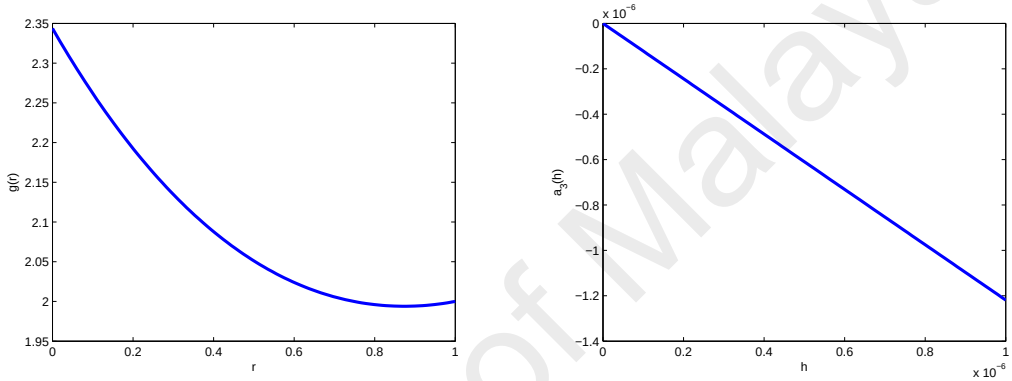

(a) Graph of $g(r)$ for $0 < r < 1$. (b) Values of a_3 where $0 < h < 10^{-6}$

Figure 4.23: Stability analysis.

Based on the Routh-Hurwitz criterion, the ODE system (4.2.1) is stable at $(0,0,0)$ if and only if:

$$a_1 > 0$$

$$a_3 < a_1 a_2$$

$$a_3 > 0 \tag{4.2.9}$$

But $a_3 < 0$ for all $h > 0$ (Fig. (4.23) (b)) because $a_3(0) = 0$ and $a_3(h)$ is a decreasing function on $[0,1]$. Hence:

$$a_3(h) < 0 \tag{4.2.10}$$

Therefore system (4.2.1) is unstable at the equilibrium point $(0,0,0)$. □

The following corollary is a direct result of Theorem (4.2.3).

Corollary 4.2.1. *Suppose that S denotes the set of all values q such that system* (4.2.1) *is stable at equilibrium point* $\mathbf{0} \in \mathbb{R}^3$ *corresponding to all* $0 < r < 1$. *Then:*

$$\inf_q S = 0.5 \tag{4.2.11}$$

4.2.2 Numerical simulation: Lifespan and bifurcation analysis

In this section, we study the influence of system parameters on lifespan and also provide a numerical bifurcation analysis of the ODE system (4.2.1). This is a linear system with three parameters, q, r and n_0. The numerical simulations were carried out using the MATLAB software package.

4.2.2 (a) Parameters' influence on the lifespan

Based on the tumor lifespan definition provided in Equation (4.52), we demonstrate that parameter q has the highest impact on the lifespan.

Figure (4.24) shows the effect of parameter μ on the tumor lifespan for $r = 0.2$, which is similar to the result in (Keinj et al., 2012). Figure (4.25) depicts the effect of parameter μ on the tumor lifespan for different initial condition values: $n_0 = 10^3,\ 10^7$ and 10^{10}. The blue solid line and red dash line represent the tumor lifespan corresponding to $\mu = 0.1$ and $\mu = 1$, respectively. In this case, it is clear that when μ changes from 0.1 to 1 there is a slight change in tumor lifespan (L).

Table (4.3) shows the variation in the tumor lifespan for the fixed value of $n_0 = 100$ and different values of parameters q and r. The tumor lifespan is clearly stabilized for $q \geq 0.8$.

This result emphasizes that the effect of parameter q on tumor lifespan is more dominant

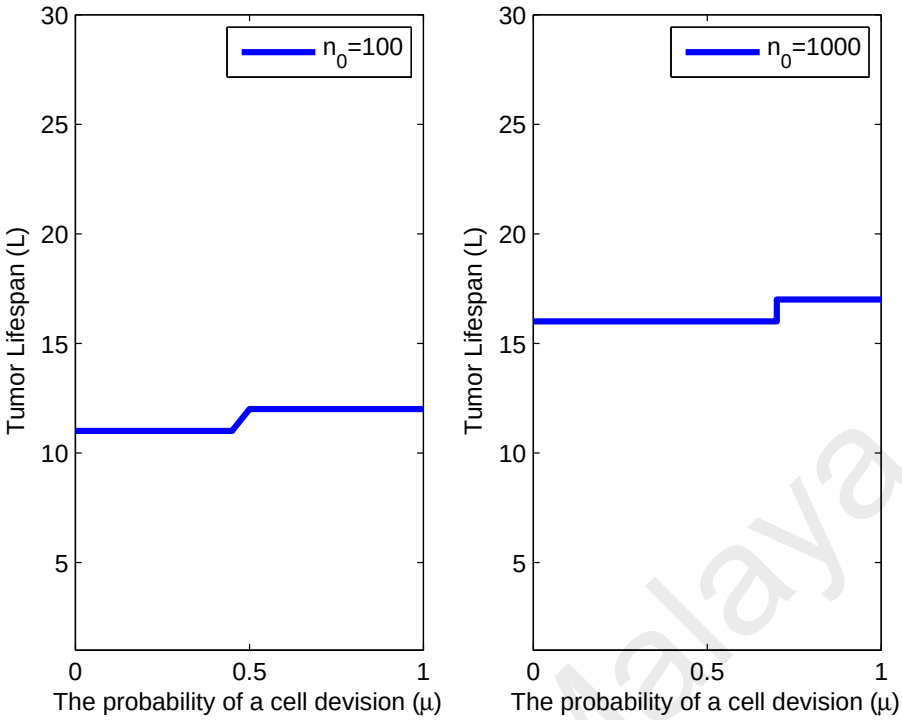

Figure 4.24: The influence of parameter μ on tumor lifespan for $q = 0.6$ and $r = 0.2$. (a) $n_0 = 100$, (b) $n_0 = 1000$.

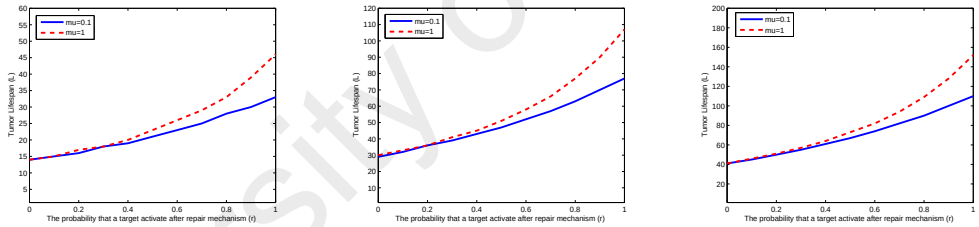

(a) $n_0 = 10^3$ (b) $n_0 = 10^7$ (c) $n_0 = 10^{10}$

Figure 4.25: Influence of μ on tumor lifespan where n_0 changes from 10^3 to 10^{10} when $q = 0.6$ and $0 < r < 1$.

than the other parameters (see Figure (4.26)). In addition, corresponding to the fixed parameter value $q = 0.9$, the tumor lifespan changes are insignificant for $0 < r < 1$ and $10^2 < n_0 < 10^5$ (see Table (4.4)). The variations in tumor lifespan (L) with respect to the changes in the initial tumor cell numbers, n_0, are depicted in Figure (4.27) and are in very good agreement with the results in (Keinj et al., 2012).

Table 4.3: Influence of parameters (q) and (r) on the tumor lifespan (L) for $n_0 = 100$.

$q \diagdown r$	0.1	0.2	0.3	0.4	0.5	0.6	0.7	0.8
0.5	14	16	19	23	28	36	50	77
0.6	11	12	13	14	16	17	20	23
0.7	9	9	10	10	11	11	12	13
0.8	7	8	8	8	8	8	9	9
0.9	6	6	6	6	7	7	7	7

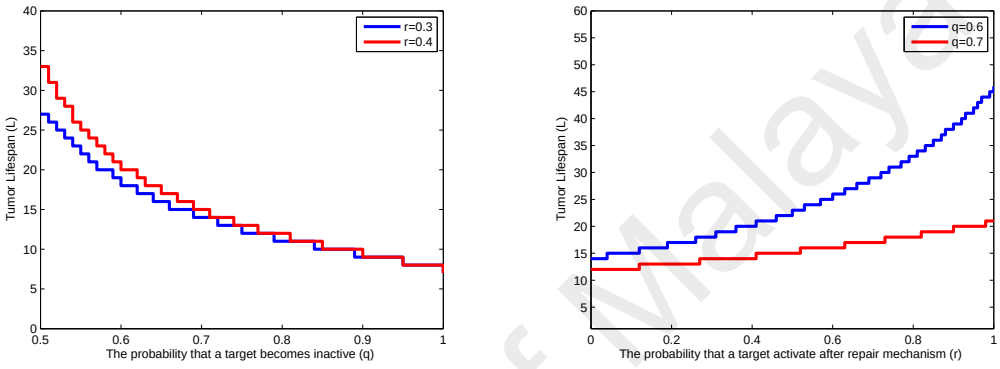

(a) (b)

Figure 4.26: (a) Influence of inactivation probability (q) on tumor lifespan (L). The blue and red solid lines represent the tumor lifespan values corresponding to $r = 0.3$ and $r = 0.4$, respectively. (b) Influence of the reactivation probability of a target after a dose fraction (r) on tumor lifespan (L). The blue and red solid lines represent the tumor lifespan values corresponding to $r = 0.3$ and $r = 0.4$, respectively

Table 4.4: Tumor lifespan for $q = 0.9$ when n_0 varies between 10^2 and 10^5.

$n_0 \diagdown r$	0.1	0.2	0.3	0.4	0.5	0.6	0.7	0.8
10^2	6	6	6	6	7	7	7	7
10^3	9	9	9	9	9	10	10	10
10^4	12	12	12	12	12	12	13	13
10^5	14	15	15	15	15	15	16	16

4.2.3 Bifurcation analysis

The system (4.2.1) is stable if all eigenvalues have negative real parts. For $q = 0.6$ and $r = 0.2$, the eigenvalues are evaluated as:

$$\lambda_1 = -0.4672,\ \lambda_2 = -0.8422,\ \lambda_3 = -0.9501 \tag{4.2.12}$$

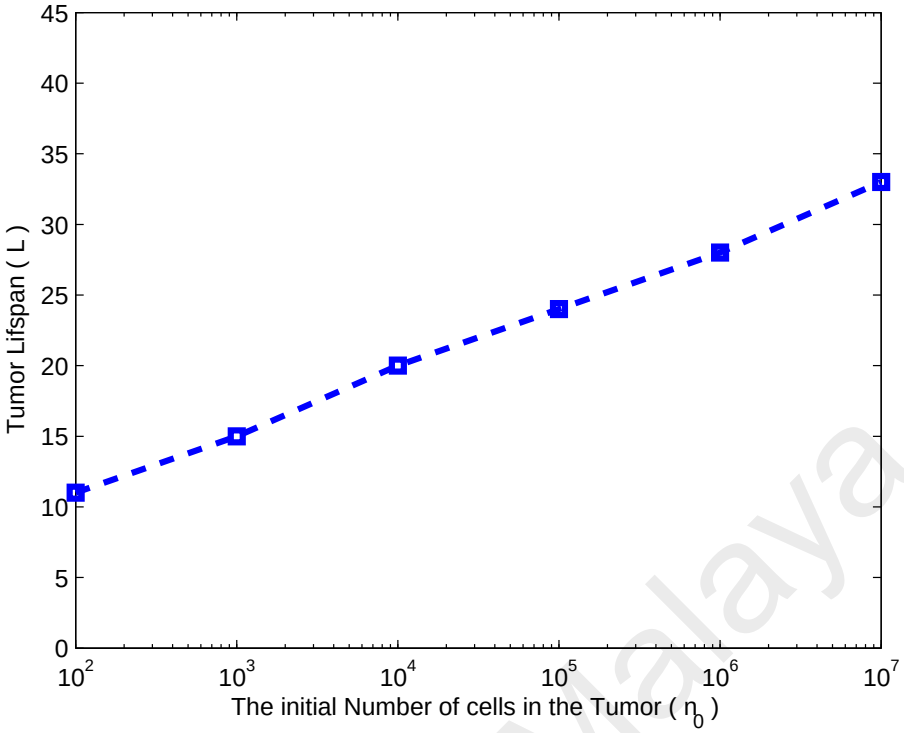

Figure 4.27: Variations in tumor lifespan (L) with respect to changes in the initial number of tumor cells (n_0) for $r = 0.1$ and $q = 0.5$.

This indicates that this system is asymptotically stable at the equilibrium point, $(0,0,0)$ (see Figure(4.28)). Also, for $q = 0.2$ and $r = 0.4$ the eigenvalues are calculated as:

$$\lambda_1 = 0.3225,\ \lambda_2 = -0.4636,\ \lambda_3 = -0.8404 \tag{4.2.13}$$

This shows that the system is unstable (see Figure(4.29)). The system phase-plane diagrams are provided in Figure(4.30).

The system parameters stability ranges for cases $\mu = 1$, $\mu = 0.5$ and $\mu = 0.1$ are depicted in Figure (4.31.a), Figure (4.31.b) and Figure (4.31.c), respectively. Here, no significant differences are observed in the stability regions of the system (4.2.1) for different values of μ.

Regarding the bifurcation value of the parameter q, we have studied several cases. The value of q is changed with different values of r. The results clearly demonstrate that the

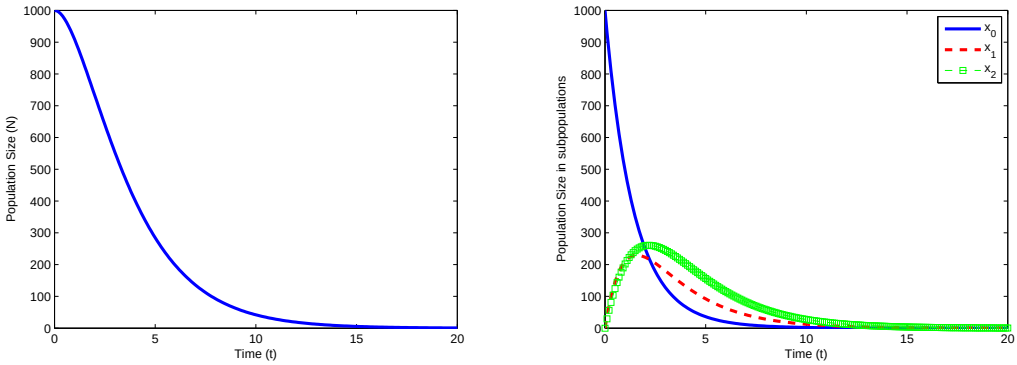

(a) Tumor (b) Subpopulations

Figure 4.28: Dynamics of all tumor cells ($N(t)$) and subpopulations $x_0(t)$, $x_1(t)$ and $x_2(t)$, for $q = 0.6$ and $r = 0.2$.

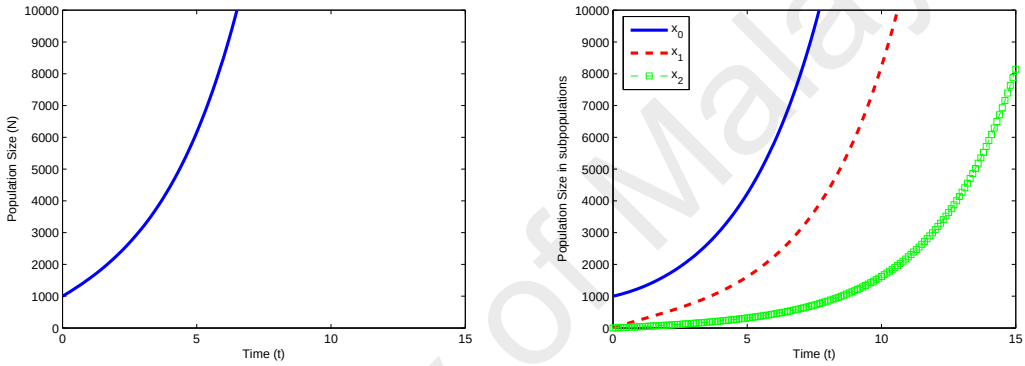

(a) Tumor (b) Subpopulations

Figure 4.29: Dynamics of all tumor cells ($N(t)$) and subpopulations $x_0(t)$, $x_1(t)$ and $x_2(t)$, for $q = 0.2$ and $r = 0.4$.

system is stable for $q \geq 0.5$ (see Figure (4.32), Figure (4.33) and Figure (4.34)).

According to the discussion provided in section (4.4.3), the system is generally stable when the Routh-Hurwitz criterion is satisfied. In this case, the three conditions of Theorem (4.2.2) can be represented as 3D graphs with respect to parameters q and r, which are depicted in Figure (4.35). A stability region is characterized by the intersection of these surfaces, is illustrated in Figure (4.36).

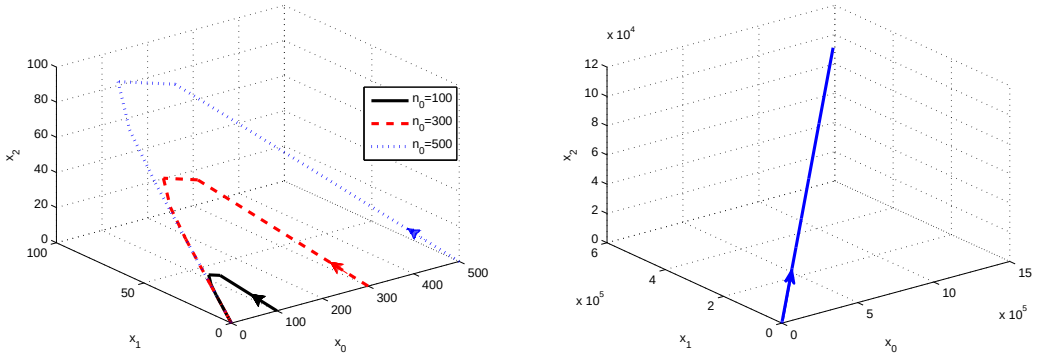

(a) Stable system (b) Unstable system

Figure 4.30: System phase diagram where (a) $(0,0,0)$ is stable for $q = 0.6$ and $r = 0.4$ (b) $(0,0,0)$ is unstable for $q = 0.2$ and $r = 0.4$.

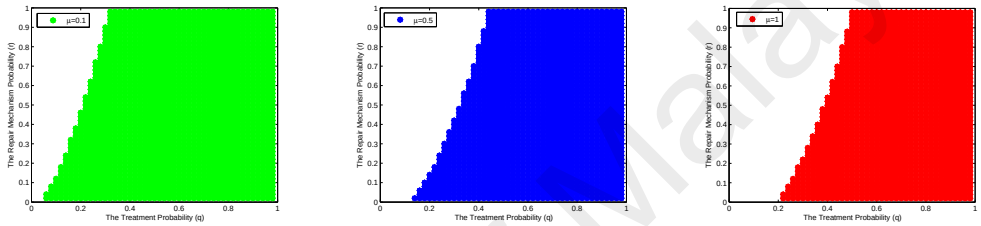

(a) $\mu = 0.1$ (b) $\mu = 0.5$ (c) $\mu = 1$

Figure 4.31: Stability region of the system(4.2.1) with respect to the values of $\mu = 0.1$, $\mu = 0.5$ and $\mu = 1$.

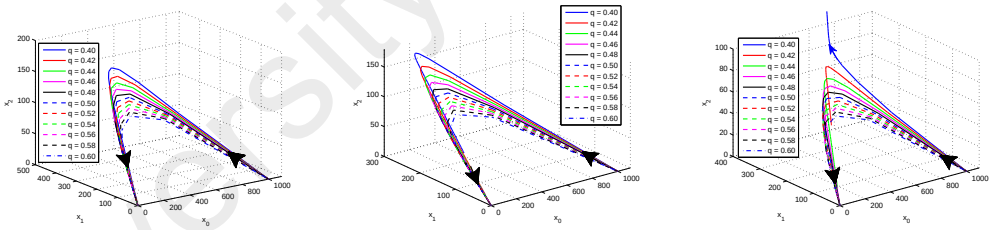

(a) $r = 0.4$ (b) $r = 0.5$ (c) $r = 0.6$

Figure 4.32: 3-D diagram of the population dynamics of subpopulations x_0, x_1 and x_2. $n_0 = 1000$, and q varies from 0.4 to 0.6 with step size 0.05. Here, r changes: (a) $r = 0.4$, (b) $r = 0.5$, (c) $r = 0.6$.

4.3 The general case of m targets

Now Suppose that m is an arbitrary integer.

System (2.2.1) can be written as:

$$\dot{x}(t) = A(q,r)\, x(t) \tag{4.3.1}$$

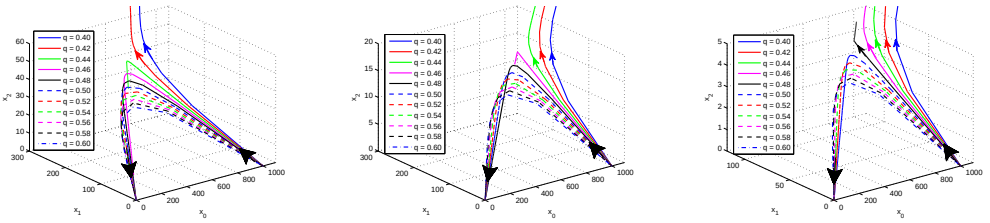

(a) $r = 0.7$ (b) $r = 0.8$ (c) $r = 0.9$

Figure 4.33: 3-D diagram of the population dynamics of subpopulations x_0, x_1 and x_2. $n_0 = 1000$, and q varies from 0.4 to 0.6 with step size 0.05. Here, r changes: (a) $r = 0.7$, (b) $r = 0.8$, (c) $r = 0.9$.

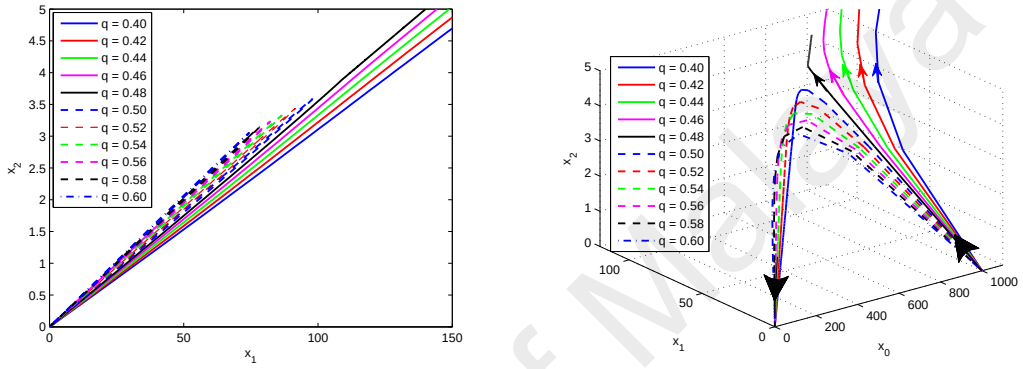

(a) Phase Diagram $x_1 - x_2$ (b) 3D Bifurcation diagram.

Figure 4.34: System bifurcation analysis, where q varies between 0.4 and 0.6 and $r = 0.9$. The system is stable when $q \geq 0.5$

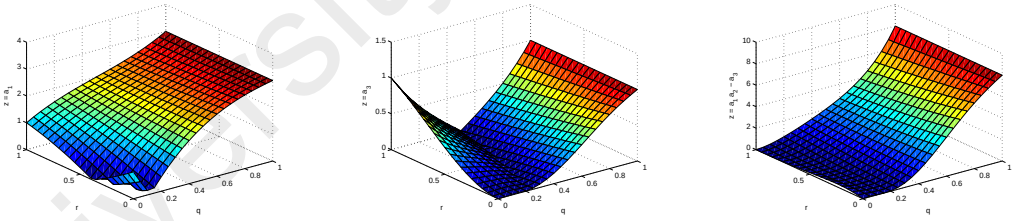

(a) $|a_1(q,r)|$ (b) $|a_1(q,r)a_2(q,r) - a_3(q,r)|$ (c) $|a_3(q,r)|$

Figure 4.35: 3-D plot for $|a_1(q,r)|$, $|a_1(q,r)a_2(q,r) - a_3(q,r)|$ and $|a_3(q,r)|$. The system(4.2.1) is stable if and only if these functions are positive.

where matrix A is described as:

$$A_{tk} = \begin{cases} \Pi(0,0) + \mu(1-q)^m - 1 & i,j = 0 \\ \Pi(i,i) - 1 & i = j \quad and \quad i \neq 0 \\ \Pi(j,i) & i \neq j \end{cases} \tag{4.3.2}$$

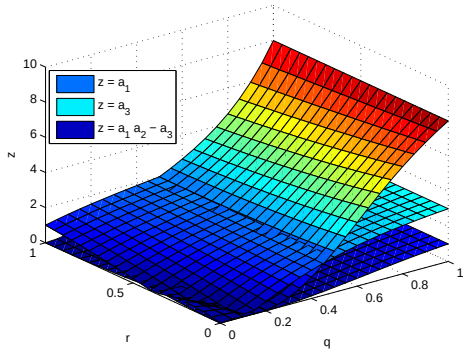

(a) a_1, $a_1a_2 - a_3$ and a_3

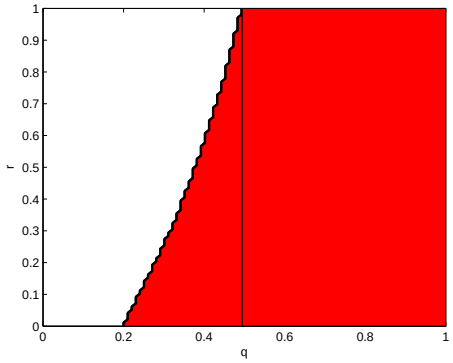

(b) The Stability Region

Figure 4.36: Intersection of the area in which functions $a_1(q,r)$ and $a_3(q,r)$ are positive and $a_1(q,r)\,a_2(q,r) > a_3(q,r)$. The Routh-Hurwitz Criterion is satisfied for all values of q and r in the blue region.

where $t = i+1$ and $k = j+1$. Therefore

$$A_{11} = \Pi(0,0) + \mu(1-q)^m - 1$$

and for $2 \leq t \leq m$

$$\begin{aligned} A_{tt} &= \Pi(t-1,t-1) - 1 \\ &= \Pi(i,i) - 1 \end{aligned} \tag{4.3.3}$$

Lemma 4.3.1. *Suppose that $B = A^\top$. If R_t defines as*

$$R_t = \sum_{k \neq t} B_{tk} \tag{4.3.4}$$

therefore

1.

$$R_t > 0 \tag{4.3.5}$$

2.

$$B_{tt}+R_t=\begin{cases}\mu(1-q)^m-q^m & i=0\\ -q^{(m-i)} & 1\le i\le(m-1)\end{cases} \tag{4.3.6}$$

Proof. 1. According to Equation(2.2.2), for any $1\le t\le m$

$$\begin{aligned}R_t &= \sum_{k\neq t}B_{tk}\\ &= \sum_{j\neq i}\Pi(i,j)\\ &> 0\end{aligned} \tag{4.3.7}$$

2. First consider that $B=A^\top$ and $t=1$. Therefore:

$$\begin{aligned}\sum_{k=1}^{m}B_{1k} &= B_{11}+\sum_{k=2}^{m}B_{1k}\\ &= \Pi(0,0)+\mu(1-q)^m-1+\sum_{j=1}^{m-1}\Pi(0,j)\\ &= \Pi(0,0)+\mu(1-q)^m-1+(1-\Pi(0,0)-\Pi(0,m))\\ &= \mu(1-q)^m-q^m\end{aligned} \tag{4.3.8}$$

Moreover, for $2\le t\le m$

$$\begin{aligned}\sum_{k=1}^{m}B_{tk} &= B_{tt}+\sum_{k\neq t}B_{tk}\\ &= (\Pi(i,i)-1)+\sum_{j\neq i}\Pi(i,j)\\ &= -\Pi(i,m)\\ &= -q^{m-i}\end{aligned} \tag{4.3.9}$$

□

The main result of this section is written as follows:

Theorem 4.3.1. *For any $m \geq 2$, $0 < \mu \leq 1$ and $0 < r < 1$, the system $\dot{\mathbf{x}} = A(q,r)\mathbf{x}$ is stable at equilibrium point $\mathbf{0}$, where $q > 0.5$.*

Proof. To complete the proof we must show each eigenvalue of matrix A has negative real part. To provide this we will show that for any $q > 0.5$, $0 < r < 1$ and $m \geq 2$ any point of Gershgorin circles $D(A_{tt}, R_t)$ have negative real part, where $1 \leq t \leq m$. For this purpose we apply Gershgorin Theorem on matrix $B = A^{\top}$.

Based on Lemma.(4.3.1),

$$B_{tt} + R_t = \begin{cases} \mu(1-q)^m - q^m & i = 0 \\ -q^{(m-i)} & 1 \leq i \leq (m-1) \end{cases} \tag{4.3.10}$$

Not that function q^m is an increasing function when $q > 0$ and m is an integer. Therefore, for $1 - q < 0.5 < q$ we have:

$$\mu(1-q)^m < (1-q)^m < q^m \tag{4.3.11}$$

where $0 \leq \mu \leq 1$.

Consequently, $B_{tt} \in \mathbb{R}$ and $B_{tt} + R_t < 0$ where $q > 0.5$ (Figure (4.37)). This shows that the Gershgorin Circles belong in the left side of real line. In addition, according to Gershgorin Theorem (2.2.4), each eigenvalue of matrix B belongs in one of Gershgorin discs.

Therefore, each eigenvalue of matrix B has negative real part. Hence, every eigenvalue of matrix A has negative real part. This completes the proof. □

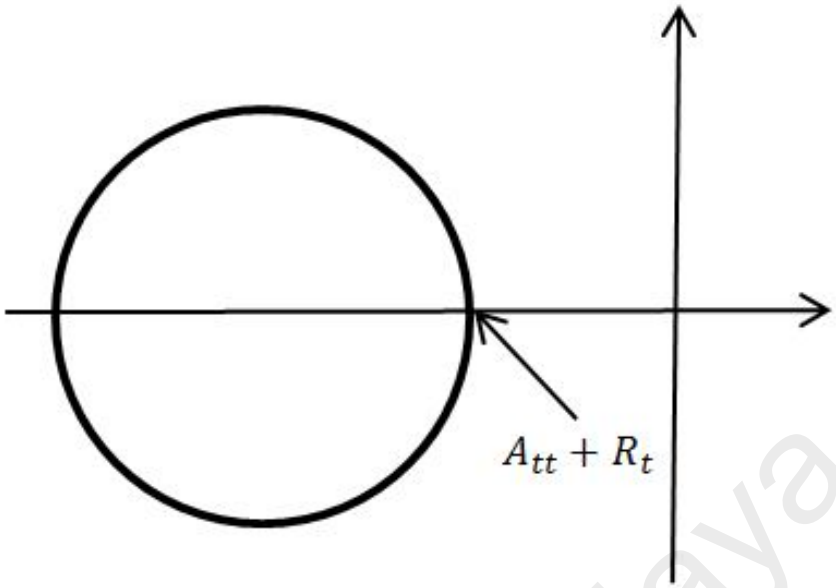

Figure 4.37: Gershgorin disc $B(A_{tt}, R_t)$.

Theorem 4.3.2. *Suppose that $m \geq 2$ is an integer, $A \in \mathbb{M}^{m\times m}$ and the set S denotes the value q such that the system (4.3.1) be stable corresponding to all $0 < r < 1$ and $0 < \mu \leq 1$. Therefore:*

$$\inf_q A = 0.5 \tag{4.3.12}$$

Proof. According to Theorem (4.3.1), the system (2.2.1) is stable where $q > 0.5$.

Now suppose that $\varepsilon > 0$. Therefore, corresponding to $q_0 = 0.5 - \varepsilon$ and for $m = 2$ there exists $r_0 = 1 - \varepsilon$ such that the system (2.2.1) is unstable. Hence:

$$\inf_q A = 0.5 \tag{4.3.13}$$

□

4.4 SDE Model

A SDE model for the tumor cells population has been proposed in Equation(3.3).

4.4.1 Existence and Uniqueness of the solutions

Since the coefficient functions are linear they are globally Lipschitz, so standard theorems on global existence and uniqueness of solutions hold (Kloden & Platen, 1992).

4.4.2 Explicit Solution

Using multi-dimensional Îto formula, a vector linear stochastic differential equations, the explicit solution to the system (3.3.5) is written as (Kloden & Platen, 1992):

$$X(t) = e^{(A-\frac{1}{2}B^2)t+BW(t)}X(0) \tag{4.4.1}$$

When $X(0)$ is constant. The expected value of $X(t)$ solves the deterministic equation:

$$dE[X(t)] = AE[X(t)]dt \tag{4.4.2}$$

which results in:

$$E[X(t)] = e^{At}E[X(0)] \tag{4.4.3}$$

4.4.3 Linear Moment Stability Analysis

In this section, the stability of stochastic differential equations is introduced. There are several kinds of stability questions and several ways to define stability for stochastic differential equations.

Theorem 4.4.1. *Suppose that A is the matrix in Equation* (3.3.6)*. System*

$$dE[X(t)] = AE[X(t)]dt \tag{4.4.4}$$

is stable if and only if

$$(1+\frac{q_1}{\alpha})(1+\frac{q_2}{\beta})(1+\frac{q_3}{\gamma})>2 \tag{4.4.5}$$

Proof. Suppose that λ_1, λ_2, and λ_3 are the eigenvalues of matrix A. Therefore

$$\mathrm{tr}(A)=-[(\alpha+q_1)+(\beta+q_2)+(\gamma+q_3)]=\lambda_1+\lambda_2+\lambda_3 \tag{4.4.6}$$

$$\det(A)=2\alpha\beta\gamma-[(\alpha+q_1)(\beta+q_2)(\gamma+q_3)]=\lambda_1\ \lambda_2\ \lambda_3 \tag{4.4.7}$$

In addition

$$\begin{aligned}\mathrm{tr}^2(A) &= [(\alpha+q_1)+(\beta+q_2)+(\gamma+q_3)]^2\\ \mathrm{tr}(A^2) &= (\alpha+q_1)^2+(\beta+q_2)^2+(\gamma+q_3)^2\end{aligned} \tag{4.4.8}$$

The system(4.4.4) is stable if and only if

$$\mathrm{tr}(A)<0 \tag{4.4.9}$$

$$\mathrm{tr}^2(A)-\mathrm{tr}(A^2)>0 \tag{4.4.10}$$

$$\det(A)<0 \tag{4.4.11}$$

From Equation(4.4.6) and Equation (4.4.8), it is clear that

$$\mathrm{tr}(A) < 0 \tag{4.4.12}$$

$$\mathrm{tr}^2(A)-\mathrm{tr}(A^2) > 0 \tag{4.4.13}$$

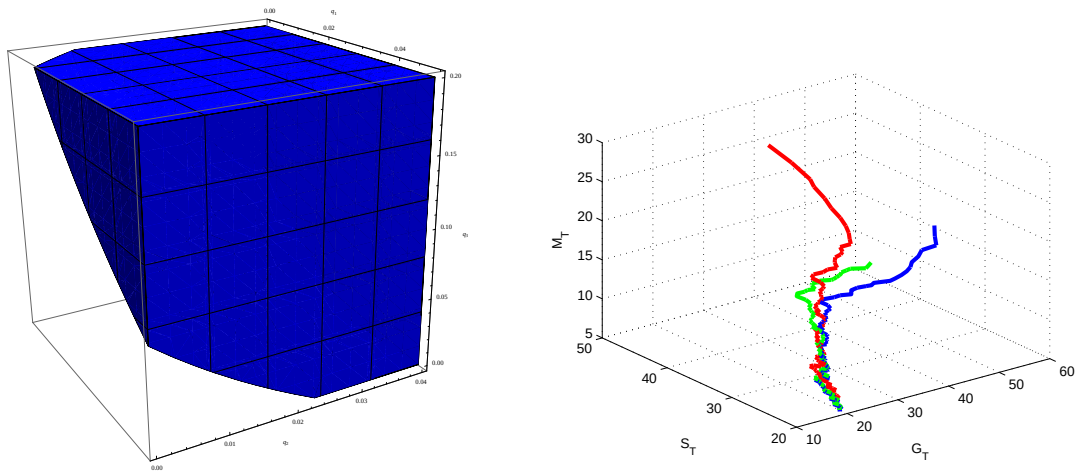

(a) The stability region of the system (4.4.4) (b) Phase Diagram *G-S-M*.

Figure 4.38: Stability region of the system.

Therefore the system is stable if and only if

$$2\alpha\beta\gamma - [(\alpha+q_1)(\beta+q_2)(\gamma+q_3)] < 0 \tag{4.4.14}$$

which proves the result. □

Remark 4.4.1. *Figure (4.38.a) and Figure (4.38.b) demonstrate the stability region and the system phase diagram, which are corresponding to parameters q_1, q_2, and q_3, respectively. The initial values $(30,40,30)$, $(50,30,20)$ and $(49,39,12)$ are depicted in the phase diagram with red, blue and green lines, respectively.*

4.4.4 Simulation Results

The Euler-Maruyama and Milstein algorithms are two common numerical methods for solving stochastic differential equations (Kloden & Platen, 1992). Both parametric and nonparametric methods could be applied to estimate the model parameters.

The selection for the parameters are as follows. We have estimated parameters α, β, and γ based on the experimental data provided for these parameters in (Sutherland et al., 1983). The other parameters such as q_i's, σ_i's and the initial conditions are considered

constants. They are selected randomly based on the nature of the problem and the order of the magnitudes of these constants.

The nonparametric method is applicable to both Euler-Maruyama and Milstein algorithms, and the parametric method is only applicable to the Euler-Maruyama algorithm. We have utilized the modified version of the SDE_Toolbox 1.4.1 of MATLAB for the simulation (Pena, 2004).

Note that in this analysis the transition rates are considered constants. Therefore these values are stable over time. However, the cell death rates are variable and highly dependent on the type and magnitude of treatment.The estimated values corresponding to the transition rates are reported in Table (4.6). Moreover, the values given in Table (4.5) were selected for the death rates.

Table 4.5: Experiment-dependent parameters

Parameter	Estimated Value
q_1	0.06 (hr^{-1})
q_2	0.02 (hr^{-1})
q_3	0.1 (hr^{-1})

As mentioned before, the initial values reported by Sutherland et al. (Sutherland et al., 1983) are used for subpopulations G, S and M. These values are:

$$\begin{aligned} \hat{G}(0) &= 49\% \\ \hat{S}(0) &= 39\% \\ \hat{M}(0) &= 12\% \end{aligned} \tag{4.4.15}$$

Remark 4.4.2. *The constants which are used in the simulation are as follows (Table(4.6)):*

Table 4.6: Initial Values of model parameters.

Parameter	Initial Value	Type of parameter
α	0.04328	Free
β	0.0824	Free
γ	0.3655	Free
G	49	Constant
S	39	Constant
M	12	Constant
q_1	0.06	Constant
q_2	0.02	Constant
q_3	0.1	Constant
σ_1	0.0375	Constant
σ_2	0.0141	Constant
σ_3	0.0327	Constant

4.4.4 (a) The Euler-Maruyama Algorithm–Parametric Method

In this case, the model is run 100 times and the data is generated. The parameters are estimated by a parametric method. In addition, the Euler-Maruyama algorithm with step size $h = 0.01$ is used to solve Equation (3.3.5) with parameter values in Equation (4.4.15). Using the parametric method, the main parameters α, β andγ are estimated and provided in Table(4.7).

Table 4.7: Estimated parameter values with 95% confidence intervals for the transition rates using the parametric method

Parameter	Estimated Value	95% Confidence Interval
α	0.04328	[-0.0052, 0.0918]
β	0.0824	[0.0315, 0.1333]
γ	0.3655	[0.1744, 0.9055]

Figures (4.39.a), (4.40.a) and (4.41.a) show the simulation results of 100 trajectories of

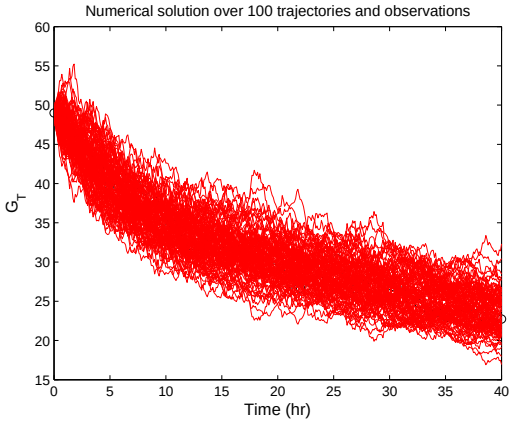

(a) Time Evolution of G_T

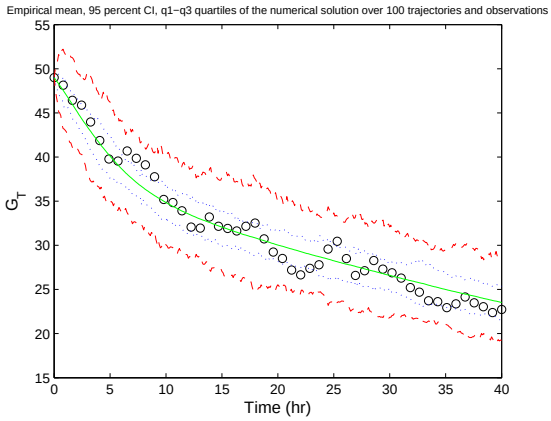

(b) Time Evolution of G_T

Figure 4.39: Cell population dynamics for subpopulation G over 100 trajectories by solving Equation(3.3.5). Here, the black circles are the trajectories corresponding to the observed numbers of cells (parametric method). The blue lines represent the first and third quartiles of the simulated trajectories and the red lines illustrate 95% confidence interval areas obtained by taking, at each time, the 2.5^{th} and 97.5^{th} percentiles of the simulated trajectories. The green line is the empirical mean of the process.

the cell population dynamics for subpopulations G, S and M, respectively. In Figures (4.39.b), (4.40.b) and (4.41.b), the black circles represent the trajectories corresponding to the estimated values in Table (4.7).

In addition, the red and blue lines in the right graph columns, represent the 95% empirical confidence interval, and the first and third quartiles of the 100 trajectories numerical solutions for the cell population dynamics in subpopulations G, S and M, respectively. The green solid line signifies the point-by-point sample mean of the trajectories.

Now, suppose that G_{40}, S_{40} and M_{40} represent the sizes of subpopulations G, S and M corresponding to 100 times running the simulation. Applying the Monte-Carlo simulation yields the process, statistical analyses (i.e., mean value, variance, median, 95%-percent confidence interval for the trajectories, first and third quartiles, process skewness and kurtosis). The results are given in the Table (4.8).

Finally, the number of cells in each subpopulation after applying the last dose fraction are shown in Figures (4.8.a), (4.8.b), and (4.8.c).

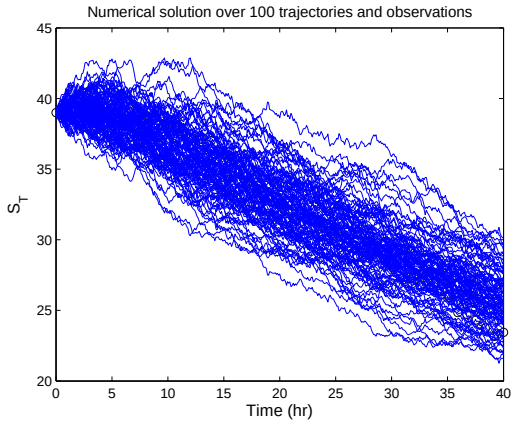

(a) Time Evolution of S_T

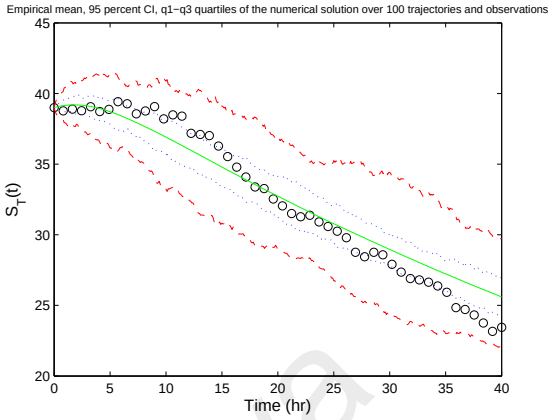

(b) Time Evolution of S_T

Figure 4.40: Cell population dynamics for the subpopulation S over 100 trajectories by solving Equation (3.3.5). Here, the black circles are the trajectories corresponding to the observed numbers of cells (parametric method). The blue lines represent the first and third quartiles of the simulated trajectories and the red lines illustrate 95% confidence interval areas obtained by taking, at each time, the 2.5^{th} and 97.5^{th} percentiles of the simulated trajectories. The green line is the empirical mean of the process.

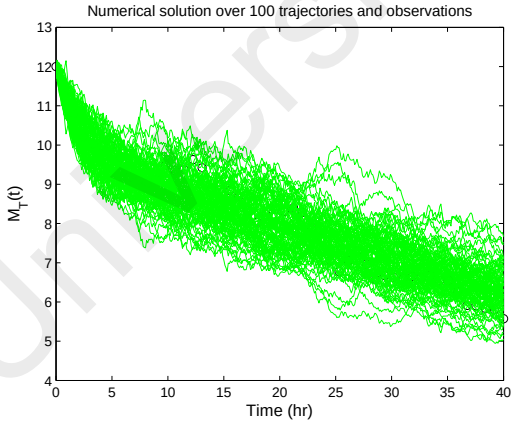

(a) Time Evolution of M_T

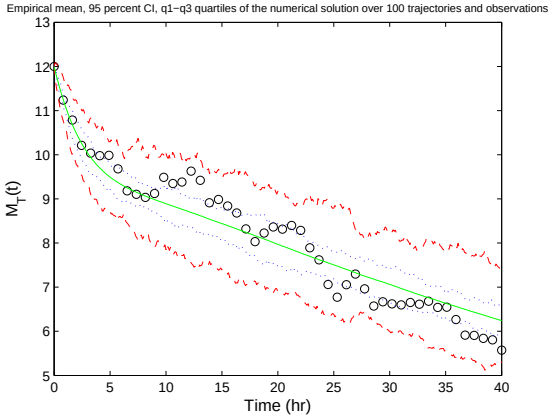

(b) Time Evolution of M_T

Figure 4.41: Cell population dynamics for the subpopulation M over 100 trajectories by solving Equation (3.3.5). Here, the black circles are the trajectories corresponding to the observed numbers of cells (parametric method). The blue lines represent the first and third quartiles of the simulated trajectories and the red lines illustrate 95% confidence interval areas obtained by taking, at each time, the 2.5^{th} and 97.5^{th} percentiles of the simulated trajectories. The green line is the empirical mean of the process.

Table 4.8: Monte Carlo Statistics for the G, S and M subpopulations at time T=40 hours.

	$G_{40}(t)$	$S_{40}(t)$	$M_{40}(t)$
Process Mean	23.53	25.60	6.24
Process Variance	6.84	4.14	0.29
Process Median	23.37	25.52	6.21
95 % confidence interval for the trajectories	[19.24, 28.34]	[21.94, 29.75]	[5.31, 7.31]
Process First and Third quartiles	[21.60, 25.38]	[24.27, 27.01]	[5.83, 6.61]
Process Skewness	0.37	0.16	0.21
Process Kurtosis	3.42	2.42	2.63

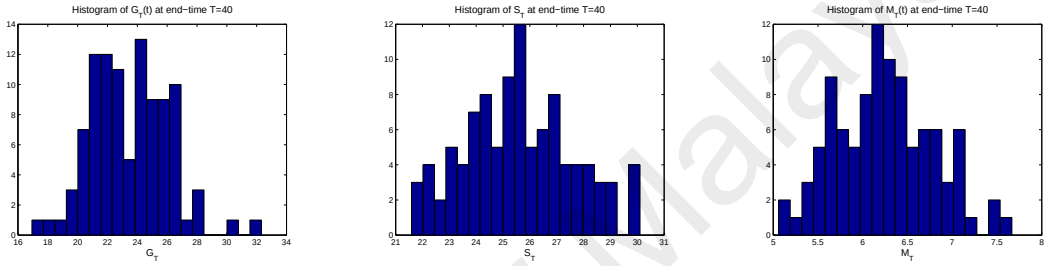

(a) G (b) S (c) M

Figure 4.42: Histogram of the observed number of cells in each subpopulation at time T=40 over 100 trajectories with Euler-Maruyama approximation.

4.4.4 (b) The Euler-Maruyama Algorithm–Nonparametric Method

In this section the model is run 100 times. The parameters are estimated by nonparametric method and the Euler-Maruyama method with step size $h = 0.01$ is used to solve Equation(3.3.5) numerically with the initial parameter values

$$G_T(0) = 49,\ S_T(0) = 39,\ M_T(0) = 12 \tag{4.4.16}$$

The main parameters α, β, and γ are estimated and the results are presented in Table(4.9).

Figures (4.43), (4.44) and (4.45) represent the simulation of 100 trajectories of the cell population dynamics in subpopulations G, S and M, respectively.

The picture descriptions are similar to the parametric ones.

Similar to the parametric case, the statistical analysis of the process is provided in Ta-

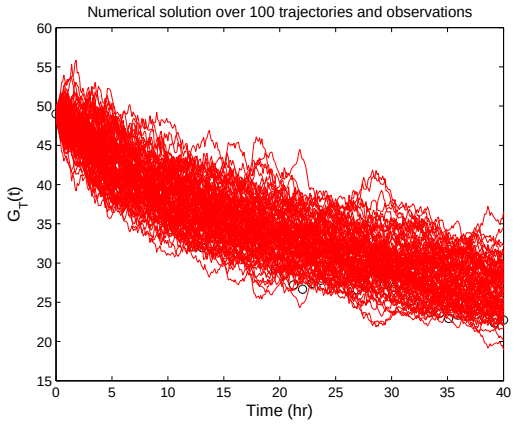

(a) Time Evolution of G_T

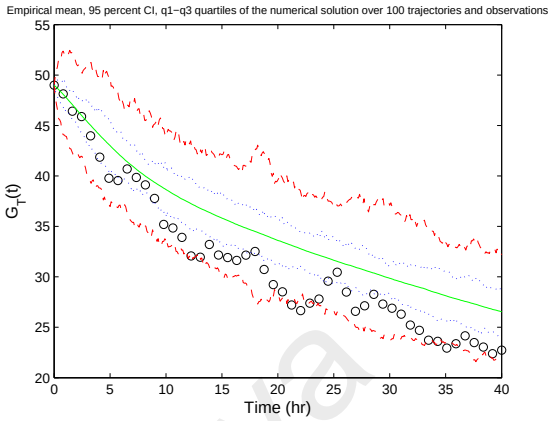

(b) Time Evolution of G_T

Figure 4.43: Cell population dynamics for subpopulation G. The black circles show the trajectories corresponding to the observed data (nonparametric method). The blue lines represent the first and third quartiles of the simulated trajectories and the red lines illustrate the 95% confidence interval areas obtained by taking, at each time, the 2.5^{th} and 97.5^{th} percentiles of the simulated trajectories. The green line is the empirical mean of the process.

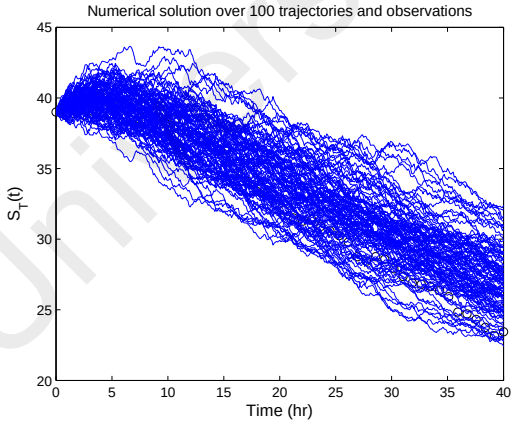

(a) Time Evolution of S_T

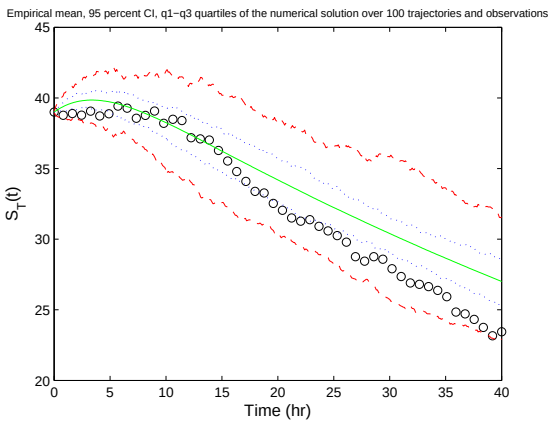

(b) Time Evolution of S_T

Figure 4.44: Cell population dynamics for subpopulation S. The black circles show the trajectories corresponding to the observed data (nonparametric method). The blue lines represent the first and third quartiles of the simulated trajectories and the red lines illustrate the 95% confidence interval areas obtained by taking, at each time, the 2.5^{th} and 97.5^{th} percentiles of the simulated trajectories. The green line is the empirical mean of the process.

Table 4.9: Estimated parameter values and 95% confidence intervals of the movement rates using the nonparametric method.

Parameter	Estimated Value	95% Confidence Interval
γ	0.2088	[-0.3365, 0.7543]
α	0.0770	[-0.0240, 0.1779]
β	0.0890	[0.0385, 0.1394]

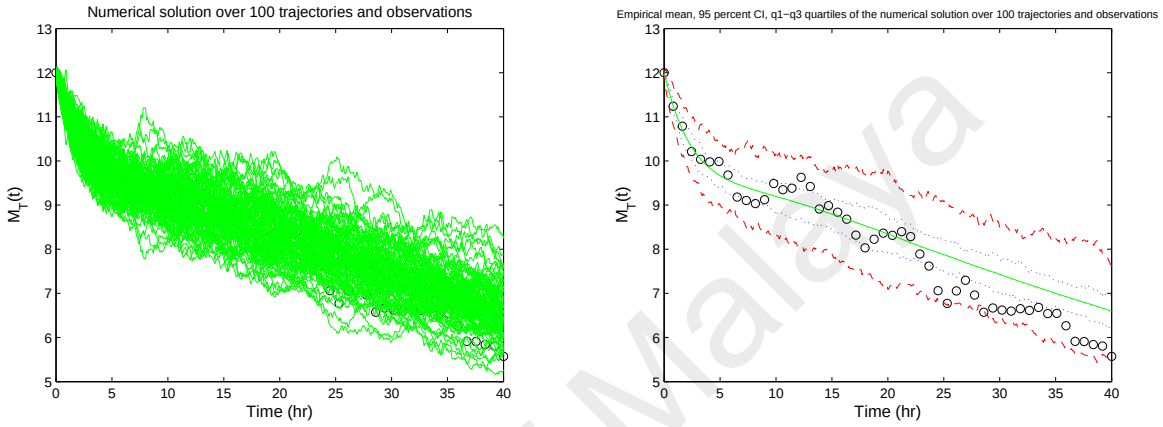

(a) Time Evolution of M_T (b) Time Evolution of M_T

Figure 4.45: Cell population dynamics for subpopulation M. The black circles show the trajectories corresponding to the observed data (nonparametric method). The blue lines represent the first and third quartiles of the simulated trajectories and the red lines illustrate the 95% confidence interval areas obtained by taking, at each time, the 2.5^{th} and 97.5^{th} percentiles of the simulated trajectories. The green line is the empirical mean of the process.

ble(4.10).

Table 4.10: Monte Carlo Statistics for the G, S and M subpopulations at time T=40 hours.

	G_{40}	S_{40}	M_{40}
Process Mean	26.54	27.01	6.60
Process Variance	9.66	5.24	0.33
Process Median	26.42	26.99	6.57
95% confidence interval for the trajectories	[21.88, 32.20]	[22.90, 31.58]	[5.64, 7.65]
Process First and Third quartiles	[24.21, 28.58]	[25.44, 28.61]	[6.24, 6.95]
Process Skewness	0.35	0.20	0.23
Process Kurtosis	3.15	2.54	2.83

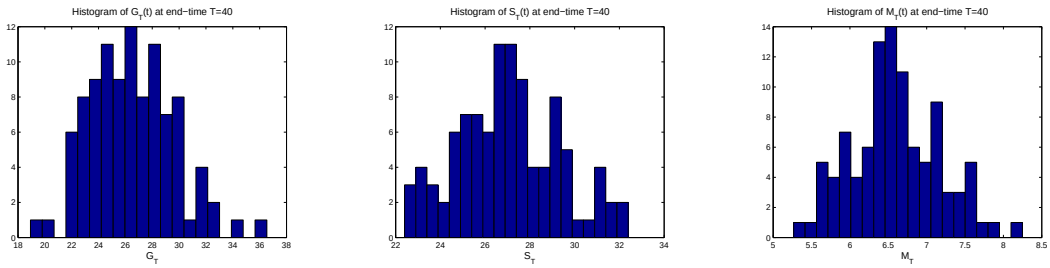

(a) G (b) S (c) M

Figure 4.46: Histogram of the observed number of cells in each subpopulation at time T=40 over 100 trajectories with Euler-Maruyama approximation.

4.4.4 (c) Milstein Method

The model is run 100 times and the Milstein method with step size 0.01 is used to solve the SDE system (3.3.4) numerically, with the same initial parameter values used with the E-M method. Again, the parametric method is used to estimate the main parameters α, β, and γ. The outcomes are presented in Table (4.11).

The figures listed in Figure (4.47), Figure(4.48) and Figure (4.49) display the results for this method with the same description as in the case of the E-M method.

Table 4.11: Estimated parameter values and 95% confidence intervals of the movement rates using the nonparametric method

Parameter	Estimated Value	95% Confidence Interval
α	0.0770	[-0.0240, 0.1779]
β	0.0890	[0.0385, 0.1394]
γ	0.2088	[-0.3365, 0.7543]

Suppose that Q_{40}, S_{40} and M_{40} represent the sizes of subpopulations G, S and M corresponding to 100 simulation times. Table(4.12) illustrates the results of applying the Monte-Carlo simulation of the process statistical analyses (i.e., the mean value, variance, median, 95% confidence interval for the trajectories, first and third quartiles, process skewness and kurtosis).

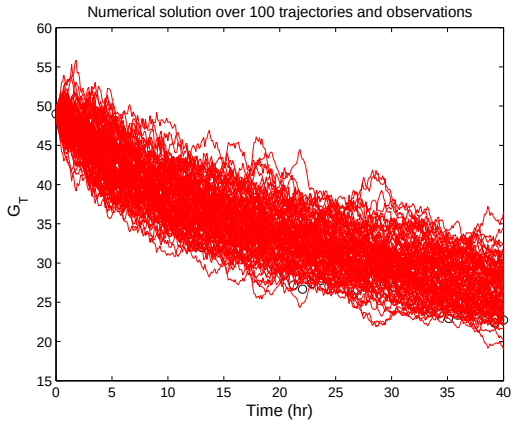

(a) Time Evolution of G_T

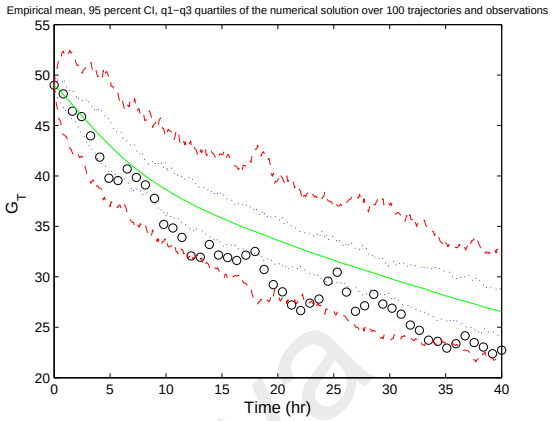

(b) Time Evolution of G_T

Figure 4.47: Cell population dynamics for subpopulation G. The black circles show the trajectories corresponding to the observed data (nonparametric method). The blue lines represent the first and third quartiles of the simulated trajectories and the red lines illustrate the 95% confidence interval areas obtained by taking, at each time, the 2.5^{th} and 97.5^{th} percentiles of the simulated trajectories. The green line is the empirical mean of the process.

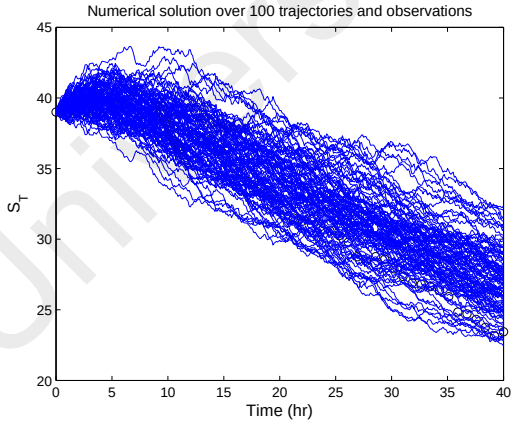

(a) Time Evolution of S_T

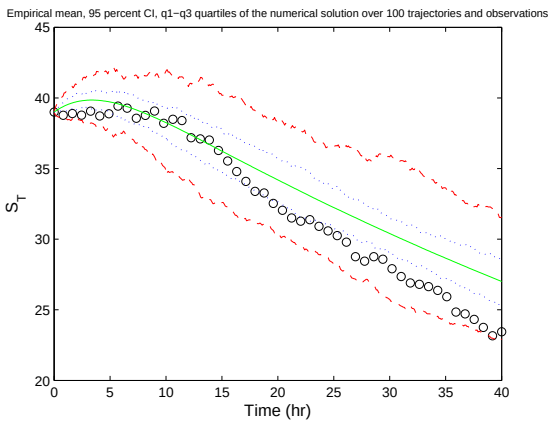

(b) Time Evolution of S_T

Figure 4.48: Cell population dynamics for subpopulation S. The black circles show the trajectories corresponding to the observed data (nonparametric method). The blue lines represent the first and third quartiles of the simulated trajectories and the red lines illustrate the 95% confidence interval areas obtained by taking, at each time, the 2.5^{th} and 97.5^{th} percentiles of the simulated trajectories. The green line is the empirical mean of the process.

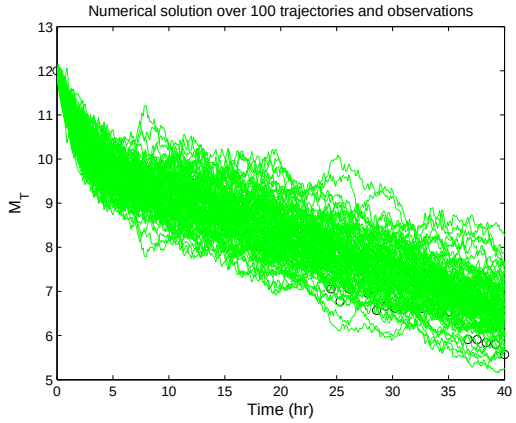

(a) Time Evolution of M_T

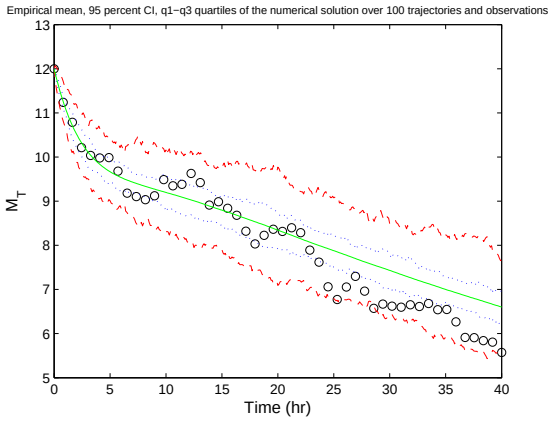

(b) Time Evolution of M_T

Figure 4.49: Cell population dynamics for subpopulation M. The black circles show the trajectories corresponding to the observed data (nonparametric method). The blue lines represent the first and third quartiles of the simulated trajectories and the red lines illustrate the 95% confidence interval areas obtained by taking, at each time, the 2.5^{th} and 97.5^{th} percentiles of the simulated trajectories. The green line is the empirical mean of the process.

Table 4.12: Monte Carlo Statistics for the G, S and M subpopulations at time T=40 hours.

	$G_{40}(t)$	$S_{40}(t)$	$M_{40}(t)$
Process Mean	26.54	27.01	6.60
Process Variance	9.66	5.24	0.33
Process Median	26.42	26.99	6.57
95% confidence interval for the trajectories	[21.88, 32.20]	[22.90, 31.58]	[5.64, 7.65]
Process First and Third quartiles	[24.21, 28.58]	[25.44, 28.61]	[6.24, 6.95]
Process Skewness	0.35	0.20	0.23
Process Kurtosis	3.15	2.54	2.83

4.4.4 (d) Whole tumor population dynamics

Using

$$N_T = G_T + S_T + M_T \tag{4.4.17}$$

The entire cell population dynamics (N_T) over 20 trajectories and observed data are depicted in Figures (4.51.a) and (4.51.b).

Based on the results, it is evident that there is no significant difference in cell population dynamics between the two parametric (Figure (4.51.a)) and nonparametric (Figure (4.51.b)) methods.

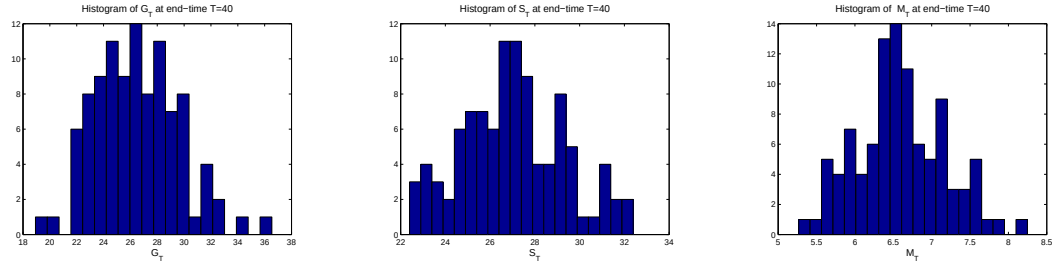

(a) G (b) S (c) M

Figure 4.50: Histogram of the observed number of cells in each subpopulation at time T=40 over 100 trajectories with Milstein approximation.

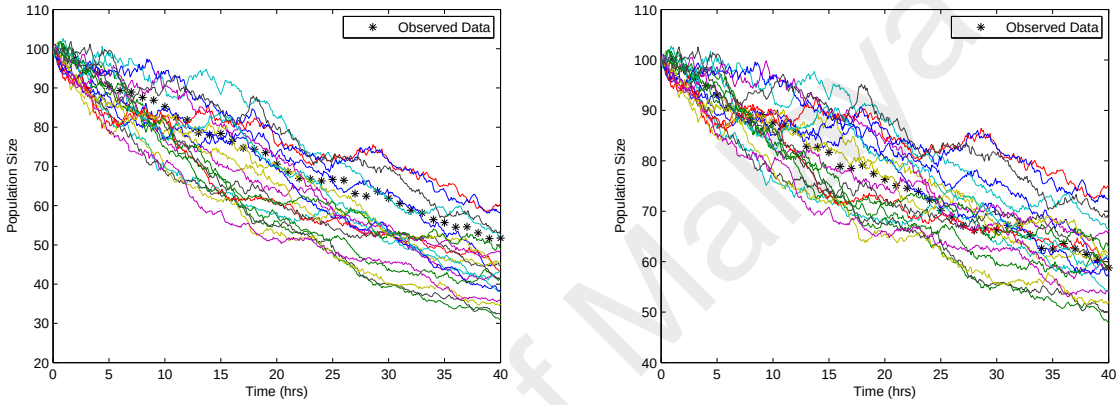

(a) Time Evolution of N_T (b) Time Evolution of N_T

Figure 4.51: (a) Cell population dynamics in the whole tumor over 20 trajectories, where the system of SDEs (3.3.5) is solved by Euler-Maruyama algorithm and the parameters are estimated by a parametric method; (b) Cell population dynamics in the whole tumor over 20 trajectories, where the system of SDEs (3.3.5) is solved by Euler-Maruyama or Milstein algorithm and the parameters are estimated by nonparametric method.

4.4.4 (e) Lifespan

According to definition (3.4.1), the tumor lifespan can be defined when the population size is decreasing after receiving the treatment. In this part The simulation is run 200 times and for each time the tumor lifespan is evaluated. Figure (4.52.a) shows the tumor lifespan corresponding to each sample, and Figure (4.52.b) represents histogram of the tumor lifespan.

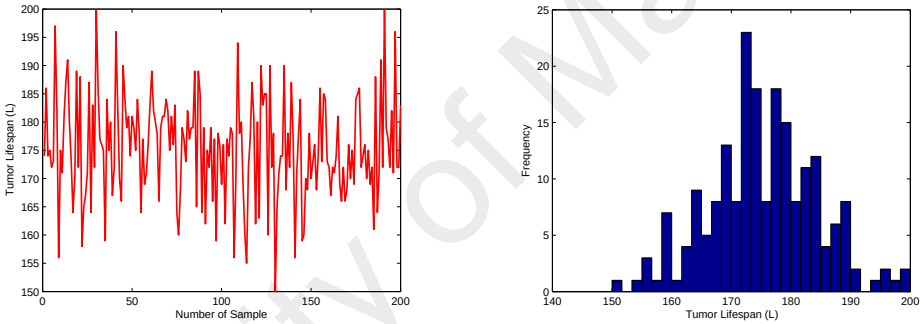

(a) Tumor lifespan (L) for 200 simulations (b) Histogram of tumor lifespan (L) for 200 simulations

Figure 4.52: Lifespan diagrams.

CHAPTER 5

EXPERIMENTAL RESULTS

The experiments have been done in **Translational Core Laboratory** (TCL) which is located at 11^th level of Pediatrics building at University of Malaya.

5.1 Methodology

5.1.1 Chemical and reagent

1. 70% Ethanol with distilled water.
2. 50 μg/ml of stock propidium iodide.
3. 100 mg/ml of stock RNase (Ribonuclease I)

5.1.2 Cell Cultures

Cell line: MCF7 purchased from American Type Culture Collection (ATCC).

Culture media: DMEM (ref: 111965-092, Gibco) supplemented with 10% FBS (Fetal Bovine Serum)(Ref:10270, Gibco) and 1% of penicillin-streptomycin (Ref: 15140122, Gibco).

5.1.3 Seeding and Radiation

The number of 7E5 cells per well was seeded in seven(7) 10 cm Petri dishes and the plates were labeled as control 0, control 24, irradiated 24, control 48, irradiated 48, control 72 and irradiated 72.

The cells have been harvested and treated by $2ml$ of Trypsine. Then the cells were kept in incubator for 5 minutes at 37^oC.

Subsequently, the cells were fixed in zero, 24, 48 and 72 houre after radiation.

Moreover, a large number of doublet cells were observed in the last experiment. Therefore, the flow cytometry was run for ECC1 cell this time and it was observed that the doublets are mainly because the MCF-7 cells like to stitch each other.

Then the cells were irradiated in the department of Oncology with the magnitude of 2 Gray. The details of the linear accelerator are:

- Brand: Varian
- Model: 2100CD
- Country: Palo Alto, California, USA

The duration of radiation is between 20-33 seconds.

5.1.4 Cell Cycle Assay

5.1.4 (a) Cell Counting Using Hemocytometer

The number of cells was counted by using hemocytometer.

5.1.4 (b) Preparing Cells

To prepare the cells, hemocytometer is cleaned with alcohol. The cells are spun by centrifuge at 500g. Thereafter, the media is removed and kept 3-4 μl to have higher concentration.

Subsequently, the cells are mixed by using a pipette. Finally, 100 μl of cells are mixed with 400 μl of Trypan Blue.

5.1.4 (c) Protocol

First, 2 μl of the mixture of Trypan Blue and cell suspension were taken and applied to the hemocytometer. Then both chambers were filled underneath the coverslip, allowing

the cell suspension to be drawn out by capillary action.

Using a microscope, it was focused on the grid lines of the hemocytometer with a 4X objective. Subsequently, the live, unstained cells (live cells do not take up Trypan Blue and are bright under microscope) were counted in one set of 16 squares.

When counting, employ a system whereby cells are only counted when they are set within a square or on the right-hand or bottom boundary line.

Following the same guidelines, dead cells stained with Trypan Blue (blue color cells) can also be counted for a viability estimate.

Finally, the hemacytometer was moved to the next set of 16 corner squares and carry on counting until all 4 sets of 16 corners are counted (Figure 5.1).

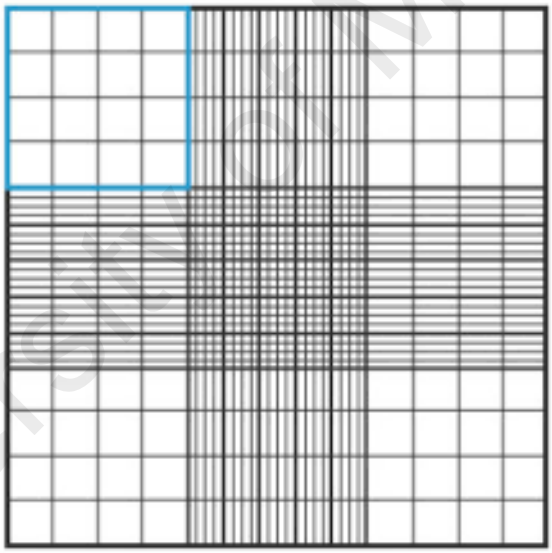

Figure 5.1: Cell counting by using hemocytometer.

5.1.4 (d) Cell's Viability

To calculate the viability of cells the following procedure was used: First, the average cell count from each of the sets of 16 corner squares is taken.Then this average is Multiplied by 10,000.

In this experiment the dilution factor is considered as 5. Therefore, the obtained number is Multiplied by 5 to correct for the 1:5 dilution from the Trypan Blue addition.

The final value is the number of viable cells/mL in the original cell suspension.

The live and dead cell count is added together to obtain a total cell count. Finally, Dividing the live cell count by the total cell count, the viability percentage is calculated.

5.1.4 (e) PI staining

The protocol of cell cycle assay by flow cytometry is as follow:

Cells were washed using PBS Then the cells were treated by 1-2 μl of Trypsin. Thereafter, cells were kept in incubator (37^{o}C and 5% CO_2) for 5 minutes.

Then cells were counted as explained in section (5.1.4 (a)). Subsequently, cells were spun at 500 g for 6 minutes to remove the In the next step, the cells were washed with 1 ml of PBSCells were fixed in cold 70% ethanol. To minimize clumping, the ethanol were added drop-wise to the pellet while vortexing. The cells were incubated at 4^{o}C for 30 minutes.

Then cells were washed two times with 1ml of PBS and spun at 850g. The cells were treated with 50 μl of a 100 μg/ml ribonuclease. This will ensure only DNA, not RNA, was stained.

Finally, 200 μl of PI (from 50 μg/ml stock solution) were added to the suspension.

5.2 Result

In the previous experiments, cells were received only one dose fraction with the magnitude of 2 Gy. To be more realistic, the number of dose fractions of radiation were increased into three consequent does fraction. The magnitude of each dose fraction was considered as 2Gy.

Finally, cell cycle analysis has been done by flow cytometry. The result of cell cycle analysis for time points 0, 24, 48 and 72 hours post radiation are presented in Figure.(5.2). The proportion of cells in each phase of cell cycle (G_1, S and G_2/M) in each time point and cell's viability are presented in Figure.(5.3) and Figure.(5.4), respectively. Finally, the data is summarized in Table.(5.1).

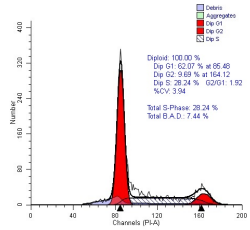

(a) Control 0 hours

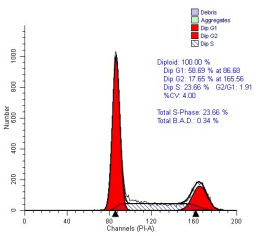

(b) Control 24 hours

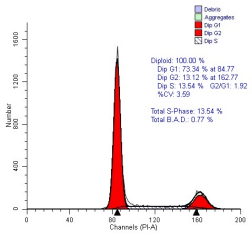

(c) Irradiated 24 hours

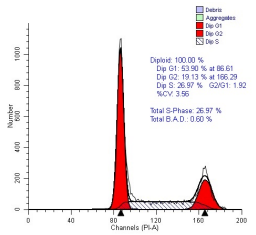

(d) Control 48 hours

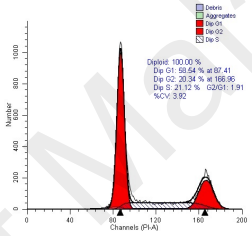

(e) Irradiated 48 hours

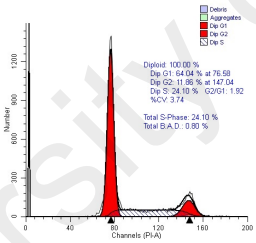

(f) Control 72 hours

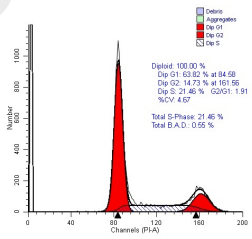

(g) Irradiated 72 hours

Figure 5.2: Cell cycle analysis for cells at time points zero, 24, 48 and 72 hours after radiation in two cases control and irradiated cells.

5.3 Simulation and Parameter Estimation

As shown in section(5.2), the MCF-7 cells were harvested and fixed at specific time points zero, 24, 48 and 72 hours post radiation. the collected cells were analyzed using flow cytometry method and the results are shown in Table(5.1).

By using the curve fitting method of MATLAB software, the appropriate curves were fitted to the data and the population size at time points 8, 16, 32, 40, 56 and 64 hours post radiation were generated corresponding to each sub-population. Subsequently, the data

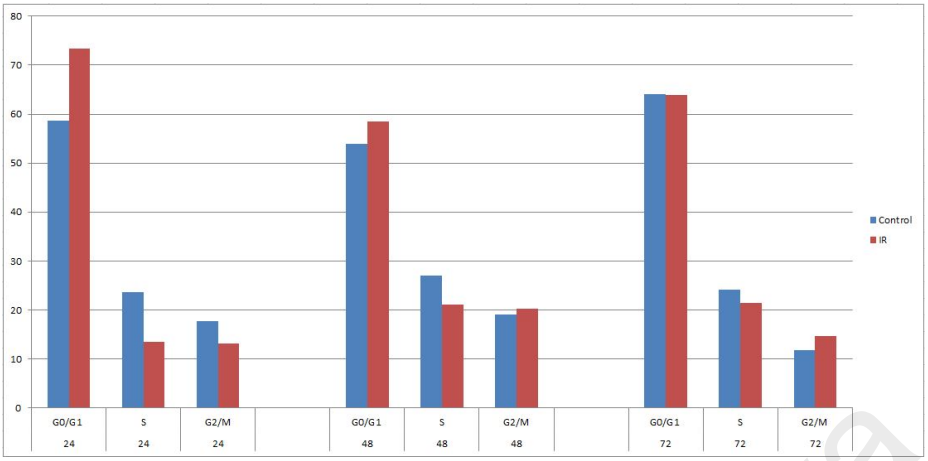

Figure 5.3: The proportion of cells in G_1, S and G_2/M phase for cells at the time of radiation (time 0) and 24, 48 and 72 hours after radiation in two cases control and irradiated cells. The blue and red colors are for control and irradiated cells, respectively.

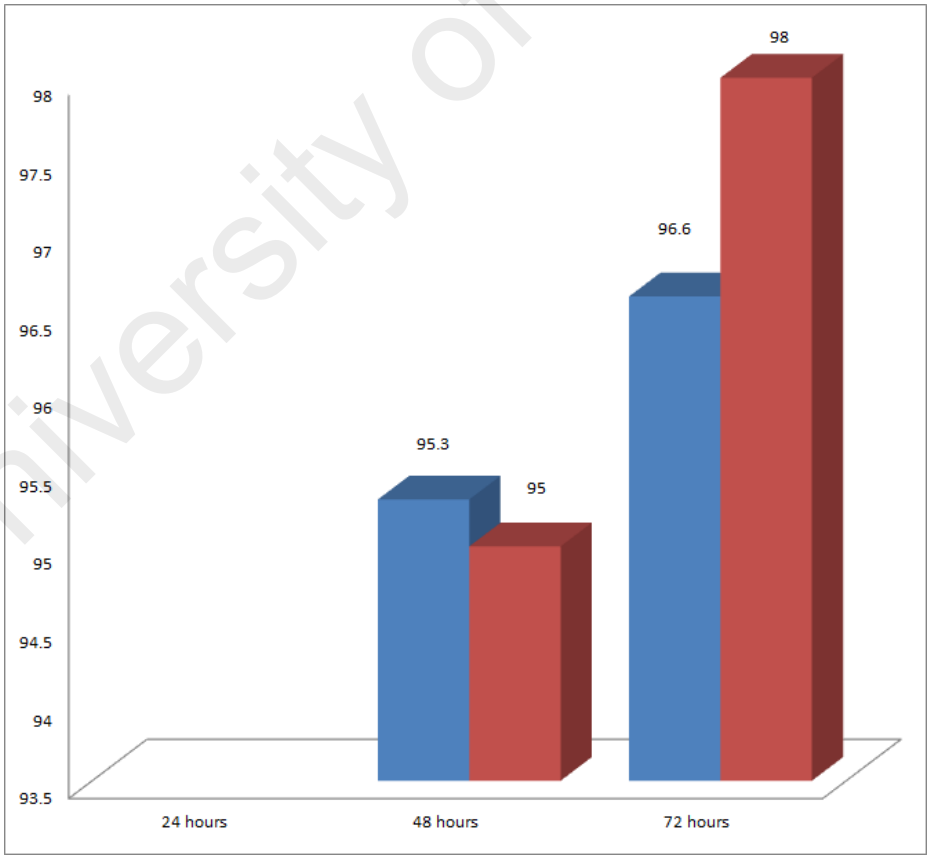

Figure 5.4: Cells viability for cells 24, 48 and 72 hours after radiation in two cases control and irradiated cells. The blue and red color show the control and irradiated cells, respectively.

Table 5.1: Proportion of cells in G_1, S and G_2/M phase corresponding to the fourth experiment.

Time point	$G\%$	$S\%$	$M\%$	CV %
Control 0 hours	62.07	28.24	9.69	3.94
Control 24 hours	58.69	23.66	17.65	4
Irradiated 24 hours	73.34	13.54	13.12	3.59
Control 48 hours	53.90	26.97	19.13	3.56
Irradiated 48 hours	58.54	21.12	20.34	3.92
Control 72 hours	64.04	24.10	11.86	3.74
Irradiated 72 hours	63.82	21.43	14.73	4.67

were aggregated in Table(5.2)

5.3.0 (a) The Euler-Maruyama Algorithm–Parametric Method

Here, the model is run 100 times and the data is generated. The parameters are estimated by a parametric method. In addition, the Euler-Maruyama algorithm with step size $h = 1$ is used to solve Equation(3.3.5) with parameter values in Equation(5.3.1).

$$\begin{aligned} G(0) &= 450,000 \\ S(0) &= 204,740 \\ M(0) &= 70,250 \end{aligned} \tag{5.3.1}$$

Using the parametric method, the main parameters q_1, q_2 and q_3 are estimated and provided in Table(5.3).

Figures(5.5.a), (5.6.a) and (5.7.a) show the simulation results of 100 trajectories of the cell population dynamics for subpopulations G, S and M, respectively. In Figures(5.5.b), (5.6.b) and (5.7.b), the black circles represent the trajectories corresponding to the estimated values in Table(5.3).

In addition, the red and blue lines in the right graph columns, represent the 95% empirical

Table 5.2: The population size in G_1, S and G_2/M phase.

Time point	G	S	M
Control 0 hours	450,000	204,740	70,250
Control 8 hours	523,544	205,549	107,441
Irradiated 8 hours	560,376	139,628	80,149
Control 16 hours	529,177	202,625	132,991
Irradiated 16 hours	597,804	110,320	92,326
Control 24 hours	498,865	201,110	150,025
Irradiated 24 hours	586,720	108,320	107,360
Control 32 hours	464,625	206,067	161,784
Control 32 hours	551,155	125,295	125,818
Irradiated 40 hours	458,400	222,736	171,338
Control 40 hours	515,744	152,732	148,284
Control 48 hours	512,050	256,215	181,735
Irradiated 48 hours	504,908	182,160	175,330
Control 56 hours	657,948	311,730	196,534
Irradiated 56 hours	542,414	205,388	207,533
Control 64 hours	927,681	394,358	218,486
Irradiated 64 hours	653,163	213,760	245,469
Control 72 hours	1,352,845	509,113	250,543
Irradiated 72 hours	861,570	198,860	289,710

Table 5.3: Estimated parameter values with 95% confidence intervals for the death rates using the parametric method

Parameter	Estimated Value	95% Confidence Interval
q_1	0.0292	[0.01191 , 0.04769]
q_2	0.1219	[0.1219 , 0.1219]
q_3	-0.15725	[-0.17467 , -0.12983]

confidence interval, and the first and third quartiles of the 100 trajectories numerical solutions for the cell population dynamics in subpopulations G, S and M, respectively. The green solid line signifies the point-by-point sample mean of the trajectories.

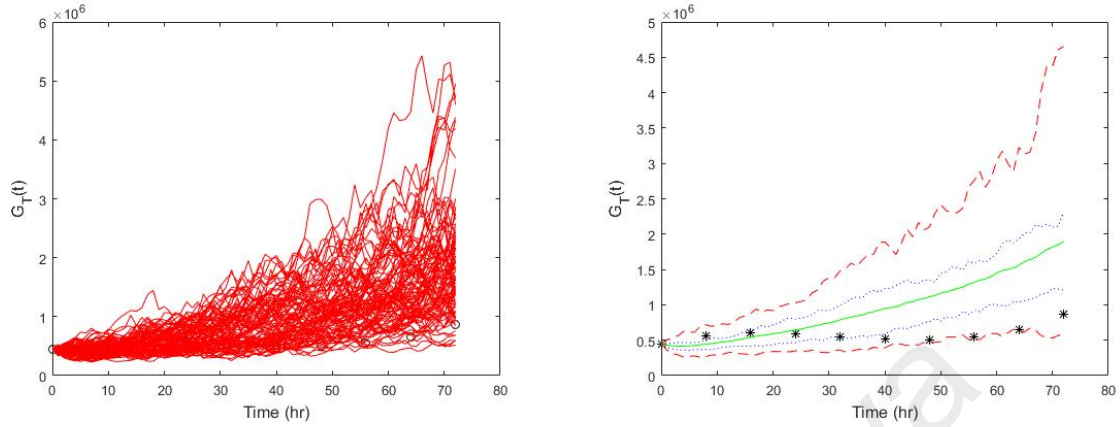

(a) Time Evolution of G_T (b) Time Evolution of G_T

Figure 5.5: Cell population dynamics for subpopulation G over 100 trajectories by solving Equation(3.3.5). Here, the black circles are the trajectories corresponding to the observed numbers of cells (parametric method). The blue lines represent the first and third quartiles of the simulated trajectories and the red lines illustrate 95% confidence interval areas obtained by taking, at each time, the 2.5^{th} and 97.5^{th} percentiles of the simulated trajectories. The green line is the empirical mean of the process.

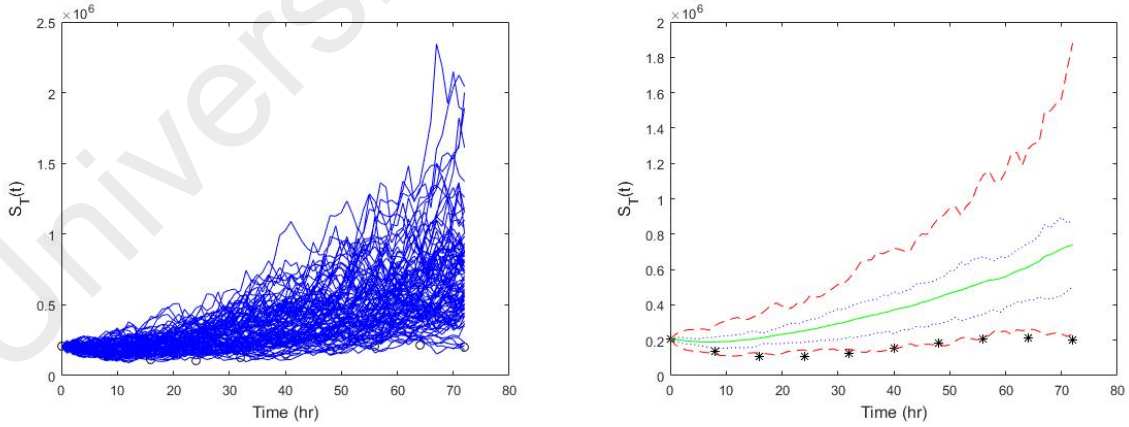

(a) Time Evolution of S_T (b) Time Evolution of S_T

Figure 5.6: Cell population dynamics for the subpopulation S over 100 trajectories by solving Equation(3.3.5). Here, the black circles are the trajectories corresponding to the observed numbers of cells (parametric method). The blue lines represent the first and third quartiles of the simulated trajectories and the red lines illustrate 95% confidence interval areas obtained by taking, at each time, the 2.5^{th} and 97.5^{th} percentiles of the simulated trajectories. The green line is the empirical mean of the process.

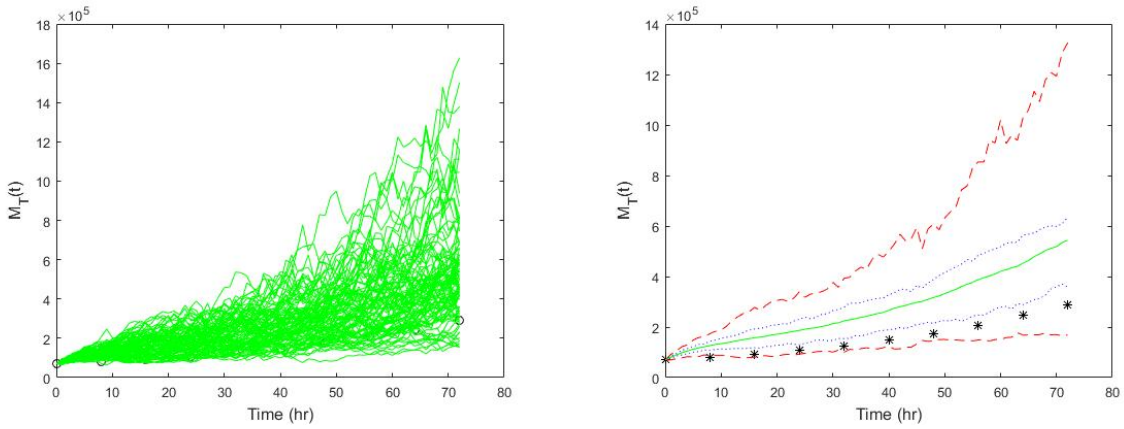

(a) Time Evolution of M_T (b) Time Evolution of M_T

Figure 5.7: Cell population dynamics for the subpopulation M over 100 trajectories by solving Equation(3.3.5). Here, the black circles are the trajectories corresponding to the observed numbers of cells (parametric method). The blue lines represent the first and third quartiles of the simulated trajectories and the red lines illustrate 95% confidence interval areas obtained by taking, at each time, the 2.5^{th} and 97.5^{th} percentiles of the simulated trajectories. The green line is the empirical mean of the process.

5.3.0 (b) The Euler-Maruyama Algorithm–Nonparametric Method

In this section the model is run 100 times. The parameters are estimated by nonparametric method and the Euler-Maruyama method with step size $h = 1$ is used to solve Equation(3.3.5) numerically with the initial parameter values in Equation (5.3.1) The main parameters q_1, q_2, and q_3 are estimated and the results are presented in Table(5.4).

Figures(5.8), (5.9) and (5.10) represent the simulation of 100 trajectories of the cell population dynamics in subpopulations G, S and M, respectively.

Table 5.4: Estimated parameter values and 95% confidence intervals of the death rates using the nonparametric method.

Parameter	Estimated Value	95% Confidence Interval
q_1	0.024	[-0.003016, 0.05108]
q_2	0.1219	[0.1219, 0.1219]
q_3	-0.016902	[-0.186265, -0.151771]

The picture descriptions are similar to the parametric ones.

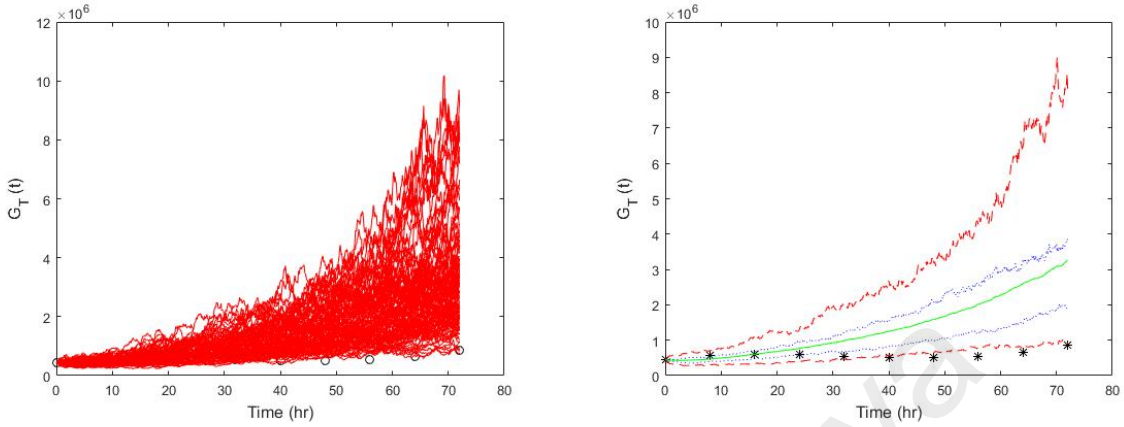

(a) Time Evolution of G_T (b) Time Evolution of G_T

Figure 5.8: Cell population dynamics for subpopulation G. The black circles show the trajectories corresponding to the observed data (nonparametric method). The blue lines represent the first and third quartiles of the simulated trajectories and the red lines illustrate the 95% confidence interval areas obtained by taking, at each time, the 2.5^{th} and 97.5^{th} percentiles of the simulated trajectories. The green line is the empirical mean of the process.

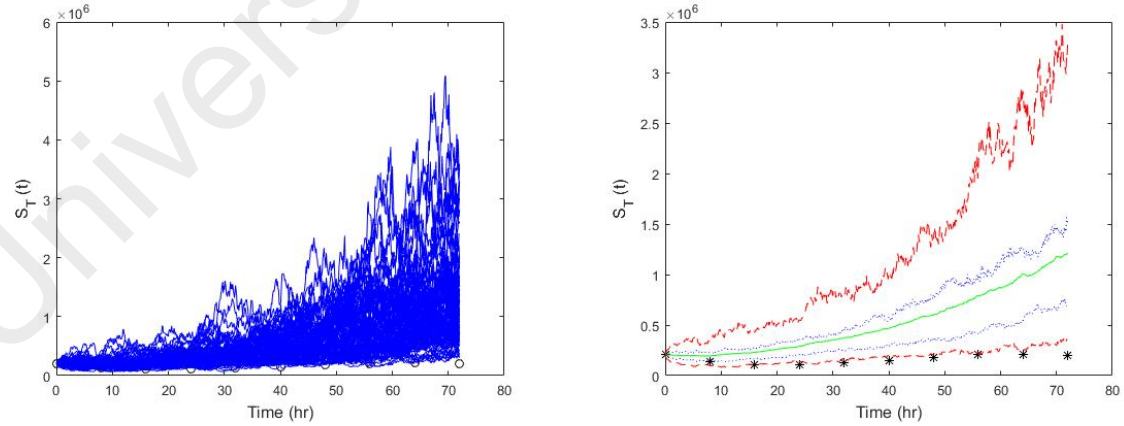

(a) Time Evolution of S_T (b) Time Evolution of S_T

Figure 5.9: Cell population dynamics for subpopulation S. The black circles show the trajectories corresponding to the observed data (nonparametric method). The blue lines represent the first and third quartiles of the simulated trajectories and the red lines illustrate the 95% confidence interval areas obtained by taking, at each time, the 2.5^{th} and 97.5^{th} percentiles of the simulated trajectories. The green line is the empirical mean of the process.

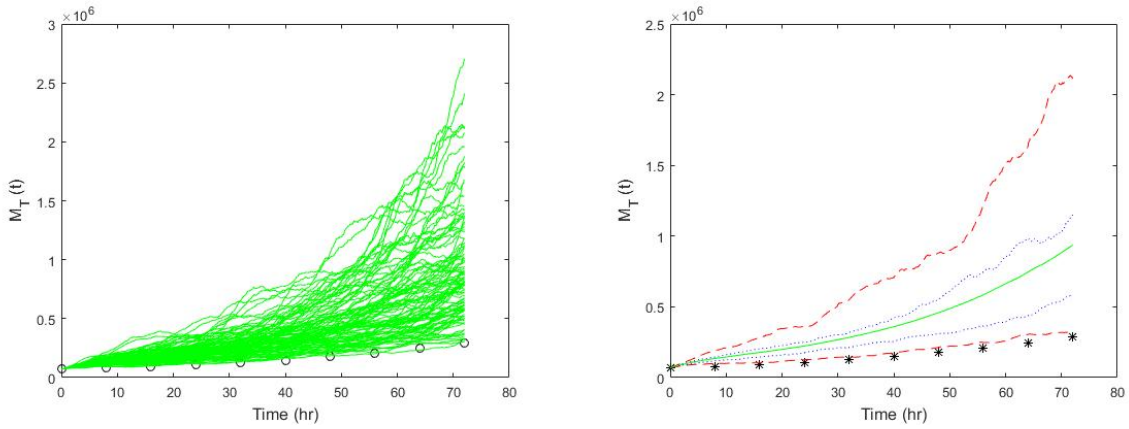

(a) Time Evolution of M_T (b) Time Evolution of M_T

Figure 5.10: Cell population dynamics for subpopulation M. The black circles show the trajectories corresponding to the observed data (nonparametric method). The blue lines represent the first and third quartiles of the simulated trajectories and the red lines illustrate the 95% confidence interval areas obtained by taking, at each time, the 2.5^{th} and 97.5^{th} percentiles of the simulated trajectories. The green line is the empirical mean of the process.

5.3.0 (c) Milstein Method

The model is run 100 times and the Milstein method with step size 1 is used to solve the SDE system (3.3.4) numerically, with the same initial parameter values used with the E-M method. Again, the parametric method is used to estimate the main parameters q_1, q_2, and q_3. The outcomes are presented in Table (5.5).

The figures (5.11), (5.12) and (5.13) display the results for this method with the same description as in the E-M method.

Table 5.5: Estimated parameter values and 95% confidence intervals of the death rates using the nonparametric method

Parameter	Estimated Value	95% Confidence Interval
q_1	0.0247215	[-0.001597, 0.05104]
q_2	0.121898	[0.10332, 0.14048]
q_3	-0.1694768	[-0.18642, -0.151713]

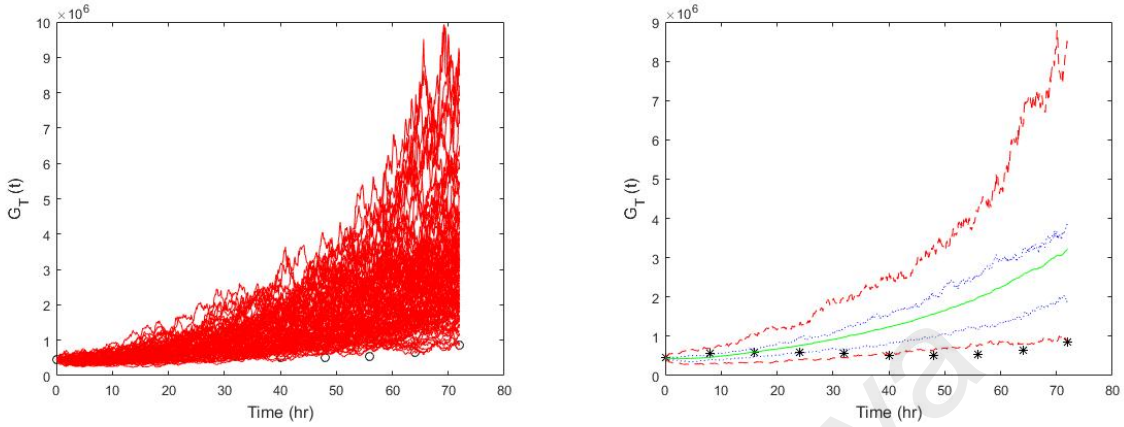

(a) Time Evolution of G_T (b) Time Evolution of G_T

Figure 5.11: Cell population dynamics for subpopulation G. The black circles show the trajectories corresponding to the observed data (nonparametric method). The blue lines represent the first and third quartiles of the simulated trajectories and the red lines illustrate the 95% confidence interval areas obtained by taking, at each time, the 2.5^{th} and 97.5^{th} percentiles of the simulated trajectories. The green line is the empirical mean of the process.

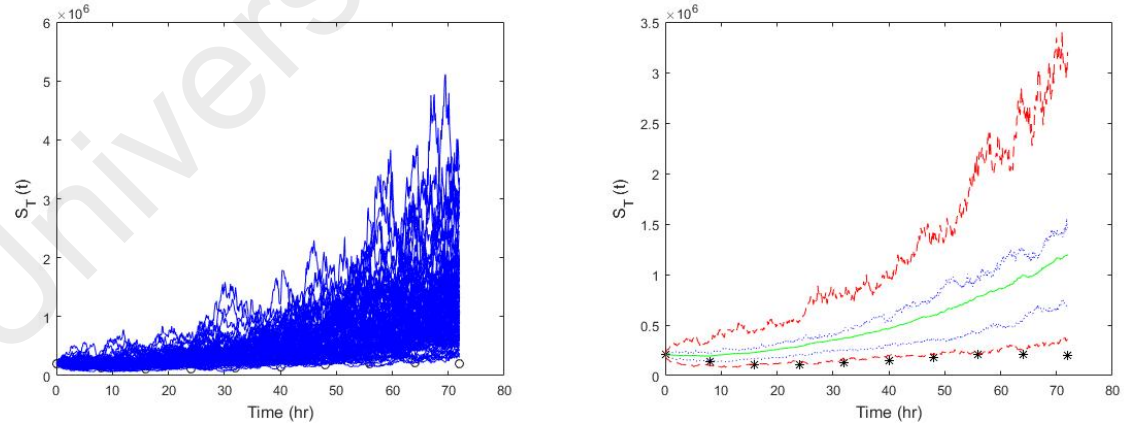

(a) Time Evolution of S_T (b) Time Evolution of S_T

Figure 5.12: Cell population dynamics for subpopulation S. The black circles show the trajectories corresponding to the observed data (nonparametric method). The blue lines represent the first and third quartiles of the simulated trajectories and the red lines illustrate the 95% confidence interval areas obtained by taking, at each time, the 2.5^{th} and 97.5^{th} percentiles of the simulated trajectories. The green line is the empirical mean of the process.

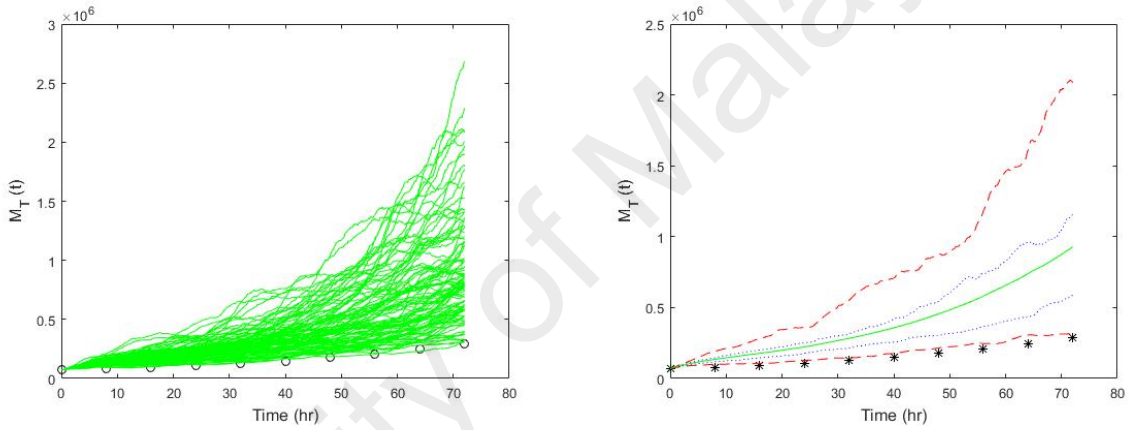

(a) Time Evolution of M_T (b) Time Evolution of M_T

Figure 5.13: Cell population dynamics for subpopulation M. The black circles show the trajectories corresponding to the observed data (nonparametric method). The blue lines represent the first and third quartiles of the simulated trajectories and the red lines illustrate the 95% confidence interval areas obtained by taking, at each time, the 2.5^{th} and 97.5^{th} percentiles of the simulated trajectories. The green line is the empirical mean of the process.

CHAPTER 6

DISCUSSION

6.1 Remind the purpose of this study

As discussed, two mathematical models are presented in this study to model the population dynamics of tumor cell population dynamics after treating by radiation therapy. The first model is driven based on the damage of cell's targets which are caused by radiation particles. In this model tumor cell's population is divided into m subpopulations $x_0, x_1, \cdots, x_{m-1}$ where x_i denotes the subpopulation with i deactivated targets.

Then the population dynamics of the tumor cells is modeled by using a system of linear ODEs. This model has five parameters which are q, the probability that a target becomes deactivated after a dose fraction of radiation, r, the probability that a target becomes active again after the action of repair mechanism, n_0, the total number of cells at time point zero post radiation, m, the number of targets in each cell and μ, the probability that a cell in subpopulation x_0 give birth.

Radiation may cause single and double-strand breaks but sometimes it is difficult to separate cells with single-strand break and cells with double-strand breaks. Based on these evidence, the model is considered in three cases, $m = 2$, $m = 3$ and general m. Subsequently, using Routh-Hurwitz criterion and Gershgorin theorem, the system stability is studied.

Cell cycle position of cells is another which researchers has been used to model the cell's population dynamics. Based on the flow cytometry results, we divide the tumor cell's population into 3 main sub-populations G, S and G_2/M, according to the cell cycle position.

Then, the population dynamics of tumor cells is modeled by using a three-dimensional SDE. Subsequently, the transition rates are estimated in the steady-state condition. Then, the SDE are solved numerically based on Euler-Maruyama and Milstein methods.

A series of experiments were done on MCF-7 cell line and the cells were analyzed by using flow cytometry method and the total number of cells in sub-populations G, S and G_2/M were counted. Finally, the death rates are estimated by using a parametric and non-parametric parameter estimation methods and based the obtained experimental data. Finally, a novel definition is proposed for the tumor lifespan which is defined as the minimum dose fraction of radiation needed to kill all tumor cells.

6.2 A summary of results

To summarize the results, the main novelties and achievements of the proposed models are:

6.2.1 The ODE model of tumor cells population dynamics

1. The model presents an intuitive and simple formula for cell proliferation Eq. (3.2.7) and tumor lifespan Eq. (4.52).

2. The proposed model comprises the dynamics of a tumor cell population due to the effect of treatment on cells through the each cell's reaction to radiation. For instance, after applying the first dose fraction and after the repair mechanism, a cell may remain in subpopulation x_0 or move to other sub-populations, x_i, $i = 1,\ldots,(m-1)$, or it may die. Therefore, the cells' reaction to treatment is different in this model and can be interpreted as heterogeneity.

3. By using the model, we confirmed that the treatment effect parameter (q) plays a more important role than the repair mechanism parameter (r). We demonstrate that $q = 0.5$ is a bifurcation value, meaning the system (4.2.1) is stable for all $0 < r < 1$.

4. We showed that the death rate of subpopulation x_i has less impact than that of subpopulation x_j when $i < j$, which means that cells with j deactivated targets are more radiosensitive than cells with i deactivated targets. Therefore, damaged cells are unable to resist radiation, which is in complete agreement with evidence provided in (Keinj et al., 2011, 2012).

5. In reality, radiation particles have different effects on different cells, representing treatment heterogeneity. For example, at the beginning of treatment, large numbers of cells with single-strand breaks and small numbers of cells with double-strand breaks are affected by treatment. Therefore, treatment heterogeneity is introduced in the model through Corollary (3.2.1).

6.2.2 The SDE model of tumor cells population dynamics

1. In the first step, existence and uniqueness of the solution is studied. Then the Stochastic Differential Equation is solved analytically.

2. The system stability is studied and it is shown that the system is stable if and only if

$$(1+\frac{q_1}{\alpha})(1+\frac{q_2}{\beta})(1+\frac{q_3}{\gamma}) > 2 \tag{6.2.1}$$

   In simple words, if the equation(6.2.1) satisfies, the population size goes to zero. Moreover it shows that the treatment is effective.

3. Based on the results, it is evident that there is no significant difference in cell population dynamics between parametric (Figure (4.51.a)) and nonparametric (Figure (4.51.b)) methods. The tumor lifespan is estimated and presented in Figure (4.52).

4. Figures (4.51) shows the effectiveness of the radiation. According to the figures, tumor population has a decreasing trend when $q_1 = 0.06$, $q_2 = 0.02$ and $q_3 = 1$.

5. Using experimental data provided by Satherland et. al, the transition rates were estimated. But that data was not enough to estimate the death rates. Therefor, a series of experiments were designed and appropriate data was produced to estimate the death rates.

6. The model was run hundred times and the death rates are estimated by using both parametric and non-parametric methods. The results of Table (5.3), Table (5.4) and Table (5.5) show that the parametric method is more accurate than the non-parametric method in this experiment. However, there is not significant difference between the results obtained from parametric and non-parametric methods.

7. Estimated values for q_1, q_2 and q_3 (Tables (5.3), (5.4) and (5.5)) show that, the death rates in subpopulations S and M are the maximum and minimum. This evidence shows that cells prefer to stay in subpopulation M.

8. According to the figure (5.4), $G2/M$ arrest is happened which is in complete agreement with the results which are obtained from Tables (5.3), (5.4) and (5.5).

9. The data is on the lower bound of 95% confidence interval when the parameters are estimated by using the non-parametric method (figures (5.8), (5.9), (5.10), (5.11), (5.12) and (5.13)).

10. The real data is more close to the average value obtained from simulated data (green line) in figure (5.5)) compare to figure (5.8) and figure (5.11)

6.3 Future Works

In future, both models will be improved as follows:

1. In reality, it is difficult to distinguish cells with single and double-strand breaks. But it is possible to detect SSBs and DSBs together by using the flow cytometry

assays such as **TUNEL** assay. Subsequently, we can divide the population into two subpopulation, cells with and without DNA fragmentation. Then, we will be able to design appropriate experiments to detect and count the number of cells with DNA fragmentation and finally, the ODE model will be calibrated and verified by using the experimental real data.

2. To improve the ODE model, we can consider the most important parameter of the model as a function of time so the ODE model will transform to a non-linear SDE model which is very interesting for mathematicians.

3. In the SDE model, the rate of movement from sub-population G to sub-population S is considered as a constant value. However, in real this rate is a function of time. To improve this model this rate (α) will be considered as a function of time. Ten by using experimental data the best fit for $\alpha(t)$ will be obtained.

4. Then delay terms will be added to the movement rate. By this term, the model will be able to directly consider the delay which happens by cell cycle arrest.

CHAPTER 7

CONCLUSION

In this study, two new mathematical frameworks were proposed to model the population dynamics of heterogeneous tumor cells after the treatment with external beam radiation. The first model is derived based on the Target Theory and Hit Theory. According to these theories, the tumor population is divided into m different sub-populations based on the different effects of ionizing radiations on human cells. This model consists of a system of differential equations with random variable coefficients representing the dynamics transition rates between sub-populations. The model is also describing the heterogeneity of the cell damage and the repair mechanism between two consecutive dose fractions.

In the second model, we study the population dynamics of breast cancer cells treated with radiotherapy by using a system of stochastic differential equations. According to the cell cycle, each cell belongs to one of three subpopulations G, S, or M, representing gap, synthesis, and mitosis subpopulations. Cells in the M subpopulation are highly radio-sensitive, whereas cells in the S subpopulation are highly radio-resistant. Therefore, in the process of radiotherapy, cell death rates of different subpopulations are not equal. In addition, since flow cytometry is unable to detect apoptotic cells accurately, the small changes in cell death rate in each subpopulation during treatment are considered. Therefore, a new definition for the lifespan of the tumor based on population size is introduced. Tumor Lifespan is defined as the minimum number of dose fractions needed to remove the whole tumor.

The stability of the first model is studied by considering three cases. For the first and second cases, we assumed that each cell has two and three targets ($m = 2$ and $m = 3$).

Applying Routh-Hurwitz criterion, it is proven that the system is stable when the probability that one target becomes deactivated after the application of a dose fraction (q) is greater than or equal to 0.5.

Finally, the system stability for the third case is investigated analytically when each cell assumed has m targets. By using Gershgorin theorem, it is shown that the system is stable where $q > 0.5$.

In the second model, the existence and uniqueness of the solution are proven and an explicit solution for the SDE model is presented. Moreover, the system stability is investigated via a necessary and sufficient condition on model parameters. The transition rates are estimated in a steady state condition. Subsequently, the model is solved numerically using Euler-Murayama and Milstein methods and the other parameters of the model are estimated using parametric and nonparametric simulated likelihood estimation parameter methods.

Finally, we did a number of experiments on MCF-7 breast cancer cell line. The cell cycle analysis assay has been used to analyze experimental data. Then the obtained data is applied and able to calibrate and verify our models.

REFERENCES

Adam, J., & Bellomo, N. (1997). *A survey of models for tumor-immune system dynamics*. Springer Science & Business Media.

Adam, J., & Bellomo, N. (2012). *A survey of models for tumor-immune system dynamics*. Springer Science & Business Media.

Aït-Sahalia, Y. (2002). Maximum likelihood estimation of discretely sampled diffusions: A closed-form approximation approach. *Econometrica*, *70*(1), 223–262.

Ait-Sahalia, Y. (2002). [numerical techniques for maximum likelihood estimation of continuous-time diffusion processes]: Comment. *Journal of Business & Economic Statistics*, *20*(3), 317–321.

Aït-Sahalia, Y., et al. (2008). Closed-form likelihood expansions for multivariate diffusions. *The Annals of Statistics*, *36*(2), 906–937.

Albano, G., & Giorno, V. (2006). A stochastic model in tumor growth. *Journal of Theoretical Biology*, *242*(2), 329–336.

Alcock, J., & Burrage, K. (2004). A genetic estimation algorithm for parameters of stochastic ordinary differential equations. *Computational Statistics & Data Analysis*, *47*(2), 255–275.

Alper, T. (1979). *Cellular radiobiology*. CUP Archive.

Antipas, V. P., Stamatakos, G. S., Uzunoglu, N. K., Dionysiou, D. D., & Dale, R. G. (2004). A spatio-temporal simulation model of the response of solid tumours to radiotherapy in vivo: parametric validation concerning oxygen enhancement ratio and cell cycle duration. *Physics in Medicine and Biology*, *49*(8), 1485.

Araujo, R. P., & McElwain, D. S. (2004). A history of the study of solid tumour growth: the contribution of mathematical modelling. *Bulletin of Mathematical Biology*, *66*(5), 1039–1091.

Aten, J. A., Stap, J., Krawczyk, P. M., van Oven, C. H., Hoebe, R. A., Essers, J., & Kanaar, R. (2004). Dynamics of dna double-strand breaks revealed by clustering of damaged chromosome domains. *Science*, *303*(5654), 92–95.

Atwood, K., & Norman, A. (1949). On the interpretation of multi-hit survival curves. *Proceedings of the National Academy of Sciences*, *35*(12), 696–709.

Bajzer, Z., Marušić, M., & Vuk-Pavlović, S. (1996). Conceptual frameworks for mathematical modeling of tumor growth dynamics. *Mathematical and Computer Modelling*, *23*(6), 31–46.

Basse, B., Baguley, B. C., Marshall, E. S., Wake, G. C., & Wall, D. J. (2004). Modelling cell population growth with applications to cancer therapy in human tumour cell

lines. *Progress in Biophysics and Molecular Biology*, *85*(2), 353–368.

Bastogne, T., Samson, A., Vallois, P., Wantz-Mezieres, S., Pinel, S., Bechet, D., & Barberi-Heyob, M. (2010). Phenomenological modeling of tumor diameter growth based on a mixed effects model. *Journal of Theoretical Biology*, *262*(3), 544–552.

Beamish, H., & Lavin, M. (1994). Radiosensitivity in ataxia-telangiectasia: anomalies in radiation-induced cell cycle delay. *International Journal of Radiation Biology*, *65*(2), 175–184.

Begg, R., Wall, D. J., & Wake, G. C. (2010). On a multicompartment age-distribution model of cell growth. *IMA Journal of Applied Mathematics*, hxq010.

Bellomo, N., & Delitala, M. (2008). From the mathematical kinetic, and stochastic game theory to modelling mutations, onset, progression and immune competition of cancer cells. *Physics of Life Reviews*, *5*(4), 183–206.

Bellomo, N., Li, N., & Maini, P. K. (2008). On the foundations of cancer modelling: selected topics, speculations, and perspectives. *Mathematical Models and Methods in Applied Sciences*, *18*(04), 593–646.

Bellomo, N., & Preziosi, L. (2000). Modelling and mathematical problems related to tumor evolution and its interaction with the immune system. *Mathematical and Computer Modelling*, *32*(3), 413–452.

Bentzen, S. M. (1993). Quantitative clinical radiobiology. *Acta Oncologica*, *32*(3), 259–275.

Bernard, S., & Herzel, H. (2006). Why do cells cycle with a 24 hour period? *Genome Informatics*, *17*(1), 72–79.

Beskos, A., Papaspiliopoulos, O., Roberts, G. O., & Fearnhead, P. (2006). Exact and computationally efficient likelihood-based estimation for discretely observed diffusion processes (with discussion). *Journal of the Royal Statistical Society: Series B (Statistical Methodology)*, *68*(3), 333–382.

Bibby, B. M., Jacobsen, M., & Sørensen, M. (2004). *Estimating functions for discretely sampled diffusion-type models*. Department of Applied Mathematics and Statistics, University of Copenhagen.

Borkenstein, K., Levegrün, S., & Peschke, P. (2004). Modeling and computer simulations of tumor growth and tumor response to radiotherapy. *Radiation Research*, *162*(1), 71–83.

Brandt, M. W., & Santa-Clara, P. (2002a). [numerical techniques for maximum likelihood estimation of continuous-time diffusion processes]: Comment. *Journal of Business & Economic Statistics*, *20*(3), 321–324.

Brandt, M. W., & Santa-Clara, P. (2002b). Simulated likelihood estimation of diffusions with an application to exchange rate dynamics in incomplete markets. *Journal of Financial Economics*, *63*(2), 161–210.

Brenner, D. J., Hlatky, L., Hahnfeldt, P., Huang, Y., & Sachs, R. (1998). The linear-quadratic model and most other common radiobiological models result in similar predictions of time-dose relationships. *Radiation Research*, *150*(1), 83–91.

Burton, A. C. (1966). Rate of growth of solid tumours as a problem of diffusion. *Growth*, *30*(2), 157–176.

Byrne, H., Alarcon, T., Owen, M., Webb, S., & Maini, P. (2006). Modelling aspects of cancer dynamics: a review. *Philosophical Transactions of the Royal Society of London A: Mathematical, Physical and Engineering Sciences*, *364*(1843), 1563–1578.

Chaplain, M. A. (2008). Modelling aspects of cancer growth: insight from mathematical and numerical analysis and computational simulation. In *Multiscale problems in the life sciences* (pp. 147–200). Springer.

Chapman, J. (2007). Target theory revisited: Why physicists are essential for radiobiology research. *Clinical Oncology*, *19*(3), S12.

Cohen, L. (1971). A cell population kinetic model for fractionated radiation therapy 1: I. normal tissues. *Radiology*, *101*(2), 419–427.

Collis, S. J., DeWeese, T. L., Jeggo, P. A., & Parker, A. R. (2005). The life and death of dna-pk. *Oncogene*, *24*(6), 949–961.

Cramer, W. (1934). The prevention of cancer. *The Lancet*, *223*(5758), 1–5.

Crowther, J. (1924). Some considerations relative to the action of x-rays on tissue cells. *Proceedings of the Royal Society of London. Series B, Containing Papers of a Biological Character*, *96*(674), 207–211.

Curtis, S. B. (1986). Lethal and potentially lethal lesions induced by radiation—a unified repair model. *Radiation Research*, *106*(2), 252–270.

Dacunha-Castelle, D., & Florens-Zmirou, D. (1986). Estimation of the coefficients of a diffusion from discrete observations. *Stochastics: An International Journal of Probability and Stochastic Processes*, *19*(4), 263–284.

Dahm-Daphi, W. A. J., C. Sass. (2000). Comparison of biological effects of dna damage induced by ionizing radiation and hydrogen peroxide in cho cells. *International Journal of Radiation Riology*, *76*(1), 67–75.

Dale, R. G., Jones, B., et al. (2007). *Radiobiological modelling in radiation oncology*. British Inst of Radiology.

Daşu, A., & Denekamp, J. (1999). Superfractionation as a potential hypoxic cell radiosensitizer: prediction of an optimum dose per fraction. *International Journal of Radiation Oncology* Biology* Physics*, *43*(5), 1083–1094.

Daşu, A., Toma-Daşu, I., & Karlsson, M. (2005). The effects of hypoxia on the theoretical modelling of tumour control probability. *Acta Oncologica*, *44*(6), 563–571.

Datta, R., Cole, A., & Robinson, S. (1976). Use of track-end alpha particles from241 am to study radiosensitive sites in cho cells. *Radiation Research*, *65*(1), 139–151.

Daukste, L. (2012). Mathematical modelling of cancer cell population dynamics.

Dawson, A., & Hillen, T. (2006). Derivation of the tumour control probability (tcp) from a cell cycle model. *Computational and Mathematical Methods in Medicine*, *7*(2-3), 121–141.

Dertinger, H., & Jung, H. (2013). *Molecular radiation biology: the action of ionizing radiation on elementary biological objects*. Springer Science & Business Media.

Dessauer, F. (1922). On several actions of radiation. *Z fur Physik*, *12*, 38–42.

Di Leonardo, A., Linke, S. P., Clarkin, K., & Wahl, G. M. (1994). Dna damage triggers a prolonged p53-dependent g1 arrest and long-term induction of cip1 in normal human fibroblasts. *Genes & Development*, *8*(21), 2540–2551.

Dionysiou, D., Stamatakos, G., Gintides, D., Uzunoglu, N., & Kyriaki, K. (2008). Critical parameters determining standard radiotherapy treatment outcome for glioblastoma multiforme: a computer simulation. *The Open Biomedical Engineering Journal*, *2*, 43.

Dionysiou, D. D., & Stamatakos, G. S. (2006). Applying a 4d multiscale in vivo tumor growth model to the exploration of radiotherapy scheduling: the effects of weekend treatment gaps and p53 gene status on the response of fast growing solid tumors. *Cancer Informatics*, *2*.

Ditlov, V. (2009). Track theory and radiation effects. *Radiation Measurements*, *44*(9), 1100–1104.

Donaghey, C. E. (1980). Cellsim: cell cycle simulation made easy. *International Review of Cytology*, *66*, 171–210.

Donaghey, C. E. (1983). Cellsim and cellgrow: tools for cell kinetic modeling. *ISA Transactions*, *22*(4), 21.

Düchting, W., & Vogelsaenger, T. (1981). Three-dimensional pattern generation applied to spheroidal tumor growth in a nutrient medium. *International Journal of Bio-Medical Computing*, *12*(5), 377–392.

Düchting, W., & Vogelsaenger, T. (1985). Recent progress in modelling and simulation of three-dimensional tumor growth and treatment. *Biosystems*, *18*(1), 79–91.

Duechting, W., Ginsberg, T., & Ulmer, W. (1995). Modeling of radiogenic responses induced by fractionated irradiation in malignant and normal tissue. *Stem cells*, *13*, 301–306.

Duechting, W., Lehrig, R., Ginsberg, T., Dedeleit, E., & Ulmer, W. (1992). Computer simulation and modelling of tumor spheroid growth and their relevance for optimization of fractionated radiotherapy. *Strahlentherapie und Onkologie*, *168*(6), 354–360.

Dullens, H., Van Der Tol, M., De Weger, R., & Den Otter, W. (1986). A survey of some formal models in tumor immunology. *Cancer Immunology, Immunotherapy*, *23*(3), 159–164.

Dunst, J., Stadler, P., Becker, A., Lautenschläger, C., Pelz, T., Hänsgen, G., ... Kuhnt, T. (2003). Tumor volume and tumor hypoxia in head and neck cancers. *Strahlentherapie und Onkologie*, *179*(8), 521–526.

Durham, G. B., & Gallant, A. R. (2002). Numerical techniques for maximum likelihood estimation of continuous-time diffusion processes. *Journal of Business & Economic Statistics*, *20*(3), 297–338.

Durocher, D., & Jackson, S. P. (2001). Dna-pk, atm and atr as sensors of dna damage: variations on a theme? *Current Opinion in Cell Biology*, *13*(2), 225–231.

Durrett, R., Foo, J., Leder, K., Mayberry, J., & Michor, F. (2011). Intratumor heterogeneity in evolutionary models of tumor progression. *Genetics*, *188*(2), 461–477.

Ellis, F. (1969). Dose, time and fractionation: a clinical hypothesis. *Clinical Radiology*, *20*(1), 1–7.

Endlich, L. (2000). *Goldman sachs: the culture of success*. Simon and Schuster.

Evans, L. C. (2012). *An introduction to stochastic differential equations* (Vol. 82). American Mathematical Society.

Falcetta, F., Lupi, M., Colombo, V., & Ubezio, P. (2013). Dynamic rendering of the heterogeneous cell response to anticancer treatments. *PLoS Computional Biology*, *9*(10), e1003293.

Ferlay, J., Soerjomataram, I., Dikshit, R., Eser, S., Mathers, C., Rebelo, M., ... Bray, F. (2015). Cancer incidence and mortality worldwide: sources, methods and major patterns in globocan 2012. *International Journal of Cancer*, *136*(5), E359–E386.

Fowler, J. (2014). 21 years of biologically effective dose. *The British Journal of Radiology*.

Fowler, J. F. (1989). The linear-quadratic formula and progress in fractionated radiotherapy. *The British Journal of Radiology*, *62*(740), 679–694.

Gámez, M., López, I., Garay, J., & Varga, Z. (2009). Observation and control in a model of a cell population affected by radiation. *BioSystems*, *96*(2), 172–177.

Gay, H. A., & Niemierko, A. (2007). A free program for calculating eud-based ntcp and tcp in external beam radiotherapy. *Physica Medica*, *23*(3), 115–125.

Gompertz, B. (1825). On the nature of the function expressive of the law of human mortality, and on a new mode of determining the value of life contingencies. *Philosophical Transactions of the Royal Society of London*, *115*, 513–583.

Gray, L. H., Conger, A., Ebert, M., Hornsey, S., & Scott, O. (1953). The concentration of

oxygen dissolved in tissues at the time of irradiation as a factor in radiotherapy. *The British Journal of Radiology*, *26*(312), 638–648.

Gupta, P. B., Fillmore, C. M., Jiang, G., Shapira, S. D., Tao, K., Kuperwasser, C., & Lander, E. S. (2011). Stochastic state transitions give rise to phenotypic equilibrium in populations of cancer cells. *Cell*, *146*(4), 633–644.

Gurkan-Cavusoglu, E., Schupp, J. E., Kinsella, T. J., & Loparo, K. A. (2011). Analysis of cell cycle dynamics using probabilistic cell cycle models. In *Engineering in medicine and biology society, embc, 2011 annual international conference of the ieee* (pp. 141–144).

Haddow, A. (1938). The biological characters of spontaneous tumours of the mouse, with special reference to rate of growth. *The Journal of Pathology and Bacteriology*, *47*(3), 553–565.

Han, W., & Yu, K. (2010). Ionizing radiation, dna double strand break and mutation. *Advances in Genetics Research*, *4*, 197–210.

Han, W., & Yu, K. N. (2009). Response of cells to ionizing radiation. *Advances in Biomedical Sciences and Engineering*, 204–262.

Harriss-Phillips, W., Bezak, E., & Yeoh, E. (2014). Monte carlo radiotherapy simulations of accelerated repopulation and reoxygenation for hypoxic head and neck cancer. *The British Journal of Radiology*.

Hill, A. (1928). The diffusion of oxygen and lactic acid through tissues. *Proceedings of the Royal Society of London. Series B, Containing Papers of a Biological Character*, *104*(728), 39–96.

Hill, S. E. (1928). A simple visual method for demonstrating the diffusion of oxygen through rubber and various other substances. *Science*, *67*(1736), 374–376.

Hirsch, M. W., Smale, S., & Devaney, R. L. (2012). *Differential equations, dynamical systems, and an introduction to chaos*. Academic press.

Hoeijmakers, J. H. (2001). Genome maintenance mechanisms for preventing cancer. *Nature*, *411*(6835), 366–374.

Howard, A., & Pelc, S. (1986). Synthesis of desoxyribonucleic acid in normal and irradiated cells and its relation to chromosome breakage. *International Journal of Radiation Biology and Related Studies in Physics, Chemistry and Medicine*, *49*(2), 207–218.

Hurn, A. S., Lindsay, K. A., & Martin, V. L. (2003). On the efficacy of simulated maximum likelihood for estimating the parameters of stochastic differential equations. *Journal of Time Series Analysis*, *24*(1), 45–63.

Hutchinson, F. (1985). Chemical changes induced in dna by ionizing radiation. *Progress in Nucleic Acid Research and Molecular Biology*, *32*, 115–154.

Jackson, S. P. (2002). Sensing and repairing dna double-strand breaks. *Carcinogenesis*, *23*(5), 687–696.

Jeggo, P. (1998). 5 dna breakage and repair. *Advances in Genetics*, *38*, 185–218.

Jensen, B., & Poulsen, R. (2002). Transition densities of diffusion processes: numerical comparison of approximation techniques. *The Journal of Derivatives*, *9*(4), 18–32.

Johnston, M. D., Edwards, C. M., Bodmer, W. F., Maini, P. K., & Chapman, S. J. (2007). Mathematical modeling of cell population dynamics in the colonic crypt and in colorectal cancer. *Proceedings of the National Academy of Sciences*, *104*(10), 4008–4013.

Joiner, M., & van der Kogel, A. (2009). Basic clinical radiobiology. *Basic Clinical Radiobiology. 4th ed2009*.

Källman, P., Ågren, A., & Brahme, A. (1992). Tumour and normal tissue responses to fractionated non-uniform dose delivery. *International Journal of Radiation Biology*, *62*(2), 249–262.

Karran, P. (2000). Dna double strand break repair in mammalian cells. *Current Opinion in Genetics & Development*, *10*(2), 144–150.

Keinj, R., Bastogne, T., & Vallois, P. (2011). Multinomial model-based formulations of tcp and ntcp for radiotherapy treatment planning. *Journal of Theoretical Biology*, *279*(1), 55–62.

Keinj, R., Bastogne, T., & Vallois, P. (2012). Tumor growth modeling based on cell and tumor lifespans. *Journal of Theoretical Biology*, *312*, 76–86.

Khanna, K. K., & Jackson, S. P. (2001). Dna double-strand breaks: signaling, repair and the cancer connection. *Nature Genetics*, *27*(3), 247–254.

Khoronenkova, S. V., & Dianov, G. L. (2015). Atm prevents dsb formation by coordinating ssb repair and cell cycle progression. *Proceedings of the National Academy of Sciences*, *112*(13), 3997–4002.

Kirkby, N., Burnet, N., & Faraday, D. (2002). Mathematical modelling of the response of tumour cells to radiotherapy. *Nuclear Instruments and Methods in Physics Research Section B: Beam Interactions with Materials and Atoms*, *188*(1), 210–215.

Kloden, P., & Platen, E. (1992). Numerical solution of stochastic differential equations springer. *Berlin, Germany*.

Kocher, M., Treuer, H., & Müller, R. (1997). Quantification of tumor reoxygenation during accelerated radiation therapy. *Radiology*, *205*(1), 263–268.

Kocher, M., Treuer, H., Voges, J., Hoevels, M., Sturm, V., & Müller, R.-P. (2000). Computer simulation of cytotoxic and vascular effects of radiosurgery in solid and necrotic brain metastases. *Radiotherapy and Oncology*, *54*(2), 149–156.

Kumari, S., Rastogi, R. P., Singh, K. L., Singh, S. P., & Sinha, R. P. (2008). Dna damage: detection strategies. *EXCLI J*, *7*, 44–62.

Kurz, E. U., & Lees-Miller, S. P. (2004). Dna damage-induced activation of atm and atm-dependent signaling pathways. *DNA Repair*, *3*(8), 889–900.

Laird, A. K. (1964). Dynamics of tumour growth. *British Journal of Cancer*, *18*(3), 490.

Laird, A. K., Tyler, S. A., Barton, A., et al. (1965). Dynamics of normal growth. *Growth*, *29*, 233–248.

Lea, D., & Catcheside, D. (1942). The mechanism of the induction by radiation of chromosome aberrations intradescantia. *Journal of Genetics*, *44*(2), 216–245.

Lea, D. E. (1955). Actions of radiations on living cells. *The American Journal of the Medical Sciences*, *229*(6), 709.

Lee, J. M., & Bernstein, A. (1993). p53 mutations increase resistance to ionizing radiation. *Proceedings of the National Academy of Sciences*, *90*(12), 5742–5746.

Lehnert, S. (2007). *Biomolecular action of ionizing radiation*. CRC Press.

Little, J. B. (1968). Delayed initiation of dna synthesis in irradiated human diploid cells. *Nature*, *218*(5146), 1064.

Lo, A. W. (1986). *Maximum likelihood estimation of generalized itô processes with discretely sampled data.* National Bureau of Economic Research Cambridge, Mass., USA.

Lyman, J. T. (1985). Complication probability as assessed from dose-volume histograms. *Radiation Research*, *104*(2s), S13–S19.

Marcu, L., Bezak, E., & Olver, I. (2006). Scheduling cisplatin and radiotherapy in the treatment of squamous cell carcinomas of the head and neck: a modelling approach. *Physics in Medicine and Biology*, *51*(15), 3625.

Marcu, L., Van Doorn, T., & Olver, I. (2004). Modelling of post-irradiation accelerated repopulation in squamous cell carcinomas. *Physics in Medicine and Biology*, *49*(16), 3767.

Marcu, L., Van Doorn, T., Zavgorodni, S., & Olver, I. (2002). Growth of a virtual tumour using probabilistic methods of cell generation. *Australasian Physics & Engineering Sciences in Medicine*, *25*(4), 155–161.

Martins, M., Ferreira, S., & Vilela, M. (2007). Multiscale models for the growth of avascular tumors. *Physics of Life Reviews*, *4*(2), 128–156.

Mayneord, W. V. (1932). On a law of growth of jensen's rat sarcoma. *The American Journal of Cancer*, *16*(4), 841–846.

McElwain, D., Callcott, R., & Morris, L. (1979). A model of vascular compression in

solid tumours. *Journal of Theoretical Biology*, *78*(3), 405–415.

Mottram, J. (1936). A factor of importance in the radio sensitivity of tumours. *The British Journal of Radiology*, *9*(105), 606–614.

Nagasawa, H., Keng, P., Harley, R., Dahlberg, W., & Little, J. (1994). Relationship between γ-ray-induced g2/m delay and cellular radiosensitivity. *International Journal of Radiation Biology*, *66*(4), 373–379.

Nagy, J. D. (2005). The ecology and evolutionary biology of cancer: a review of mathematical models of necrosis and tumor cell diversity. *Mathematical Biosciences and Engineering*, *2*(2), 381–418.

Nicolau, J. (2002). A new technique for simulating the likelihood of stochastic differential equations. *The Econometrics Journal*, *5*(1), 91–103.

Nicoloff, J., & Hoekstra, M. (1996). *Dna repair in higher eukaryotes, vol. 2.* Humana Press Inc., Totowa, New Jersey.

Nilsson, J., Lind, B., & Brahme, A. (2002). Radiation response of hypoxic and generally heterogeneous tissues. *International Journal of Radiation Biology*, *78*(5), 389–405.

Nomiya, T. (2013). Discussions on target theory: past and present. *Journal of Radiation Research*, *54*(6), 1161–1163.

Nordsmark, M., & Overgaard, J. (2004). Tumor hypoxia is independent of hemoglobin and prognostic for loco-regional tumor control after primary radiotherapy in advanced head and neck cancer. *Acta Oncologica*, *43*(4), 396–403.

O'Donoghue, J. (1997). The response of tumours with gompertzian growth characteristics to fractionated radiotherapy. *International Journal of Radiation Biology*, *72*(3), 325–339.

Ohnishi, T., Mori, E., & Takahashi, A. (2009). Dna double-strand breaks: their production, recognition, and repair in eukaryotes. *Mutation Research/Fundamental and Molecular Mechanisms of Mutagenesis*, *669*(1), 8–12.

O′Rourke, S., McAneney, H., & Hillen, T. (2009). Linear quadratic and tumour control probability modelling in external beam radiotherapy. *Journal of Mathematical Biology*, *58*(4-5), 799–817.

Pedersen, A. R. (1995). A new approach to maximum likelihood estimation for stochastic differential equations based on discrete observations. *Scandinavian Journal of Statistics*, 55–71.

Pena, J. M. (2004). Characterizations and stable tests for the routh–hurwitz conditions and for total positivity. *Linear Algebra and Its Applications*, *393*, 319–332.

Piantadosi, S., Hazelrig, J. B., & Turner, M. E. (1983). A model of tumor growth based on cell cycle kinetics. *Mathematical Biosciences*, *66*(2), 283–306.

Pollard, E. (1959). Radiation inactivation of enzymes, nucleic acids, and phage particles. *Reviews of Modern Physics*, *31*(2), 273.

Pollard, E. C., Guild, W. R., Hutchinson, F., & Setlow, R. B. (1955). The direct action of ionizing radiation on enzymes and antigens. *Progress in Biophysics*, *5*, 72–108.

Popple, R. A., Ove, R., & Shen, S. (2002). Tumor control probability for selective boosting of hypoxic subvolumes, including the effect of reoxygenation. *International Journal of Radiation Oncology* Biology* Physics*, *54*(3), 921–927.

Quiet, C. A., Weichselbaum, R. R., & Grdina, D. J. (1991). Variation in radiation sensitivity during the cell cycle of two human squamous cell carcinomas. *International Journal of Radiation Oncology* Biology* Physics*, *20*(4), 733–738.

Quinn, T., & Sinkala, Z. (2009). Dynamics of prostate cancer stem cells with diffusion and organism response. *BioSystems*, *96*(1), 69–79.

Rédei, G. P. (2008). *Encyclopedia of genetics, genomics, proteomics, and informatics*. Springer Science & Business Media.

Rich, T., Allen, R. L., & Wyllie, A. H. (2000). Defying death after dna damage. *Nature*, *407*(6805), 777–783.

Rischin, D., Hicks, R. J., Fisher, R., Binns, D., Corry, J., Porceddu, S., & Peters, L. J. (2006). Prognostic significance of [18f]-misonidazole positron emission tomography–detected tumor hypoxia in patients with advanced head and neck cancer randomly assigned to chemoradiation with or without tirapazamine: A substudy of trans-tasman radiation oncology group study 98.02. *Journal of Clinical Oncology*, *24*(13), 2098–2104.

Roose, T., Chapman, S. J., & Maini, P. K. (2007). Mathematical models of avascular tumor growth. *Siam Review*, *49*(2), 179–208.

Rouse, J., & Jackson, S. P. (2002). Interfaces between the detection, signaling, and repair of dna damage. *Science*, *297*(5581), 547–551.

Sachs, R., Hlatky, L., & Hahnfeldt, P. (2001a). Simple ode models of tumor growth and anti-angiogenic or radiation treatment. *Mathematical and Computer Modelling*, *33*(12), 1297–1305.

Sachs, R., Hlatky, L., & Hahnfeldt, P. (2001b). Simple ode models of tumor growth and anti-angiogenic or radiation treatment. *Mathematical and Computer Modelling*, *33*(12), 1297–1305.

Sancar, A., Lindsey-Boltz, L. A., Ünsal-Kaçmaz, K., & Linn, S. (2004). Molecular mechanisms of mammalian dna repair and the dna damage checkpoints. *Annual Review of Biochemistry*, *73*(1), 39–85.

Satow, T., & Kawai, H. (2006). Hit and target models for dna damage with indirect action. *Computers & Mathematics with Applications*, *51*(2), 257–268.

Sax, K. (1941). Types and frequencies of chromosomal aberrations induced by x-rays. In *Cold spring harbor symposia on quantitative biology* (Vol. 9, pp. 93–103).

Scott, D. W. (2015). *Multivariate density estimation: theory, practice, and visualization*. John Wiley & Sons.

Sible, J. C., & Tyson, J. J. (2007). Mathematical modeling as a tool for investigating cell cycle control networks. *Methods*, *41*(2), 238–247.

Sideris, T. C. (2013). *Ordinary differential equations and dynamical systems* (Vol. 2). Springer Science & Business Media.

Simms, K., Bean, N., & Koerber, A. (2012). A mathematical model of cell cycle progression applied to the mcf-7 breast cancer cell line. *Bulletin of Mathematical Biology*, *74*(3), 736–767.

Sinclair, W. K. (2012). Cyclic x-ray responses in mammalian cells in vitro 1. *Radiation Research*, *178*(2), AV112–AV124.

Søvik, Å., Malinen, E., Bruland, Ø. S., Bentzen, S. M., & Olsen, D. R. (2006). Optimization of tumour control probability in hypoxic tumours by radiation dose redistribution: a modelling study. *Physics in Medicine and Biology*, *52*(2), 499.

Stamatakos, G., Antipas, V., Uzunoglu, N., & Dale, R. (2014). A four-dimensional computer simulation model of the in vivo response to radiotherapy of glioblastoma multiforme: studies on the effect of clonogenic cell density. *The British Journal of Radiology*.

Stamatakos, G., et al. (2010). An advanced discrete state–discrete event multiscale simulation model of the response of a solid tumor to chemotherapy: Mimicking a clinical study. *Journal of Theoretical Biology*, *266*(1), 124–139.

Stamatakos, G. S., Georgiadi, E. C., Graf, N., Kolokotroni, E. A., & Dionysiou, D. D. (2011). Exploiting clinical trial data drastically narrows the window of possible solutions to the problem of clinical adaptation of a multiscale cancer model. *PLOS One*, *6*(3), e17594.

Starnatakos, G., Zacharaki, E. I., Makropoulou, M., Mouravliansky, N. A., Marsh, A., Nikita, K. S., & Uzunoglu, N. K. (2001). Modeling tumor growth and irradiation response in vitro-a combination of high-performance computing and web-based technologies including vrml visualization. *IEEE Transactions on Information Technology in Biomedicine*, *5*(4), 279–289.

Stramer, O., & Yan, J. (2012). On simulated likelihood of discretely observed diffusion processes and comparison to closed-form approximation. *Journal of Computational and Graphical Statistics*.

Su, T. T. (2006). Cellular responses to dna damage: one signal, multiple choices. *Annual Review of Genetics*, *40*, 187–208.

Sutherland, R. L., Hall, R. E., & Taylor, I. W. (1983). Cell proliferation kinetics of mcf-7

human mammary carcinoma cells in culture and effects of tamoxifen on exponentially growing and plateau-phase cells. *Cancer Research*, *43*(9), 3998–4006.

Sy, W.-C., & Han, P. (1982). Analysis of a stochastic model of cell survival. *Journal of Theoretical Biology*, *96*(2), 309–326.

Tannock, I. F. (1972). Oxygen diffusion and the distribution of cellular radiosensitivity in tumours. *The British Journal of Radiology*, *45*(535), 515–524.

Tell, R., Heiden, T., Granath, F., Borg, A., Skog, S., & Lewensohn, R. (1998). Comparison between radiation-induced cell cycle delay in lymphocytes and radiotherapy response in head and neck cancer. *British Journal of Cancer*, *77*(4), 643.

Teschl, G. (2012). *Ordinary differential equations and dynamical systems* (Vol. 140). American Mathematical Society Providence, RI.

Thomlinson, R., & Gray, L. (1955). The histological structure of some human lung cancers and the possible implications for radiotherapy. *British Journal of Cancer*, *9*(4), 539.

Toma-Daşu, I., Daşu, A., & Karlsson, M. (2006). Theoretical simulation of tumour hypoxia measurements. In *Oxygen transport to tissue xxvii* (pp. 369–374). Springer.

Toma-Daşu, I., Daşuu, A., & Brahmeu, A. (2009). Quantifying tumour hypoxia by pet imaging-a theoretical analysis. In *Oxygen transport to tissue xxx* (pp. 267–272). Springer.

Tuckwell, W., Bezak, E., Yeoh, E., & Marcu, L. (2008). Efficient monte carlo modelling of individual tumour cell propagation for hypoxic head and neck cancer. *Physics in Medicine and Biology*, *53*(17), 4489.

Turner, M. E. (1975). Some classes of hit-theory models. *Mathematical Biosciences*, *23*(3), 219–235.

Uzman, A. (2003). *Molecular biology of the cell: Alberts, b., johnson, a., lewis, j., raff, m., roberts, k., and walter, p.* Wiley Online Library.

Valentin, J. (2006). *Low-dose extrapolation of radiation-related cancer risk*. Elsevier London.

Valenzuela, M. T., Mateos, S., de Almodóvar, J. M. R., & McMillan, T. J. (2000). Variation in sensitizing effect of caffeine in human tumour cell lines after γ-irradiation. *Radiotherapy and Oncology*, *54*(3), 261–271.

Varga, R. S. (2009). *Matrix iterative analysis* (Vol. 27). Springer Science & Business Media.

Varga, R. S. (2010). *Geršgorin and his circles* (Vol. 36). Springer Science & Business Media.

Vilenchik, M. M., & Knudson, A. G. (2000). Inverse radiation dose-rate effects on

somatic and germ-line mutations and dna damage rates. *Proceedings of the National Academy of Sciences*, *97*(10), 5381–5386.

von Sonntag, C. (1987). *The chemical basis of radiation biology*. Taylor & Francis London.

Wake, G. C., & Byrne, H. M. (2013). Calculus from the past: multiple delay systems arising in cancer cell modelling. *The ANZIAM Journal*, *54*(03), 117–126.

Ward, J. F. (1998). Nature of lesions formed by ionizing radiation. In *Dna damage and repair* (pp. 65–84). Springer.

Weber, T. S., Jaehnert, I., Schichor, C., Or-Guil, M., & Carneiro, J. (2014). Quantifying the length and variance of the eukaryotic cell cycle phases by a stochastic model and dual nucleoside pulse labelling. *Plos Computional Biology*, *10*(7), e1003616.

Winsor, C. P. (1932). The gompertz curve as a growth curve. *Proceedings of the National Academy of Sciences*, *18*(1), 1–8.

Withers, H., Taylor, J., & Maciejewski, B. (1988). The hazard of accelerated tumor clonogen repopulation during radiotherapy. *Acta Oncologica*, *27*(2), 131–146.

Wouters, B., Weppler, S., Koritzinsky, M., Landuyt, W., Nuyts, S., Theys, J., ... Lambin, P. (2002). Hypoxia as a target for combined modality treatments. *European Journal of Cancer*, *38*(2), 240–257.

Wouters, B. G., & Brown, J. M. (1997). Cells at intermediate oxygen levels can be more important than the" hypoxic fraction" in determining tumor response to fractionated radiotherapy. *Radiation Research*, *147*(5), 541–550.

Wyman, C., & Kanaar, R. (2006). Dna double-strand break repair: all's well that ends well. *Annual Review of Genetics*, *40*, 363–383.

Zaider, M., & Minerbo, G. (2000). Tumour control probability: a formulation applicable to any temporal protocol of dose delivery. *Physics in Medicine and Biology*, *45*(2), 279.

Zhou, X.-Y., Wang, X., Hu, B., Guan, J., Iliakis, G., & Wang, Y. (2002). An atm-independent s-phase checkpoint response involves chk1 pathway. *Cancer Research*, *62*(6), 1598–1603.

LIST OF PUBLICATIONS

1. Oroji, A., Omar, M., & Yarahmadian, S. (2016). An ÃŐto stochastic differential equations model for the dynamics of the MCF-7 breast cancer cell line treated by radiotherapy. Journal of Theoretical Biology, 407, 128-137.

2. Oroji, A., bin Omar, M., & Yarahmadian, S. (2015, October). A new ODE tumor growth modeling based on tumor population dynamics. In THE 22ND NATIONAL SYMPOSIUM ON MATHEMATICAL SCIENCES (SKSM22): Strengthening Research and Collaboration of Mathematical Sciences in Malaysia (Vol. 1682, p. 020045). AIP Publishing.

3. Oroji, A., Yarahmadian, S., Seddighi, S., & Omar, M. (2018). A Mathematical Model for Tumor Cell Population Dynamics Based on Target Theory and Tumor Lifespan. arXiv preprint arXiv: 1801.07113.